DECORATIVE AND PROTECTIVE TiN COATINGS ON 304 STAINLESS STEEL USING CATHODIC ARC PVD

by

Sylwia Agnieszka Lyda

B. Sc., Wilfrid Laurier University, 2014

A THESIS SUBMITTED TO THE SCHOOL OF GRADUATE STUDIES
IN PARTIAL FULFILLMENT OF THE REQUIREMENTS FOR THE
DEGREE OF

MASTER OF APPLIED SCIENCE

in

Engineering Physics

McMaster University

Hamilton, Ontario

Submission date (April 2016)

Abstract

Titanium Nitride (TiN) coatings on the market today are known as very hard ceramic coatings most commonly deposited on metallic alloys such as stainless steel. Previous and current research into functional coatings demonstrated tremendous potential for various industrial applications. Primary focus in this research into TiN coatings is decorative coatings with scratch resistant properties specific to the cathodic arc PVD system used in this research. Individual parameters were varied while others kept constant prior to and during deposition. This created a unique set of samples in order to determine the most effective deposition recipe specific to the PVD system. Adhesion is a major factor to consider when developing coatings onto stainless steel. Two different cleaning methods are used to prepare the samples, one method being performed within a class 10,000 clean room. Initial research determined whether strong adhesion is dependent on external baking of stainless steel substrates by investigating various bake time and temperatures prior to deposition. Further research varied ion bombardment duration and voltage, TiN deposition duration, and nitrogen pressure and investigated their influence on scratch resistance and adhesion of the coatings. Scratch testing verified hardness and provided insight to the coating's resistance to delamination with linearly increasing force. From these results, it became possible to identify the quality of adhesion between the TiN coating and stainless steel substrate.

Table of Contents

List of Tables

List of Figures

Acknowledgements

I would like to express my sincere gratitude to my advisor Dr. Peter Mascher for the continuous support of my M.A.Sc. study, for his patience, motivation, and immense knowledge. His guidance helped me in all the time of research and writing of this thesis. I could not have imagined having a better advisor and mentor for my M.A.Sc. study.

I am grateful to C. Bahl and T. Boehm of SteelForm Design Inc. for allowing us to use their industrial facility and PVD system to create my samples, and to L. Martinu, J. Saphieha, and T. Schmitt of the Functional Coating and Surface Engineering Laboratory (FCSEL) at École Polytechnique de Montréal, and L. Goncharova for giving me access to their laboratory facilities for analysis.

1 Introduction

1.1 Importance of TiN Films on Stainless Steel

Stainless steel is a major alloy used in numerous industrial applications worldwide. Some applications include: interior and exterior parts in aerospace (Whittaker and Hess 2015) and automotive engineering (Hariharan, Balachandran and Sathya Prasad 2009); jewelry and watches (Yuan, Li and Wang 2013); home appliances, such as microwaves, refrigerators and dishwashers; door handles; as well as kitchen and bathroom equipment (Taiwade, et al. 2012). A major advantage of stainless steel is that it is more cost effective over other expensive high performance alloys (Hariharan, Balachandran and Sathya Prasad 2009), but it is susceptible to corrosion (Hansen, Dexter and Waite 1995) (Adler and Walters 1992), oil stains from fingerprints, and scratch damage (Adler and Walters 1992).

Functional thin films protect materials from regular wear occurring over time as well as environmental and chemical corrosion caused by moisture or acidic conditions (Vuorinen, Niemi and Korhonen 1985). Titanium Nitride (TiN), Titanium Carbide (TiC), and Titanium Carbo-Nitride (TiCN) are just a few of the many coating materials frequently used for this purpose in industrial applications (Johnson and Randhawa 1987).

TiN material demonstrates excellent mechanical properties because of its hardness. TiN is insoluble in water and has a melting point of 2950 °C (Lugscheider, et al. 1999). TiN has a Vickers hardness of 2310 +/- 380 (Nordin, Larsson and Hogmark

1999) and thermal conductivity of 11.9 W/mK (Ding, Samani and Chen 2010). It is frequently used to enhance substrate surface properties, such as sharpness, edge retention, and corrosion resistance for industrial applications of high speed steel (HSS) drill bits and milling cutters (Bull and Rickerby 1990) (Bendavid, et al. 1994) (Mohrbacher, et al. 1995) (Wu, Mohrbacher and Celis 1996) (Kobayashi and Doi 1978). Experimental results have shown that TiN films of approximately 3 μm thickness improved the lifetime of HSS drill bits by at least 10 times, depending on drilling conditions. Similarly, lifetimes of hobs, broaches, end mills, and bandsaws have been improved three to five times with the use of TiN coatings. Along with the use of TiN coatings on cutting and drilling tools, substrate geometries and finishes have been modified in order to optimize the protective films. Although wear resistance is an important property of coated tools, increased productivity is also of major importance for these applications. TiN films function as dry film lubricants (Mattox, Handbook of Physical Vapor Deposition (PVD) Processing 2010) for cutting and drilling tools, allowing them to run faster than traditional uncoated tools (Randhawa and Johnson, Technical Note: A Review of Cathodic Arc Plasma Deposition Processes and their Applications 1987).

TiN coatings are frequently used in aerospace and automotive industries to protect surfaces from high temperatures within engines and repetitive wear from sliding and grinding that would occur in suspension forks or internal gears (Zalnezhad, Sarhan and Hamdi 2013). Industries, such as aerospace engineering, also focus on scratch resistant properties; examples are gas turbine engines, used to power aircrafts, trains, ships, electrical generators, as well as tanks. Aircraft are subjected to harsh external conditions involving foreign particles, such as sand and dust particles, that impact compressor blades and impellers in the engines at high velocities. Since aircraft operate under varying conditions, lifetime durations for jet engine components differ. Coating engine components with a layer of TiN significantly reduces the amount of wear, thus improving the overall lifetime of the engine. A TiN film thickness of 12 μm is recommended for observable wear improvement. Experimental results have shown that TiC films of similar thickness further improve the lifetime of these engine components (Randhawa and Johnson, Technical Note: A Review of Cathodic Arc Plasma Deposition Processes and their Applications 1987).

Acid and moisture resistance is a crucial property for protection against corrosion. Stainless steel products are faced with accelerated corrosion in marine and chemical plant environments as well as automotive and aerospace applications. Cathodic arc physical vapour deposition (PVD) coatings are still in early stages of development for corrosion protection applications. Coatings deposited using cathodic arc PVD processes exhibit promising potential for use on raw steel sheets, plumbing and pump components, fasteners used in automotive and aerospace applications, compressor blades and impellers used in centrifugal pumps and gas turbine engines. Currently, chromium coatings deposited using electroplating methods are frequently used for external steel units in the automotive industry, but TiN coatings show promise, as TiN material is highly resistant to chemical attack (Randhawa and Johnson, Technical Note: A Review of Cathodic Arc Plasma Deposition Processes and their Applications 1987). In certain applications, water and oil repellant properties of coated stainless steel are extremely beneficial. For example, fingerprint resistance of consumer products would require an easy clean surface, which derives from hydrophobic or oleophobic properties at the surface. Hydrophobic surfaces are also favorable in water applications because they help reduce corrosion and as a result, increase performance and lifetime of the stainless steel parts (Adler and Walters 1992) (Hansen, Dexter and Waite 1995). Observing contact angles is a common method used to determine the ability of a material or surface to soak. Hydrophobic surfaces refer to surfaces that repel water, while oleophobic surfaces refer to surfaces that repel oils. **Figure 1-1** shows ranges of contact angles and their classifications. From **Figure 1-1**, it is evident that in order for a surface to be considered hydrophobic or oleophobic, the contact angle of the liquid on the surface must be large.

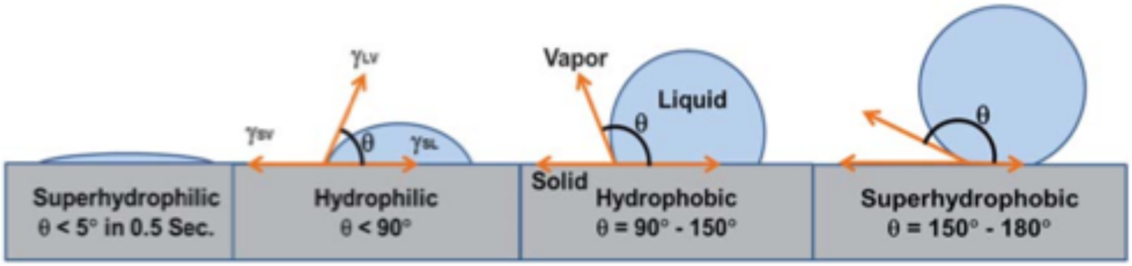

Figure 1-1. Contact angles and their classifications ranging from super hydrophilic to super hydrophobic (Nuraje, et al. 2013, with permission).

TiN coatings also are frequently used for the decorative purposes of coating jewelry, watches, automotive trims, and interior hardware, such as door knobs, plumbing fixtures and metallic trims. Sputtering and electroplating processes are traditionally used for jewelry and watch industries while sputtering and ion plating processes are popular for household hardware and appliances. TiN thin films display a characteristic gold colour, making it an excellent alternative for these applications as it significantly decreases production and consumer costs, as opposed to using genuine gold. Cathodic arc PVD processes are desirable because it offers superior quality coatings and faster production due to its capability of depositing films at very high rates (Randhawa and Johnson, Technical Note: A Review of Cathodic Arc Plasma Deposition Processes and their Applications 1987).

It is important to note that TiN material meets FDA guidelines and is not toxic, thus expanding its applications to biomedical engineering. TiN coatings can be found on scalpel and bone saw blades in operating rooms, hip and knee replacement implants (Mohseni, et al. 2015), as well as biosensors within the human body (Lima, et al. 2011). Also utilized in microelectronics, TiN coatings are considered to be highly conductive barrier metals (Nicolet 1978) used between metal contacts and an active electrical circuit (Wittmer, Struder and Melchior 1981).

1.2 Coating Systems

1.2.1 Physical Vapour Deposition (PVD)

TiN thin films are very common coatings deposited by PVD systems. In a PVD system, a pure material is evaporated into its gas phase and transported to the target substrate through the movement of the vapourized gas particles. The vapourized gas particles interact with the reactive atmosphere, creating a thin film layer of hard material (for example, Titanium (Ti) reacts with nitrogen gas (N_2) to form TiN coatings) (Knotek, Liiffler and Kriimer 1993). In comparison to other deposition techniques, PVD systems provide numerous advantages. They are less harmful to the environment than chemical vapour deposition (CVD) systems that sometimes operate using precursors with harmful byproducts that may be toxic, corrosive, or even pyrophoric. PVD processes are beneficial as they can be operated at lower temperatures, approximately 500°C, whereas CVD processes operate at approximately 1000°C (Randhawa and Johnson, Technical Note: A Review of Cathodic Arc Plasma Deposition Processes and their Applications 1987). Although plasma enhanced chemical vapour deposition (PECVD) can be operated at lower temperatures of 200°C (Schade, et al. 2006). PVD and CVD systems operate at high vacuum conditions, requiring operating supervision and water-cooling systems to deplete large heat loads (Jehn 1999). PVD technology allows for thin films to be deposited through different methods. These methods include evaporation and sputtering.

1.2.2 Cathodic Arc PVD

Cathodic arc PVD is a particular form of the evaporative PVD process. A schematic of these types of systems is shown in **Figure 1-2**. Located at the cathode of each vacuum arc, target material (for example, Ti) is evaporated, simultaneously forming a plasma of titanium ions. By applying a bias voltage, the ions are accelerated toward the substrate. With the introduction of nitrogen flow, titanium ions react with the nitrogen atoms, forming the TiN coating found on the substrate post deposition. The cathodes are supplied with a voltage. The arcs become initiated once a high voltage pulse electrode is placed near the cathode, forming highly energetic emitting areas known as cathode spots. This phenomenon is known as gas charge ignition (Randhawa and Johnson, Technical

Note: A Review of Cathodic Arc Plasma Deposition Processes and their Applications 1987). Cathode spots are of the order of 10^{-6} m in size and possess current densities as high as 10 A/μm^2 (Daalder, Random Walk of Cathode Arc Spots in Vacuum 1983). The mechanism responsible for generating a plasma of the target material is the random movement of the cathode spots, with speeds of the order 10^2 m/s (Daalder, Random Walk of Cathode Arc Spots in Vacuum 1983) (Davis and Miller 1969). Typical voltages supplied to the arcs range from 15-50V depending on the metal, semiconductor, or insulator target material. Arc currents range from 30-400A (Randhawa and Johnson, Technical Note: A Review of Cathodic Arc Plasma Deposition Processes and their Applications 1987).

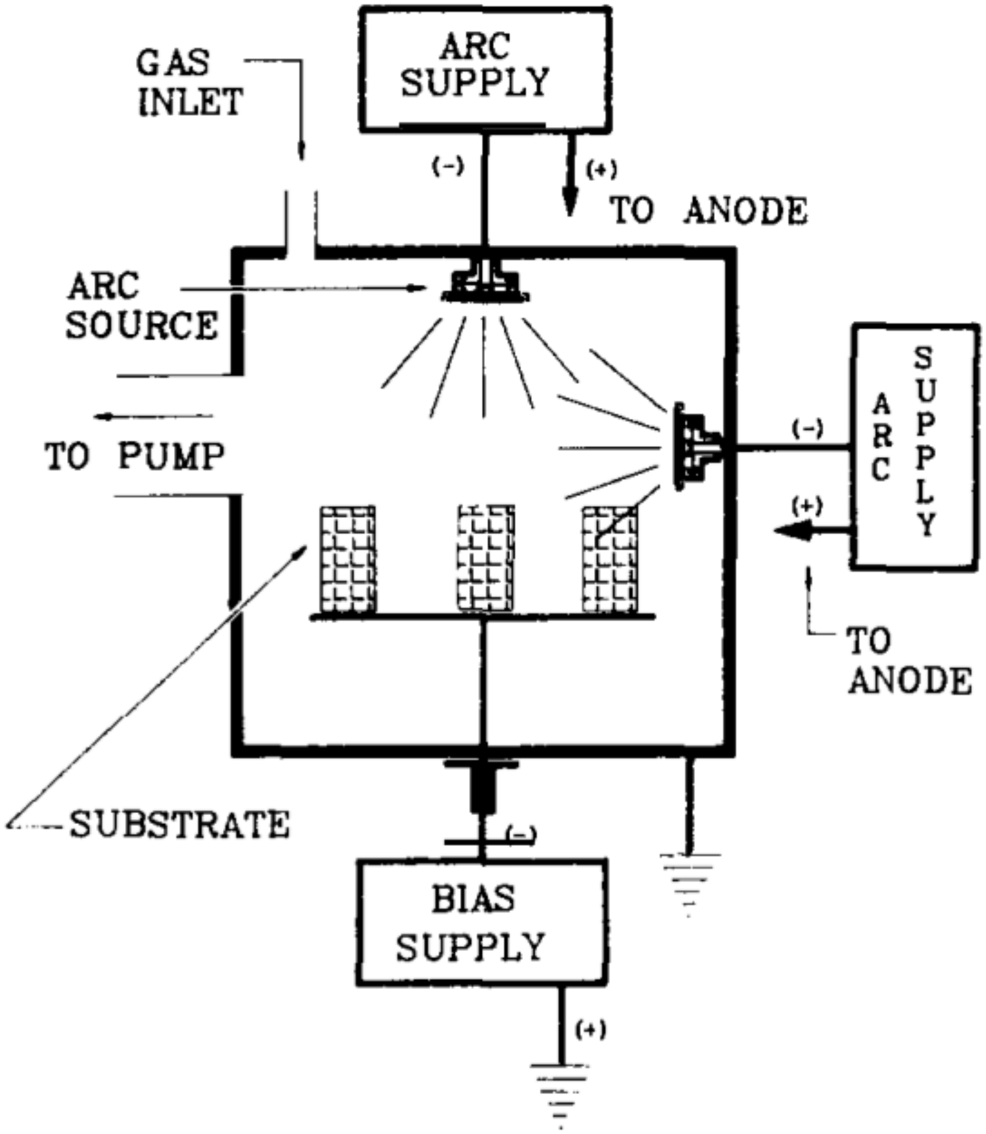

FIGURE 1-2. Schematic of the cathodic arc PVD process (Randhawa and Johnson, Technical Note: A Review of Cathodic Arc Plasma Deposition Processes and their Applications 1987, with permission).

Cathodic arc PVD systems can produce uniform coatings that maintain consistent thickness across the surface of the substrate. Superior quality coatings can be achieved due to the system's high deposition rate and low substrate temperatures (Randhawa and

Johnson, Technical Note: A Review of Cathodic Arc Plasma Deposition Processes and their Applications 1987) (Mattox, Fundamentals of Ion Plating 1973) (Andreev, et al. 1982). TiN coatings can be produced over a wide range of values for different system parameters and still maintain excellent film uniformity without affecting the stoichiometry of the TiN material. For example, varying the mass flow of nitrogen would still produce TiN coatings with correct stoichiometry, evident by its characteristic gold colour (Randhawa and Johnson, Technical Note: A Review of Cathodic Arc Plasma Deposition Processes and their Applications 1987).

Several characteristic mechanisms contribute to the high quality coating produced by cathodic arc PVD systems. Typically, 30 to 100% of evaporated target material is ionized (Kimblin 1974) (Tuma, Chen and Davies 1978) (Miller 1979) due to higher kinetic energies, resulting in a highly reactive plasma. These high amounts of ionized particles contain various charged states of the target material, including Ti, Ti^{+}, and Ti^{2+} (Davis and Miller 1969) (Lunev, Padalkaand and Khoroshikh 1977). H. Randhawa et al. suggests a high degree of ionization is directly related to the overall performance of hard coatings. In addition to the large number of ionized particles during deposition, high kinetic energies of ions establish a gradient substrate-coating interface or layer-layer interface. As a result, the degree of adhesion and coating density are improved while significantly reducing surface stresses (Randhawa and Johnson, Technical Note: A Review of Cathodic Arc Plasma Deposition Processes and their Applications 1987). Kinetic energies of ions in cathodic arc PVD processes range from 10-100 eV (Kimblin 1974) (Miller 1979) (Daalder, Cathode Spots and Vacuum Arcs 1981). The combination of high ionization within the plasma and the high kinetic energies of these ions results in high ionization efficiency, described as the ratio of ions reaching the surface of the substrate to the total number of atoms reaching the surface of the substrate per unit area. The cathodic arc PVD process proves to be the leading method of physical vapour deposition with ionization efficiency ranging from 30-50%, much higher than other PVD processes. For example, ion plating, magnetron sputtering and activated reactive evaporation methods exhibit ionization efficiencies ranging from 2-8% (Randhawa and Johnson, Technical Note: A Review of Cathodic Arc Plasma Deposition Processes and their Applications 1987).

1.2.3 Sputtering

Sputter deposition is a process that utilizes the concept of momentum transfer to remove ions from a target material and deposit them onto the desired substrate. Particles of atomic size, frequently gas ions, are propelled towards the target and bombard the surface with a high enough kinetic energy to physically eject the target atoms, causing vapourization of the material, instead of thermal vapourization from a hot source. Sputtering may be performed under vacuum conditions using an ion beam or low-pressure plasma, typically less than 5 mTorr (Mattox, Handbook of Physical Vapor Deposition (PVD) Processing 2010).

1.2.4 Evaporation

A common method of PVD is known as evaporation deposition. The process begins by thermally evaporating the source material to its gas phase within a vacuum. Typical vacuum pressures for this process range from 10^{-5}-10^{-9} Torr. The evaporated material is then projected directly toward the substrate where it condenses back to its solid form. Evaporation is known to produce relatively pure, uniform coatings because a high vacuum environment is achieved prior to the start of the process. As a result, a majority of potential contaminants is eliminated, allowing for the material to condense evenly throughout the substrate surface. However, since the material is propelled from one direction, the evaporated material would deposit non-uniformly on a substrate with considerably rough surface (Mattox, Handbook of Physical Vapor Deposition (PVD) Processing 2010).

1.3 Adhesion Properties

In order to develop high quality coatings, it is important to establish strong adhesion between the coating and the substrate. In our work, coatings are deposited onto stainless steel by layers. Transition layers are of high priority because they are responsible for the adhesion properties of the surface coating. It is important to consider using materials that demonstrate strong bonding to both the stainless steel substrate and the top layer of the coating. For example, titanium nitride and titanium carbide are both very common materials used in decorative coatings on stainless steel. Titanium nitride exhibits a gold colour, while titanium carbide exhibits a metallic black colour. In order for the titanium nitride and titanium carbide coatings to adhere onto the stainless steel, a gradient interlayer, produced through pure titanium ion bombardment and deposition, is strongly recommended. It is also extremely important to consider the thickness of the coatings, as thicker coatings exhibit greater compressive stress. If the compressive stress exceeds a certain threshold, the coating is much more likely to chip off, exposing the stainless steel substrate (Tuffy, Byrne and Dowling 2004). Thus, it is crucial to reduce surface stress to a minimum when depositing the coatings onto the stainless steel substrate.

M. Higgins et al. conducted depositions onto stainless steel using a CVD system. They coated test coupons of stainless steel with Silcolloy® amorphous silicon (a-Si) coating at 400°C and Dursan® carbosilane (CSi) coating at 450°C and tested adhesion properties as well as corrosion resistant and hydrophobic properties of the coatings. They used Auger Electron Spectrometry (AES) for depth profiling of the coatings. This method allowed the determination of the thickness of the coatings and, displayed evidence of adhesion due to the overlap between the precursor and the iron in the stainless steel, as well as confirmed the precursor materials used during depositions.

Figure 1-3 is a plot of AES depth profiling for stainless steel coated with amorphous silicon. It is also important to note that the overlap between silicon and iron in the stainless steel shows that the silicon is diffused into the surface of stainless steel. This proves that bonding of the coating to the surface of the stainless steel enhanced the adhesion properties of the coating. This area is known as the diffusion zone. From the plot shown in **Figure 1-3**, it was observed that the thickness of the a-Si coating was approximately 2000A, equivalent to 200 nm. The thickness of the diffusion zone between silicon and iron was approximately 500A, from 2000A to 2500A, showing adhesion due to bonding between the a-Si coating and the stainless steel surface.

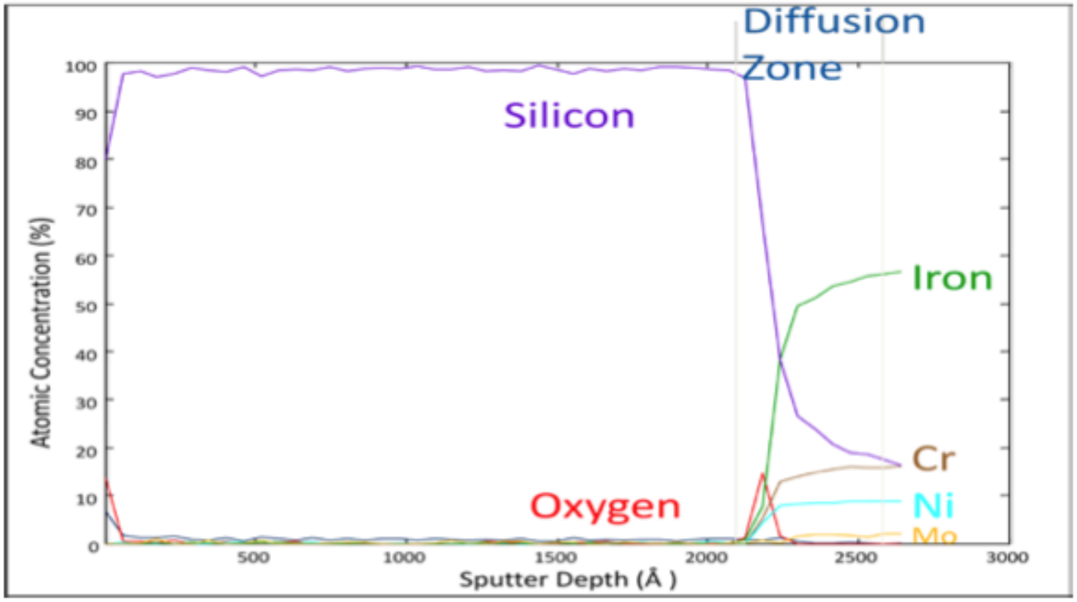

Figure 1-3. AES profile of Silcolloy® coated stainless steel (Higgins, et al. 2010, with permission).

Figure 1-4 is a plot of AES depth profiling for stainless steel coated with carbosilane. It was confirmed that carbon and silicon were present in the precursor. It was also observed that the thickness of the carbosilane coating is approximately 1200A, equivalent to 120 nm. The thickness of the diffusion zone between silicon and iron was approximately 40 nm, showing adhesion due to bonding between the carbosilane coating and the stainless steel surface (Higgins, et al. 2010).

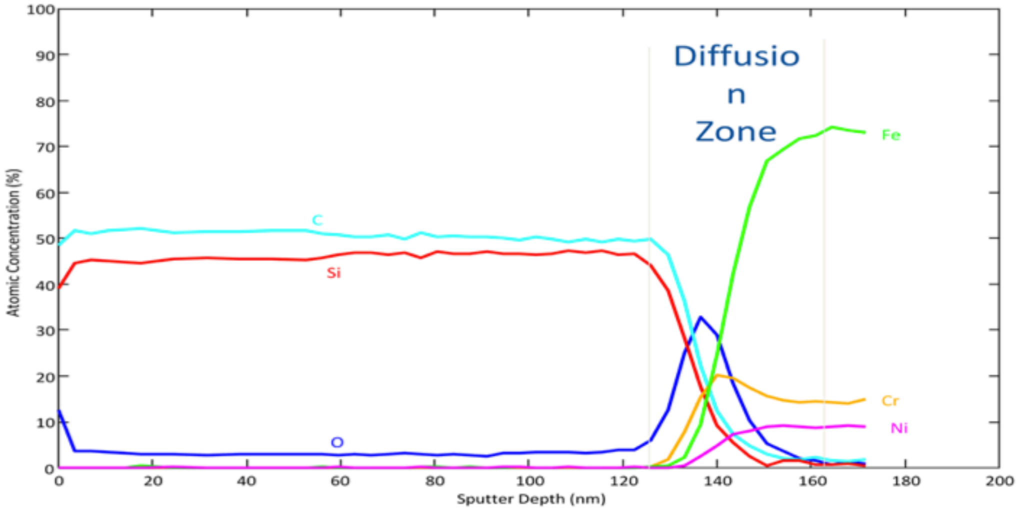

Figure 1-4. AES depth profile of Dursan® coated stainless steel (Higgins, et al. 2010, with permission).

Physical Properties and Experimental Results from Literature

M. Higgins et al. performed comparative testing of both a-Si and carbosilane coated stainless steel using various testing procedures established by the American Society for Testing and Materials (ASTM).

The ASTM G31 acid test on a stainless steel control, stainless steel coated with a-Si, as well as stainless steel coated with carbosilane required the stainless steel coupons to be exposed to 6M hydrochloric acid at 22 °C for 24 hours. The results of this test are show in **Table 1-1**, where mils per year (MPY) is a unit equivalent to approximately one thousandth of an inch. As expected, the stainless steel control demonstrated the most material loss compared to coated stainless steel, with a loss of 91.9 MPY. a-Si coated stainless steel showed an enhancement in acid resistance with a loss of 18.42 MPY, but ultimately the carbosilane coated stainless steel proved superior with a loss of only 3.29 MPY – a 27.9X enhancement over the stainless steel control (Higgins, et al. 2010).

Table 1-1. Results from comparative corrosion testing for unprotected stainless steel, stainless steel coated with a-Si, and stainless steel coated with carbosilane using immersion in 6M HCl for 24 hours at 22 °C (Higgins, et al. 2010, with permission).

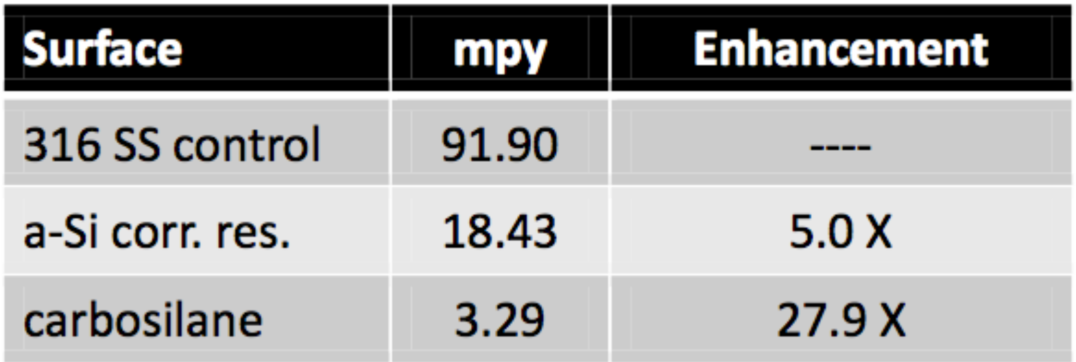

Surface	mpy	Enhancement
316 SS control	91.90	----
a-Si corr. res.	18.43	5.0 X
carbosilane	3.29	27.9 X

A comparative salt spray test was also conducted on a stainless steel control and a-Si coated stainless steel using the ASTM B117 testing method. The samples were placed in a salt spray apparatus where a sodium chloride salt solution fogged up the samples for a total of 4000 hours (Higgins, et al. 2010). Photographs of the samples after the salt spray test are shown in **Figure 1-5**. By visual observation, it was evident that the stainless steel control showed some sign of rusting while the a-Si coated stainless steel sample showed no sign of rusting or damage from the salt spray solution.

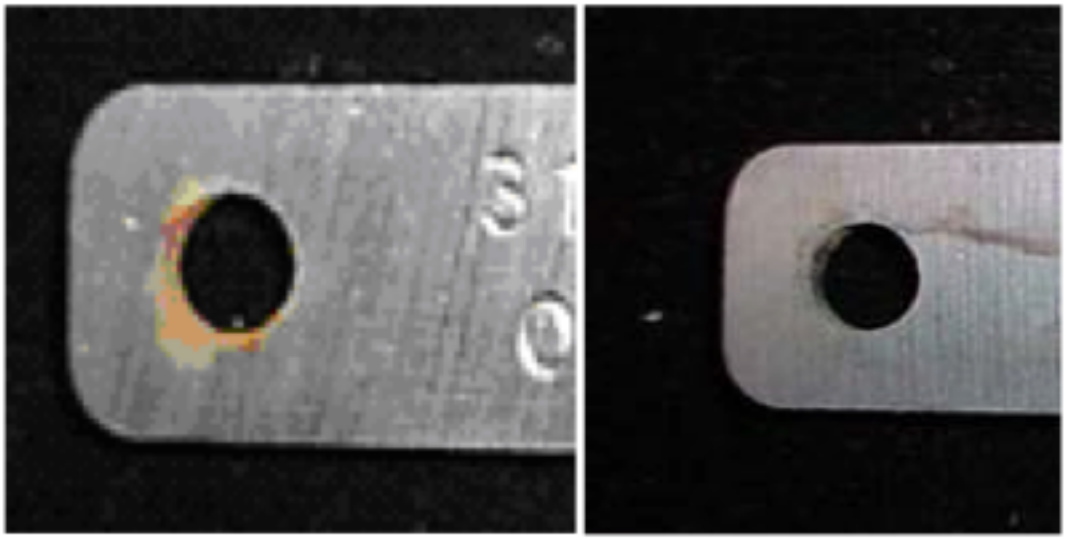

Figure 1-5. Images showing the results from 4000 hour salt spray test for unprotected stainless steel (left) and stainless steel coated with a-Si (right) (Higgins, et al. 2010, with permission).

M. Higgins et al. also performed comparative testing of the hydrophobicity of stainless steel surfaces, both uncoated and coated with a-Si or carbosilane. They observed advancing and receding contact angles on these surfaces. The results are tabulated in **Table 1-2**.

A stainless steel control was used for comparison. The stainless steel control demonstrated an advancing contact angle of 37.2° and a receding angle of 0° (Higgins, et al. 2010), meaning that the liquid dispersed completely over the stainless steel surface. Thus, the stainless steel control exhibited no hydrophobic properties. Stainless steel coated with a-Si demonstrated an advancing contact angle of 53.6° and a receding angle of 19.6°. It was concluded that stainless steel coated with a-Si demonstrated an enhancement in hydrophobicity of its surface. In comparison to a-Si coating, stainless steel coated with carbosilane showed an advancing contact angle of 100.5° and a receding angle of 63.5° (Higgins, et al. 2010), displaying a relatively distinct droplet on the surface. Stainless steel coated with carbosilane proved superior because it greatly enhanced hydrophobic properties over the uncoated and a-Si coated stainless steels.

Table 1-2. Advancing and receding angles for stainless steel control (unprotected), stainless steel coated with a-Si, and stainless steel coated with carbosilane (Higgins, et al. 2010).

Surface	**Advancing Angle (Degrees)**	**Receding Angle (Degrees)**
a-Silicon	53.6	19.6
Carbosilane	100.5	63.5
316 Stainless Steel	37.2	0

Figure 1-6 shows a visual comparison of water droplets on hydrophobic carbosilane-coated stainless steel (left, middle) and uncoated stainless steel control showing hydrophilic properties (right) (Higgins, et al. 2010). It is evident that the hydrophobicity of the coated stainless steel leads to the formation of a liquid droplet on the surface while liquids disperse over the surface of the stainless steel control since it does not demonstrate any hydrophobic properties.

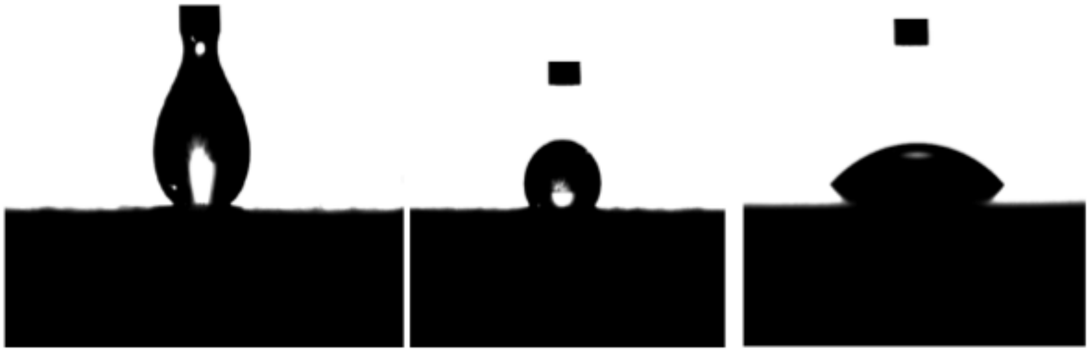

Figure 1-6. Visual comparison of water droplets on hydrophobic carbosilane-coated stainless steel (left, middle) and uncoated stainless steel control showing hydrophilic properties (right) (Higgins, et al. 2010, with permission).

D. Merl et al. investigated the protective properties against material deterioration for stainless steel disc substrates coated with nitride based hard coatings (TiAgN and TiSiN) using a Sputron system with plasma beam sputtering for deposition. The radii of the stainless steel disc substrates were 25nm while the thickness of the TiAgN and TiSiN coatings were 1.9 μm and 1.6 μm respectively. A 100 nm layer of titanium was used as a transition layer to adhere the protective coatings onto the stainless steel substrate. During deposition, the pressure of the vacuum chamber remained at 2 mPa with the flow of the nitrogen precursor set at 5 sccm. The temperature during deposition did not exceed 130°C and the bias voltage was set to -30V (Merl, et al. 2013).

Tribo-corrosion analysis was performed using a CSM tribometer apparatus with a pin-on-disc structure that is represented by the schematic shown in **Figure 1-7** (Merl, et al. 2013).

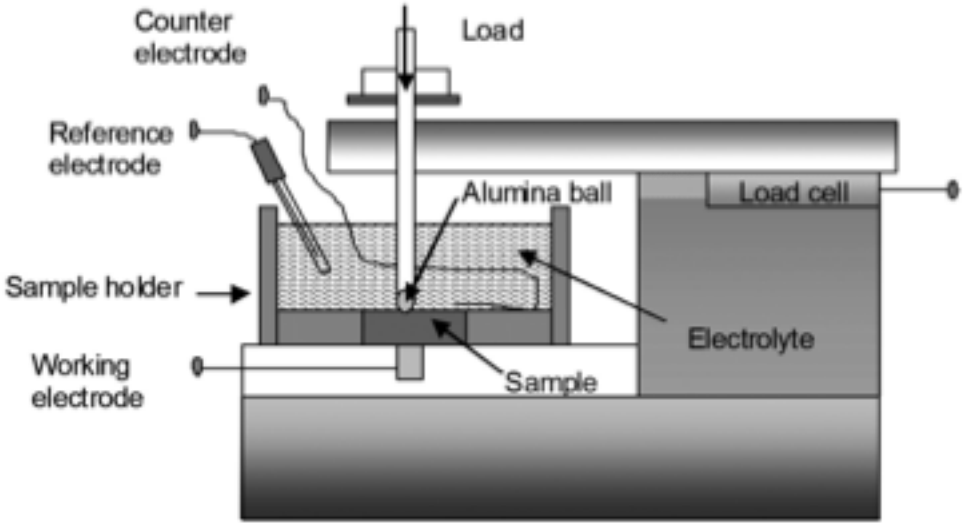

Figure 1-7. CSM tribometer apparatus with a pin-on-disc structure (Merl, et al. 2013, with permission).

Tribo-corrosion experiments focus on the investigation of both tribological properties as well as corrosion resistant properties of materials and substrates containing protective coatings (Celis, Ponthiaux and Wenger 2006) (Ponthiaux, et al. 2004). The coated and uncoated stainless steel samples were utilized as electrodes while the counter electrode was a platinum wire. The electrolyte used during the experiments was a solution that simulates fluids found within the human body, known as Hank's Solution. The composition of Hank's Solution can be found in **Table 1-3** (Merl, et al. 2013).

Table 1-3. Composition of Hank's Solution (Merl, et al. 2013).

Component	**Amount (g/L)**
NaCl	8
Na_2HPO_4	0.0475
$NaHCO_3$	0.35
KCl	0.5
KH_2PO_4	0.06
$MgCl_2.6H_2O$	0.1
$MgSO_4.7H_{2O}$	0.1
$CaCl_2$	0.18
Glucose (pH = 7.2)	1

In order to mathematically model the total loss of mass due to wear and corrosion, the basic relation begins with the simple assumption that the total loss of mass is equivalent to the sum of the loss of mass from mechanical wear and loss of mass from corrosion separately. Realistically, when corrosion and mechanical wear interact within the same system, they may cause a greater loss than if these interactions were isolated from one another. This is because corrosive effects may alter the behavior of the substrate, but also the behavior of the substrate may change due to mechanical wear on the material. Thus synergistic effects must be considered in addition to the isolated losses, as represented in **Equation (1-1)**.

$$M_{total} = M_{mechanical} + M_{corrosion} + M_{synergy} \qquad \textbf{(1-1)}$$

where M_{total} is the total material loss by mass, $M_{mechanical}$ is the loss of mass due to mechanical wear only, $M_{corrosion}$ is the loss of mass due to corrosion impact only, and

$M_{synergy}$ is the loss of mass due to both loss factors interacting together during the tribo-corrosion testing. $M_{synergy}$ may also be represented by **Equation (1-2)**.

$$M_{synergy} = M_{M\text{-}C} + M_{C\text{-}M} \qquad \textbf{(1-2)}$$

where variable $M_{M\text{-}C}$ takes into account loss of mass when mechanical wear is influencing corrosion and variable $M_{C\text{-}M}$ considers the loss of mass when corrosion is influencing mechanical wear. Therefore, **Equation (1-1)** becomes (Merl, et al. 2013):

$$M_{total} = M_{mechanical} + M_{corrosion} + M_{M\text{-}C} + M_{C\text{-}M} \qquad \textbf{(1-3)}$$

Tribo-corrosion testing conducted by D. Merl et al. involves running an aluminum ball along a circular track on the surface of the sample discs and observing mechanical wear and corrosion effects within the system before, during and after the rotations. First, the corrosion potential was measured. The results of this test may be found in **Figure 1-8**. A drop in potential was observed for all samples during rotation. The reason for this is assumed to be rust forming due to the electrolyte and being removed by the aluminum ball from mechanical wear. It can be noted that the unprotected stainless steel sample experienced the largest drop in corrosion potential. This observation can be explained by the fact that the unprotected stainless steel had undergone the most corrosion, thus producing much more oxide on the surface of the sample. Both the TiSiN and TiAgN coatings led to a smaller drop in corrosion potential during rotation of the discs. The increase in corrosion potential of all samples after rotation had stopped suggests that the sample began to reestablish an oxide layer due to rusting from the electrolyte (Merl, et al. 2013).

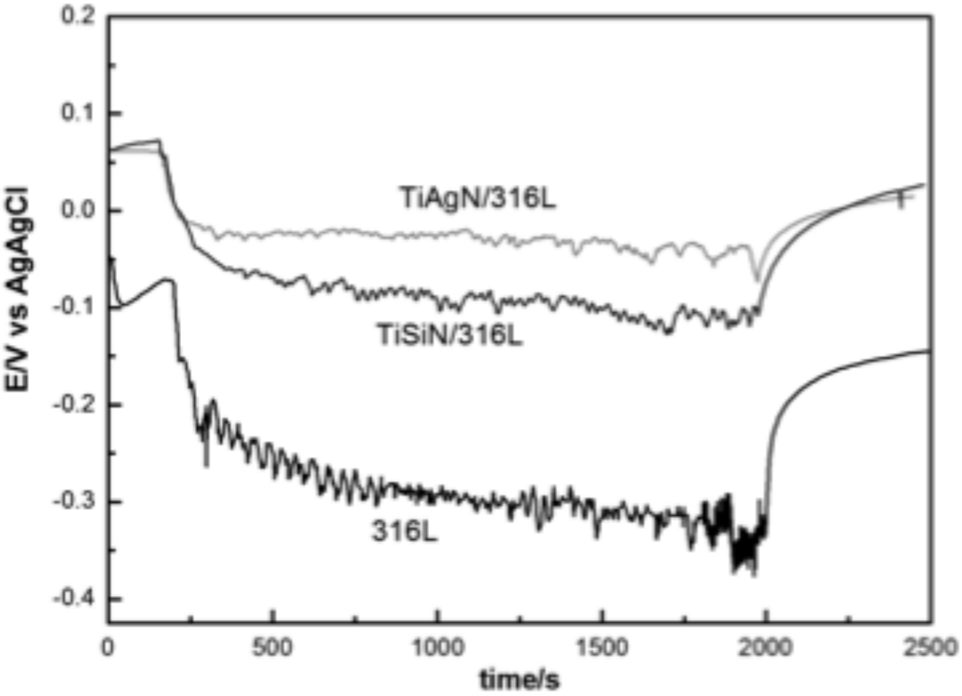

Figure 1-8. Corrosion potential before, during, and after disc rotations for unprotected stainless steel, stainless steel coated with TiSiN, and stainless steel coated with TiAgN (Merl, et al. 2013, with permission).

Post tribo-corrosion testing, the tracks of the aluminum ball along the sample surfaces were analyzed using depth profiling. These results may be found in **Figures 1-9** and **1-10**. It was observed that the unprotected sample of stainless steel suffered the most physical damage to the surface, depicted in **Figure 1-9** by showing that the unprotected stainless steel exhibited the deepest scratch depth. Both the TiSiN and TiAgN coatings led to an enhancement in terms of protection from mechanical wear in the presence of a corrosive environment, but ultimately the TiAgN coating proved superior as indicated by its shallow scratch depth shown in **Figure 1-10** and its smallest drop in corrosion potential shown in **Figure 1-8** (Merl, et al. 2013).

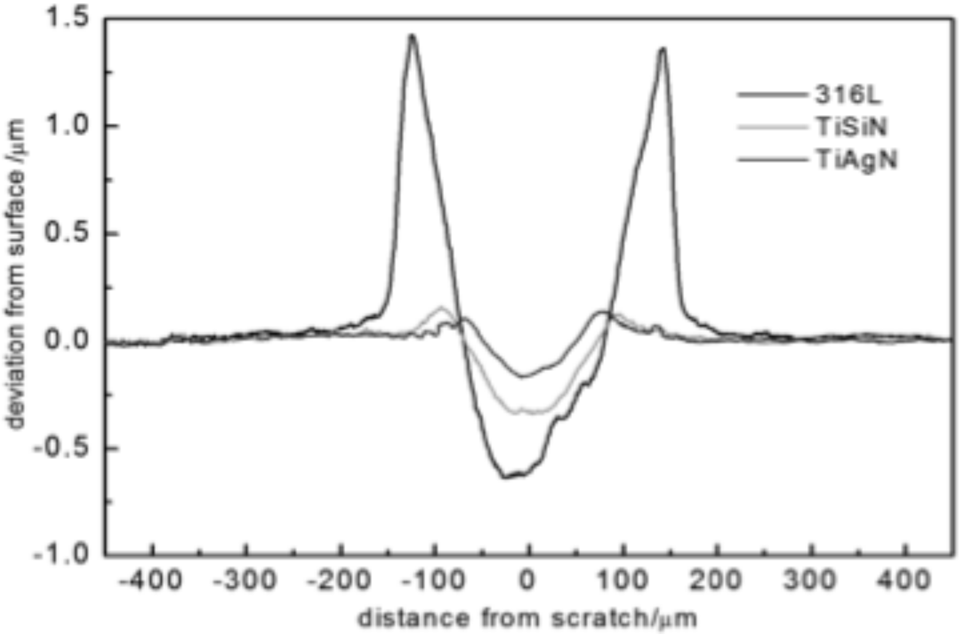

Figure 1-9. Depth profiling of wear track for unprotected stainless steel, stainless steel coated with TiSiN, and stainless steel coated with TiAgN (Merl, et al. 2013, with permission).

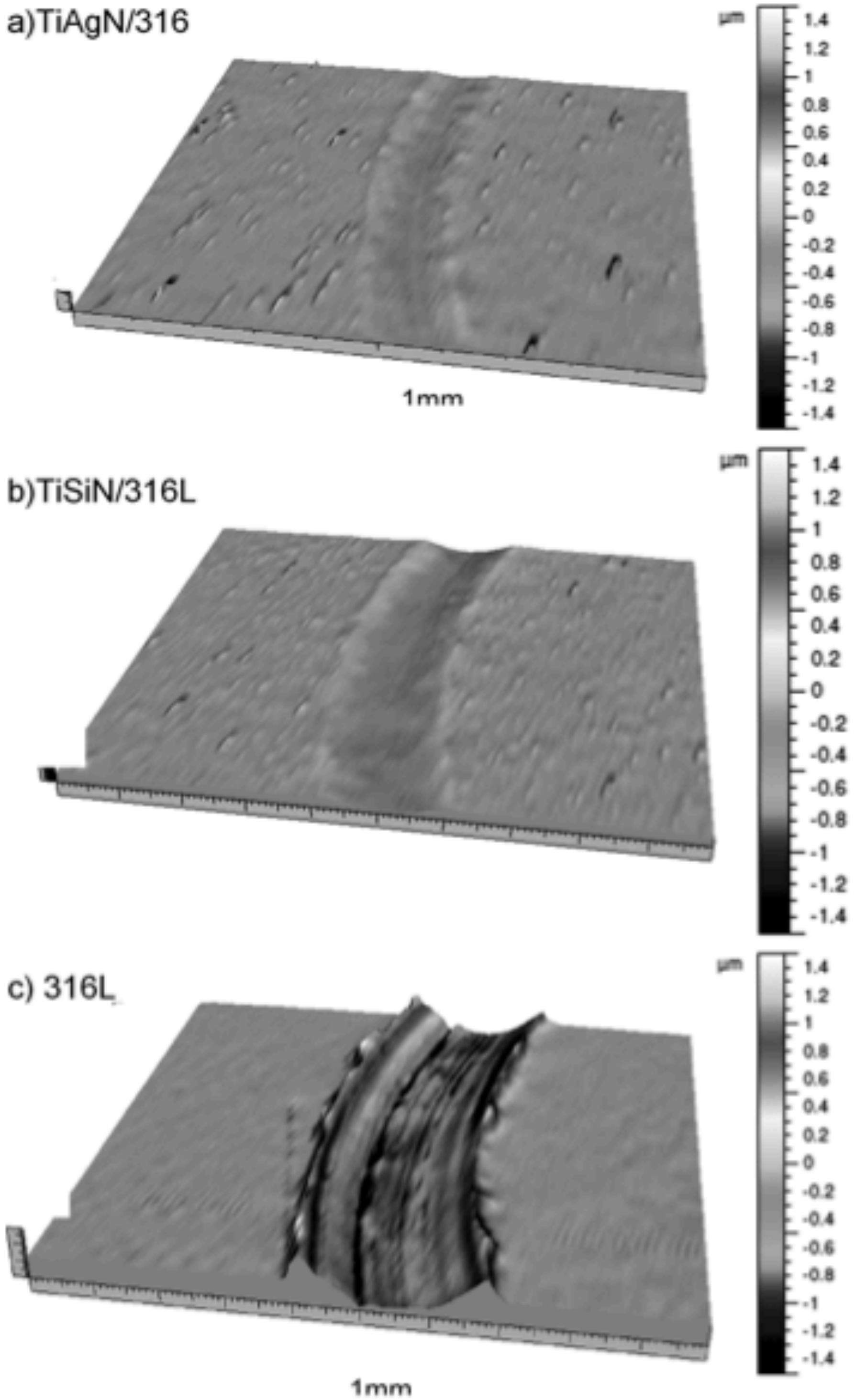

Figure 1-10. 3D micrographs of wear tracks for unprotected stainless steel, stainless steel coated with TiSiN, and stainless steel coated with TiAgN (Merl, et al. 2013, with permission).

1.4 Advantages and Disadvantages of Decorative and Protective Coatings on Stainless Steel

Decorative coatings increase aesthetics of the stainless steel product, by offering many colour options as well as the option of matte or mirror finishes. This comes as a major advantage to the consumer market. For example, when considering the retail market for jewelry and watches, offering a larger selection of colours may bring in more potential customers. For example, rose gold has become very popular within the recent years. Functional coatings can alter the properties of stainless steel in many ways. Scratch resistant coatings enhance durability of the stainless steel product. For example, an abrasion resistant watch would be highly desirable to a potential customer since watches are worn frequently and can be easily scratched from regular wear if not protected. Enhancements in hydrophobic and oleophobic properties establish easy to clean surfaces. This could be beneficial when marketing a product such as a stainless steel dishwasher or refrigerator as fingerprints easily show on unprotected stainless steel surfaces. This property would save time and money spent on cleaning with specific stainless steel cleaning products. Similarly, hydrophobic properties of thin films reduce corrosion of the stainless steel products (Higgins, et al. 2010). Low friction coatings would also be an excellent direction for research as they can be applied to a wide range of industries, especially automotive and aeronautical industries, and would greatly contribute to performance optimization in mechanical function.

Disadvantages of decorative and protective coatings include expensive production costs, depending on the material being used for deposition or maintenance of the deposition process (Higgins, et al. 2010). Deposition time is also an important factor to consider. Long deposition durations would mean slower production, resulting in a lower profit margin.

1.5 Cost Analysis

One of the major advantages of protective coatings is that they significantly decrease the overall lifetime costs of the stainless steel product. While high performance alloys minimize the degree of corrosion, initial production costs are very high in comparison to stainless steel. Stainless steel has low initial production costs but increased lifetime expenses from maintenance and repairs due to damage from mechanical wear, corrosion, as well as other factors that may affect the appearance and performance of the product. Coating the stainless steel with a protective chemical layer proved to enhance several mechanical properties, such as corrosion resistance (Higgins, et al. 2010) (Merl, et al. 2013), hydrophobic and oleophobic behaviour, and resistance against damage from mechanical wear (Merl, et al. 2013), proving that protective coatings on stainless steel are advantageous in marine applications where corrosion is significantly accelerated. Protective coatings on stainless steel are extremely cost effective because they contribute to a significant reduction in overall lifetime expenses (Higgins, et al. 2010). **Figure 1-11** shows an approximated overall cost comparison of high performance alloys, unprotected stainless steel, and coated stainless steel in corrosion prone applications. The expense approximation includes initial manufacturing and lifetime maintenance costs (Higgins, et al. 2010). It is evident that coated stainless steel products demonstrate a significant decrease of hundreds of thousands of dollars in lifetime expenses.

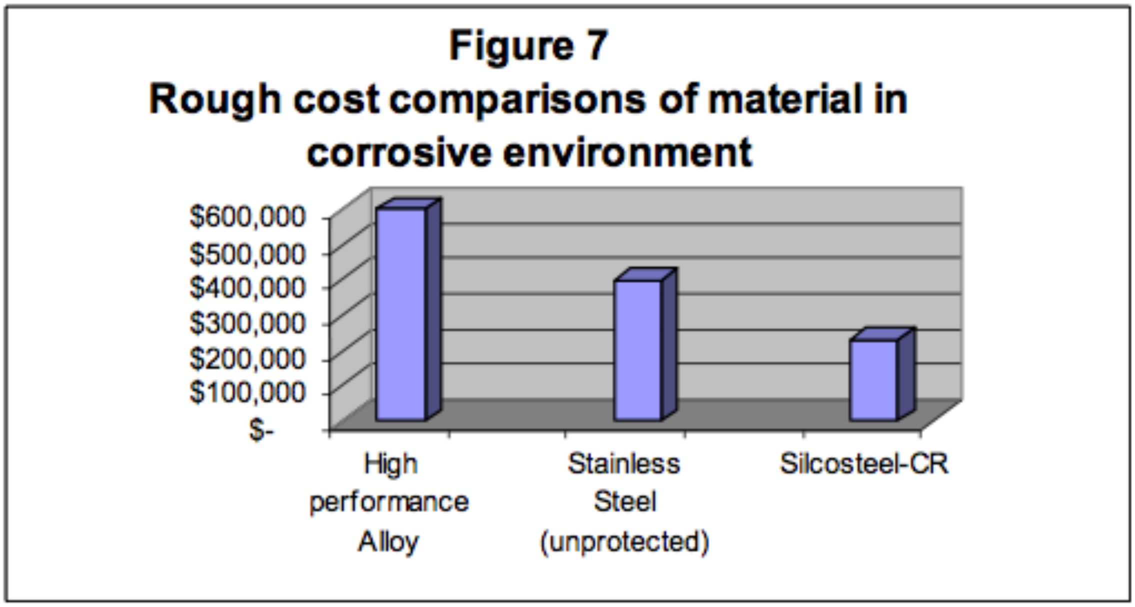

Figure 1-11. Comparative costs of different materials used in corrosion prone applications (Higgins, et al. 2010).

2 Theory

2.1 Argon Plasma Cleaning

Plasma cleaning is a key concept in this research. A bias voltage is responsible for accelerating argon ions towards the substrate. Voltage and ion acceleration have a directly proportional relationship, where the higher the bias voltage, the greater the acceleration of the argon ions. It is extremely important that the surface of the substrate be very clean prior to deposition. External cleaning of the surface cannot, however, guarantee absolute cleanliness of the substrate as there may be left over residue or oxides on the surface as samples are being loaded into the chamber. By using the most effective voltage, argon ions are accelerated towards the target substrate, breaking up any macroparticles on the surface, and thus, providing effective cleaning of the substrate prior to TiN deposition (Laing, et al. 1999).

2.2 Ion Bombardment and the Ti Interlayer

Once argon plasma cleaning has been completed, it is important to produce a gradient of titanium between the stainless steel substrate and the TiN layer. The goal is to increase adhesion of the TiN coatings by using argon plasma cleaning, ion bombardment, and ion implantation processes in combination. Ion implantation can change the surface composition of the substrate. Creating a titanium interlayer between the TiN coating and the stainless steel substrate is believed to have great benefits in the overall adhesion of the coating. For this project, titanium ions were used to create a graded interface between the stainless steel substrate and the TiN coating. Titanium ions bombard the surface of the stainless steel substrate through the use of a high voltage. As a result, atoms from the stainless steel are knocked out of place and titanium ions are implanted within the surface. Ti deposition is run for a short amount of time in order to form a thin film of titanium only, prior to introducing nitrogen. This method establishes stronger adhesion of the TiN coating based on bonding between the Ti interlayer and the stainless steel substrate as well as between the Ti interlayer and the TiN layer (Quaeyhaegens, et al.

1991). C. C. Cheng et al. suggested that establishing a Ti interlayer significantly reduces internal stresses due to the change in orientation of the outer TiN layer (Cheng, Erdemir and Fenske 1989).

3 Experimentation

3.1 Substrate Cleaning

Clean substrate surface conditions are important for producing high quality coatings. Surface contaminants can greatly affect adhesion and uniformity of the TiN coating. Such contaminants may be present throughout the surface of the substrate as a form of oxide or present on limited areas as oil residue from fingerprints or dust particles from the air. Substrate pretreatment reduces the amount of surface residue prior to coating deposition. The goal of this is to optimize coating adhesion and uniformity. Recontamination may occur on the substrate after pretreatment, but before the deposition process begins. Particles from the air or chamber walls may redeposit onto the substrate during sample transfer. For this reason, it is important to ensure thorough surface cleaning of the substrate by performing both external (performed outside the deposition system) and internal (performed within the deposition system) cleaning procedures. Internal cleaning procedures may require introducing several cleaning steps such as ion bombardment and thermal vaporization of contaminants by maintaining high temperatures within the chamber (Mattox, Handbook of Physical Vapor Deposition (PVD) Processing 2010).

Initially, TiN films were deposited onto stainless steel substrates that were laser cut into 25 mm by 25 mm squares. Two cleaning methods were used on the initial set of samples and compared to determine whether external cleaning of the substrates would improve coating adhesion. The first cleaning method is one utilized in-house at Steelforme Design Inc. The Steelforme cleaning method cleans the substrates ultrasonically and rinses them repeatedly with deionized (DI) water and alcohol. Lastly, the substrates are dried with a cotton cloth.

Steelforme Cleaning Method:

NOTE: All steps were performed while wearing gloves.

1. Ultrasonic cleaner for 3 minutes.
2. Rinse with DI water.
3. Rinse again with DI water in a separate container.
4. Rinse with alcohol in a separate container
5. Dry with cotton cloth.

The second cleaning method was performed in a class 10,000 clean room located within the Centre for Emerging Device Technologies (CEDT) at McMaster University. The McMaster cleaning method was established with the purpose of minimizing the possibility of recontamination while thoroughly cleaning the substrate. Instead of beginning with ultrasonic cleaning, the substrates were bathed in isopropanol for 3 minutes and afterwards bathed in methanol for 3 minutes prior to ultrasonic cleaning. The substrates were placed in an ultrasonic cleaner for 10 minutes, flipping the substrate over after 5 minutes. Three separate beakers of DI water were prepared in order to rinse the samples from any residual chemicals that may react with hydrochloric acid (HCl). Next, the stainless steel substrates were bathed in diluted 3.59% HCl for 3 minutes and once again rinsed with DI water, separately four times, to remove any residual acid. Finally, the substrates were dried with nitrogen gas and packaged individually.

McMaster Cleaning Method:

NOTE: All steps were performed under a highly controlled environment in a class 10,000 clean room.

1. 3 minutes in isopropanol.
2. 3 minutes in methanol.
3. Rinse in DI water.
4. Ultrasonic cleaner with DI water – 5 minutes on one side and 5 minutes on the other.
5. Rinse with DI water.
6. Rinse with DI water in separate beaker.
7. Rinse with DI water in separate beaker.
8. HCl (3.59%) for 3 minutes.
9. Rinse with DI water.
10. Rinse with DI water in separate beaker.
11. Rinse with DI water in separate beaker.
12. Rinse with DI water in separate beaker.

13. Dry with flowing nitrogen gas.
14. Package in individual bags.

Separate, individual cleaning parameters were applied to three samples. Sample 20b was only pretreated with ultrasonic cleaning for 3 minutes. Sample 20c was rinsed in alcohol only. Lastly, sample 20d was bathed in water with Comet bleach powder for 3 minutes. All samples were air dried prior to being placed into the chamber. Investigating each cleaning step was important in order to be able to determine the most effective substrate pretreatments. Effectiveness was measured by observing critical loads where coating delamination occurred, indicating the strength of adhesion.

3.2 External Bake

Heating pretreatment prior to coating deposition is essential because it helps to further clean the substrate by evaporating residual water or other particles from the surface. While thermal pretreatment has additional benefits to coating adhesion, it may also negatively affect the resulting thin film by triggering premature tribological failures. For example, overheating the substrate may provoke accelerated oxidization on the surface of the stainless steel (Ikeda and Satoh 1991). This would result in weaker mechanical properties and adhesion of the coating. The effect of thermal pretreatment was investigated in order to achieve stronger adhesion between the TiN coatings and the stainless steel substrates. Initial samples were prepared using Steelforme and McMaster cleaning methods and then placed into a Fisher Scientific, model 650-58, external furnace. The samples were baked prior to deposition using temperatures of 245, 325, and

400 °C for 20 or 40 minutes.

3.3 Instrumentation: Cathodic Arc PVD

All TiN films were deposited using a multi-arc magnetron sputtering coating machine. The system was comprised of five valves, a preceding mechanical pump, a diffusion pump, a holding pump, a roots pump, and the chamber where samples were loaded. The chamber is connected to a preceding mechanical pump, shown in **Figure 3-1**. The mechanical pump is initially run to bring the pressure within the chamber to a low vacuum level of $P = 5.0\text{x}10^2$ Pa in order to improve the quality of vacuum that the diffusion pump can achieve. When the diffusion pump begins operating at a pressure lower than atmosphere, it results in a much lower final pressure, thus creating a high vacuum condition at the end of pump down (Yan, Jianjun and Hongbin 2011). The roots pump assists the preceding mechanical pump achieve a low vacuum pressure of $P = 3\text{x}10^0$ Pa. Utilizing a preceding mechanical pump results in a faster pump down, which decreases the run time of the system, and improves the lifespan of the diffusion pump by lowering the chance of particles from the air to contaminate the oil within the diffusion pump (Mattox, Handbook of Physical Vapor Deposition (PVD) Processing 2010). If a preceding mechanical pump is not used during pump down, the oil within the diffusion pump is required to be changed more frequently, as a result significantly increasing maintenance costs of the system.

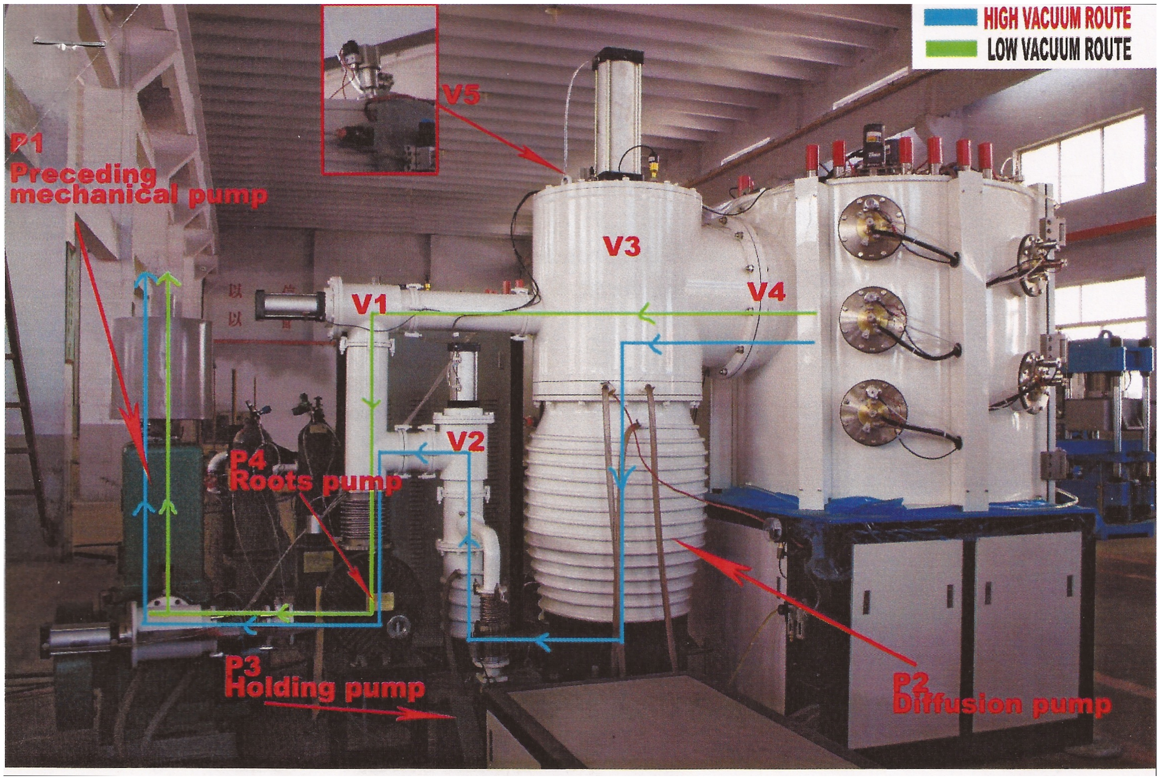

Figure 3-1. Diagram of the multi-arc magnetron sputtering coating system with pumps and valves highlighted. This system is located at Steelforme Design Inc.

The mechanical pump provides the diffusion pump with a low vacuum condition (Mattox, Handbook of Physical Vapor Deposition (PVD) Processing 2010), thus the valves to the mechanical pump must be shut off and the valves to the diffusion pump opened, which enables the diffusion pump to further lower the pressure to a high vacuum condition. Diffusion pumps use the momentum transfer process to achieve a high vacuum. The oil vapours collide with gas particles, transferring momentum from one particle to the other. As a result, the gas particles are accelerated toward the exhaust of the diffusion pump. The diffusion pump operates in order to establish a uniform flow of gas molecules under the influence of pressure differences between high vacuum and atmospheric conditions (Lee and Lee 1996). A schematic diagram of the basic components within a diffusion pump is shown in **Figure 3-2**.

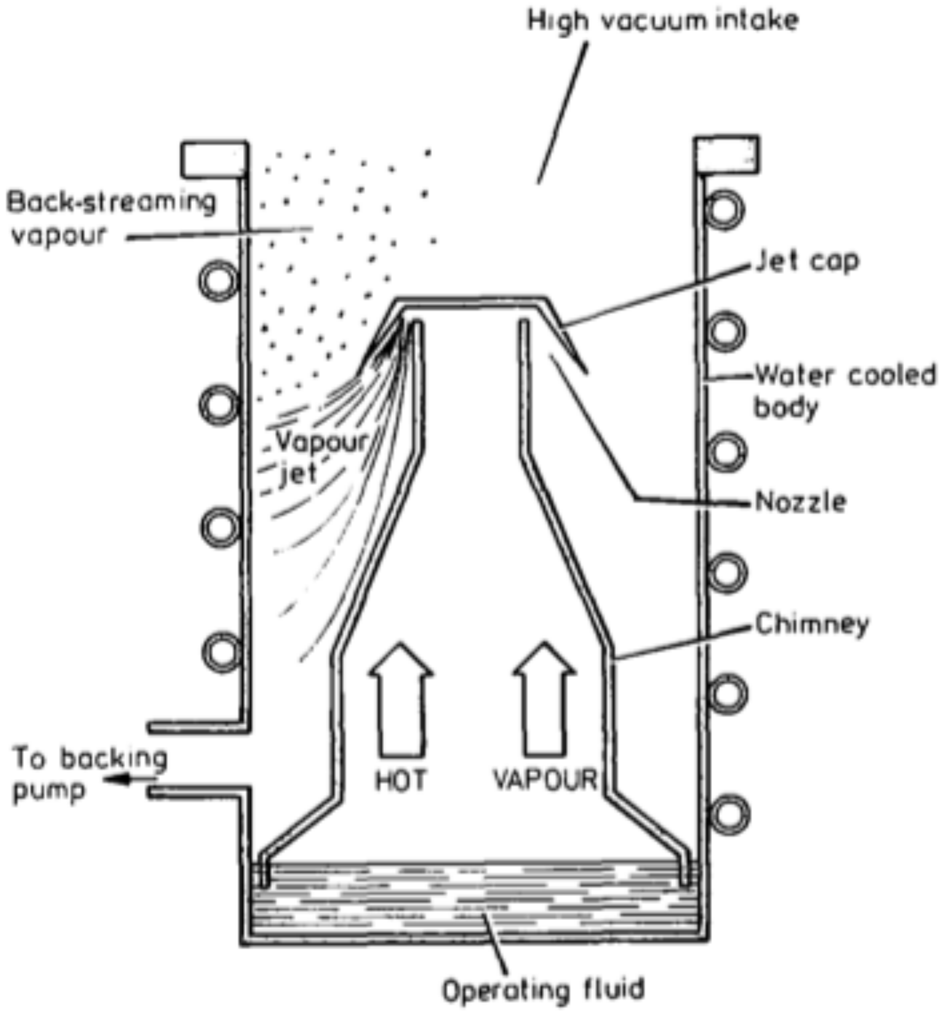

Figure 3-2. Basic elements of a diffusion pump (Harris 1977, with permission)**.**

Oil vapours are commonly used as high velocity media for this process. Oil within the diffusion pump is evaporated through the use of a heated boiler (Lee and Lee 1996). The diffusion pump used in the cathodic arc PVD system was maintained at a temperature of 230°C in order to evaporate the oil within it. The oil vapours then travel through a slit nozzle, accelerating to high velocities, producing a jet stream. Gas molecules enter through the diffusion pump inlet and pass through the stream of oil vapours. The collisions between the gas molecules and oil vapour cause a downward momentum before the oil vapours reach the outer radial walls of the diffusion pump, where they are condensed back to liquid form and return to the boiler located at the bottom of the diffusion pump. The walls of the diffusion pump must be maintained at lower temperatures in order for the oil vapours to condense. This is achieved through cooling, using air or water systems (Lee and Lee 1996). Specific to the cathodic arc PVD used for this project, a water-cooling system was implemented for the diffusion pump walls. The accelerated gas molecules are then removed thorough the use of a mechanical pump.

The jet action of the oil vapour considerably increases transmission probability due to its beaming effects. The density and velocity of the jet stream along with the molecular weight of the oil vapour particles influence the collisions between the oil vapour and gas molecules. Nozzle shape, pump geometries, boiler pressure, and gas density distribution all influence the density and velocity of the jet stream. The overall performance of the diffusion pump is directly related to the efficiency of energy transfer, which is influenced by these important factors. High gas densities impact the overall motion of the collisions between oil vapour and gas molecules, resulting in an altered jet stream due to gas flow. High oil vapour densities significantly decrease the collision efficiency due to ineffective gas penetration into the jet stream. However, low concentrations of oil vapour in the jet stream result in lower collision probabilities. Either extreme proves to be ineffective in terms of energy transfer. Experimental results suggest an optimal boiler pressure within a range of 1-2 Torr. This allowed for the density of the oil vapour to be sparse enough for the gas molecules to effectively penetrate the jet stream (Lee and Lee 1996).

It is important to optimize the pumping ratio, defined as the pressure at inlet versus pressure at outlet. This is achieved by introducing a holding pump at the diffusion pump outlet, shown in **Figure 3-1**. The holding pump is a basic mechanical pump that is only connected to the diffusion pump and not the chamber. It is able to achieve low vacuum conditions from atmospheric pressure. The holding pump functions as a buffer at the outlet, which maintains a low vacuum at the diffusion pump outlet in order for the pumping ratio to be much higher. It is important to maintain a lower pressure at the outlet of the diffusion pump, because this allows for a higher final vacuum pressure of $7.0\text{x}10^{-3}$ Pa to be achieved at the diffusion pump inlet.

It is crucial to achieve high vacuum and elevated temperatures within the chamber due to two major reasons. High vacuum environments minimize any gaseous contaminants within the chamber, thus providing a long mean free path, the average distance traveled between collisions of gas particles, between the target material and the substrate (Mattox, Handbook of Physical Vapor Deposition (PVD) Processing 2010). In addition, setting temperatures above 100°C assures that any water present within the chamber would be evaporated out. High temperatures within the chamber also increase surface mobility of the depositing material on the stainless steel surface. Surface mobility is a measure of how well particles along the surface of the substrate can rearrange. When Ti atoms reach the surface of the substrate, they have some degree of mobility before they react. Mobility of these atoms depends on various factors including the energy of the atoms, chemical bonding, and the temperature of the substrate surface. Maintaining high temperature and vacuum conditions within the chamber results in superior quality uniform coatings because of high surface mobility and film purity of TiN, which results from the reduced amount of contaminants within the chamber (Mattox, Handbook of Physical Vapor Deposition (PVD) Processing 2010).

3.4 Sample Deposition

3.4.1 System Start Up

To start up the system, it is important to ensure all valves are closed and the preceding mechanical pump and roots pump are switched off. It is required to switch the holding pump and diffusion pumped on and allow one hour for the diffusion pump to reach an operating temperature of 230°C.

3.4.2 Sample Loading and Chamber Pump Down

The following description refers to system details shown in **Figure 3-1**. To load the samples, valve 5 must be opened to vent the chamber and allow it to reach atmospheric pressure. The holding pump and diffusion pump remain on at this time to maintain its required operating temperature. Once samples are mounted onto the rotating carousel present within the chamber, the system can begin pump down, which begins with the preceding mechanical pump while valves 1 and 4 are opened. Once the chamber reaches a pressure of 5.0×10^{2} Pa, the roots pump is initiated and valves 2 and 3 open when the pressure of the chamber reaches 3.0×10^{0} Pa. Valve 1 automatically closes when valve 2 opens. Plasma cleaning is ready to begin when the chamber pressure reaches 7.0×10^{-3} Pa.

3.4.3 Plasma Cleaning

Before beginning plasma cleaning, the chamber temperature is set to 245°C. Once the chamber temperature reached the desired temperature, valve 4 is closed. The argon line on the mass flow controller is turned on and the pressure within the chamber is maintained between 2.5 and 3.0 Pa while the sample stage is rotating. The bias power supply is switched on, set to high voltage mode, and adjusted to 650 V. Plasma cleaning is run for 5 minutes before the argon line is closed and the bias power supply is switched off. Lastly, valve 4 is opened to allow for the chamber to pump down to 7.0×10^{-3} Pa.

3.4.4 Ion Bombardment

Ion bombardment begins with the chamber temperature maintained at 245°C and valve 4 closed. The bias power supply is switched on, set to high voltage mode and adjusted to values ranging from 300-500V depending on the sample run. The arcs are then switched on and run for the default time of 120 or 300 seconds depending on the sample run.

3.4.5 TiN Deposition

TiN deposition begins with the chamber temperature maintained at 245°C and valve 4 closed. The bias power supply is switched on, set to low voltage mode and adjusted to 70V. The arcs are then switched on and run for 30 seconds in order for the Ti interlayer to be deposited onto the stainless steel substrate. Following the Ti interlayer, the nitrogen gas line is opened and the pressure within the chamber is maintained between 3.0 and 4.0×10^{-1} Pa. TiN deposition is run for 10 minutes. The deposition ends when the power supply for the arcs and the bias power supply are turned off. All gases must be shut off prior to closing valves 4, 3, 2, and 1. Lastly the preceding mechanical pump and roots pump are shut off.

3.4.6 System Shut Down

Prior to system shut down, all valves, the roots pump and preceding mechanical pump are turned off. Next, the diffusion pump is shut off and given an hour to cool down while the holding pump continues to run during this time. After an hour, the holding pump is shut off.

3.5 Scratch Testing

All scratch tests were performed on a Micro Combi Tester (MCT), located in the Functional Coating and Surface Engineering Laboratory at École Polytechnique de Montréal, manufactured by Anton Paar, formerly known as CSM instruments. The MCT is used to mechanically characterize a wide variety of thin films and obtain information about fracture resistance, scratch resistance, adhesion, and hardness of these coatings. The MCT is capable of performing micro indentation, where a diamond tip is pressed with gradually increasing force until a user-defined load has been reached. Once the load is removed, the residual indentation is measured. This functionality is mainly used to determine the hardness of the coating. **Figure 3-3** shows three diamond tips used for mechanical testing: Conical, Berkovich, and Vickers.

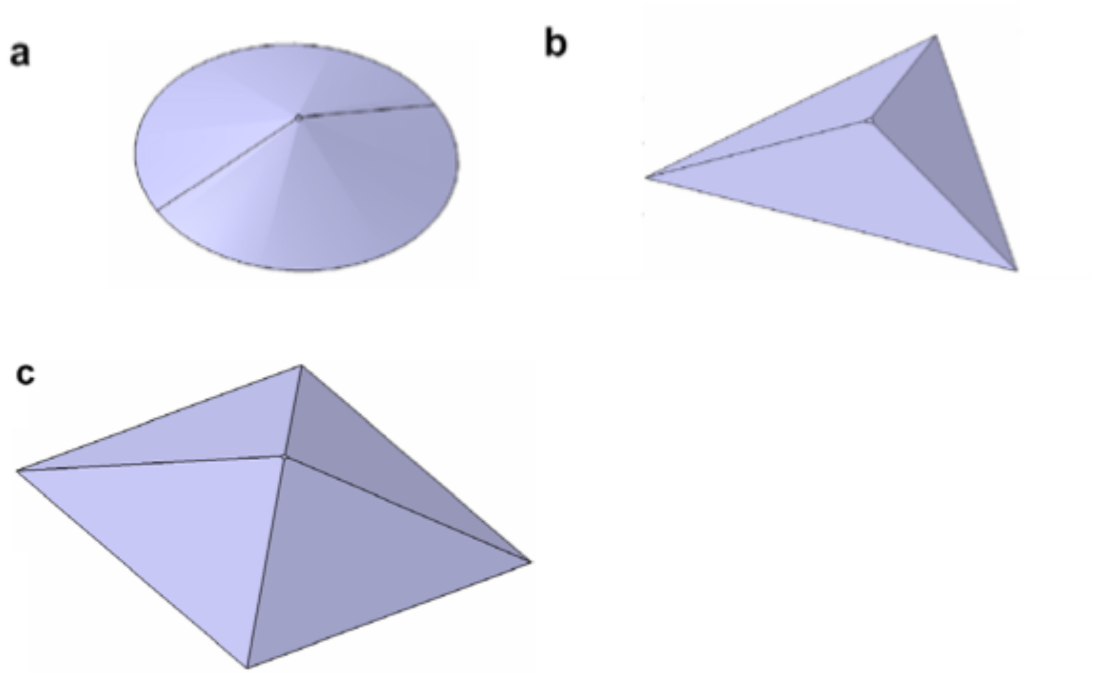

Figure 3-3. Indentation geometries for (a) Conical, (b) Berkovich, and (c) Vickers tips (Sakharova, et al. 2009, with permission).

Berkovich and Vickers are most commonly used for micro indentation in order to determine the hardness of coatings. When a load is applied to a material, this material experiences elastic displacement and some residual deformation. This is accurately described in the load displacement curve for indentation tests shown in **Figure 3-4**. Indentation hardness is determined by calculating the maximum applied load (F_L) divided by the projected contact area (A_p):

$$H = \frac{F_L}{A_p}$$

The Berkovich tip is most commonly used for indentation testing. A_p is approximated using the following fitting polynomial for the Berkovich tip geometry:

$$A_p(h_c) = C_0 h_c{}^2 + C_1 h_c + C_2 h_c^{\frac{1}{2}} + C_3 h_c^{\frac{1}{4}} + \ldots$$

where h_c is the contact depth and C_0 is 24.5 for ideal Berkovich geometry.

The area of projected contact angle is a second order function dependent on contact depth. If there are many data points during indentation, more coefficients are required, but if there are too many coefficients, the function begins to model noise and inflection points occur (Xu, et al. 1998). The following equation is used to calculate contact depth:

$$h_c = h_L - \varepsilon \frac{F_L}{S}$$

where h_L is the maximum indentation depth, ε is the error value, F_L is the maximum applied load, and S is the stiffness value. Stiffness is determined from the slope of the unloading curve shown in **Figure 3-4**.

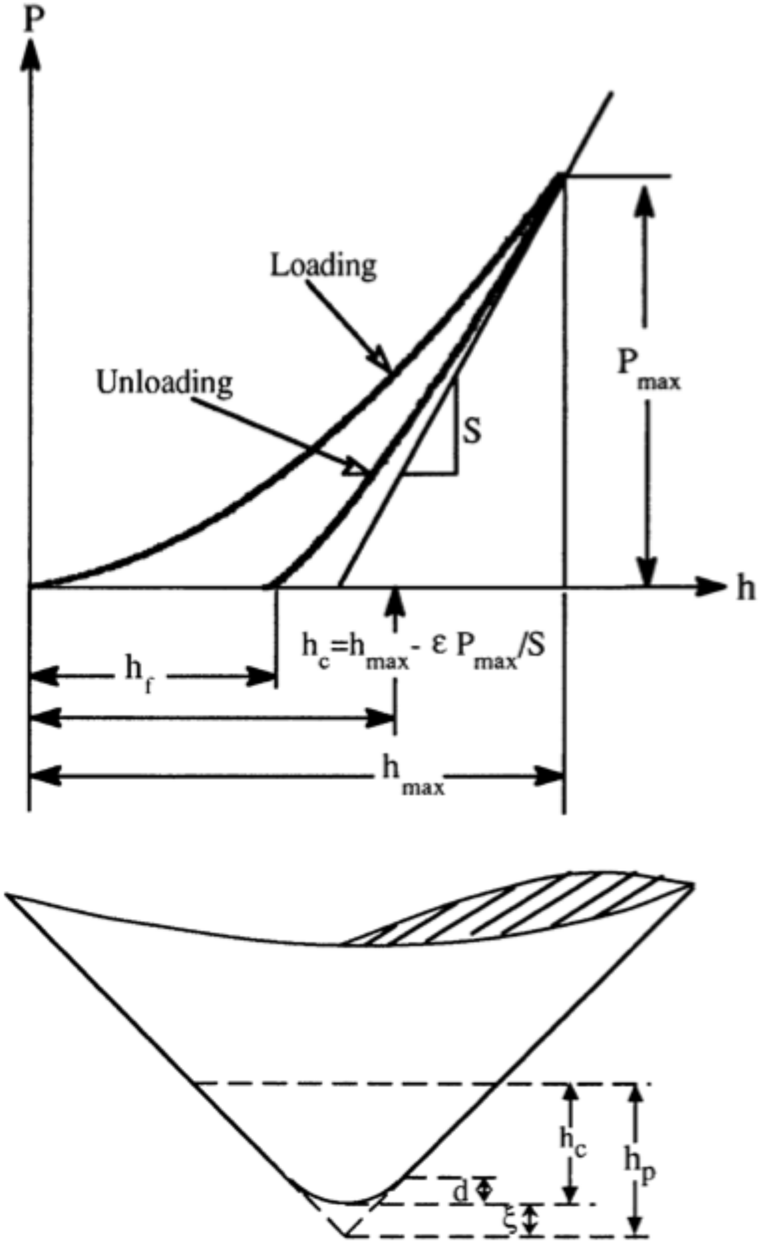

Figure 3-4. Load displacement curve for indentation testing with schematics of indentation parameters. ξ and d are determined by the roundness of the intender tip. For ideal Berkovich geometry, ξ = d = 0 (Xu, et al. 1998, with permission).

There are a few methods for evaluating coating adhesion: Scratch testing is a force method, peel testing is an energy method, and pull/topple testing is a stress method. For the purpose of this research, the MCT was used for scratch analysis. All scratch tests were performed using a spherical Rockwell diamond tip with a radius of 0.2mm. The scratch was programmed to progressive mode, where the diamond tip would run along the sample in a straight line while the applied load increased linearly with displacement, shown in **Figure 3-5**.

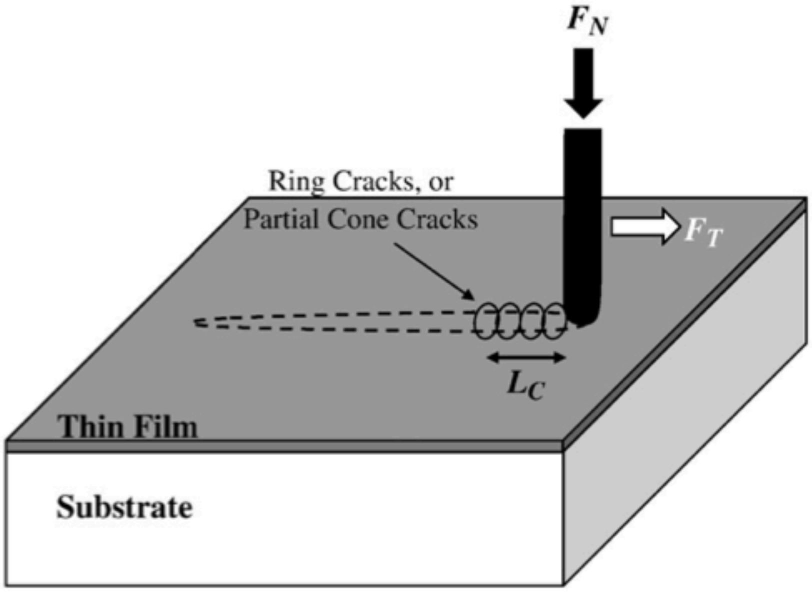

Figure 3-5. Schematic diagram of a scratch test with forces. F_N is the normal load and F_T is the tangential force. L_c is the distance between cracking failure and the end of the scratch (Borrero-López, et al. 2010, with permission).

Other scratch modes include a constant load, where a predetermined constant load, in Newtons, is applied to the surface and run along the sample without varying the load value. Incremental scratch modes use the same technique as the progressive scratch mode, but instead one varies the applied load by increments instead of gradually varying the load.

Pre-scan and post-scan measurements were performed during every scratch. These scans are done by the MCT by running the tip along the surface with a force of 15mN. They are capable of providing information on penetration depth, residual depth, and scratch load. The purpose of the pre-scan is to calibrate the indenter to the surface, as it is possible for samples to have minute slants along the substrate. The pre-scan monitors this and calibrates the MCT prior to the scratch. The post-scan runs along the scratch and helps clear any residual debris. Each scratch was programmed to extend 5mm in length with a speed of 10 mm/min. The initial and final loads were 30 mN and 20 N, respectively making the loading/unloading rate to be 39,940 mN/min. In order to obtain a consistent average, each sample was scratched five times, taking approximately an hour to perform a full scratch analysis per sample.

3.5.1 Characterizing TiN Coatings from Scratch Analysis

With each scratch, qualitative measurements needed to be taken. Every individual scratch was observed under a microscope to look for indications of critical failure modes. With each scratch, the coating would experience tension and compression stresses as the indenter scratches along the surface. This causes plastic deformation, where the coating material is pushed out the sides and plowing effects are noticeable at the end of the scratch. Spallation-buckling failure may also be apparent when delamination of the coating occurs. Overwhelming tensile, shear and compressive stresses also cause cracking failure (Mattox, Handbook of Physical Vapor Deposition (PVD) Processing 2010), where cracks within the film become visible. Cracking and spallation-buckling failures are a good indication of how well the coating adheres to the surface of the stainless steel substrate (Marder 1996)(Mattox, Thin Film Adhesion and Adhesive Failure – a Perspective 1978). These modes of failure, ranking from weak adhesion to strong adhesion, include adhesive rupture, surface buckling, adhesion/cohesion, forward cracking, and rearward cracking.

Adhesive rupture occurs when the indenter is able to fully delaminate the coating and the substrate is completely exposed. This commonly occurs when the adhesion between the coating and substrate is very weak. Surface buckling, adhesion/cohesion, and forward cracking all appear as half circle deformities in the direction of the scratch. Surface buckling consists of cracks that extend far out past the indenter path. This is representative of weaker adhesion since the scratch is affecting the coating farther away. Forward cracking failures are distinct because they only occur within the scratch and do not extend outwards. Rearward cracking is representative of strong adhesion. The coating experiences increased tensile rather than compressive stress, thus creating cracks in the opposite direction of the scratch, as shown in **Figure 3-6**.

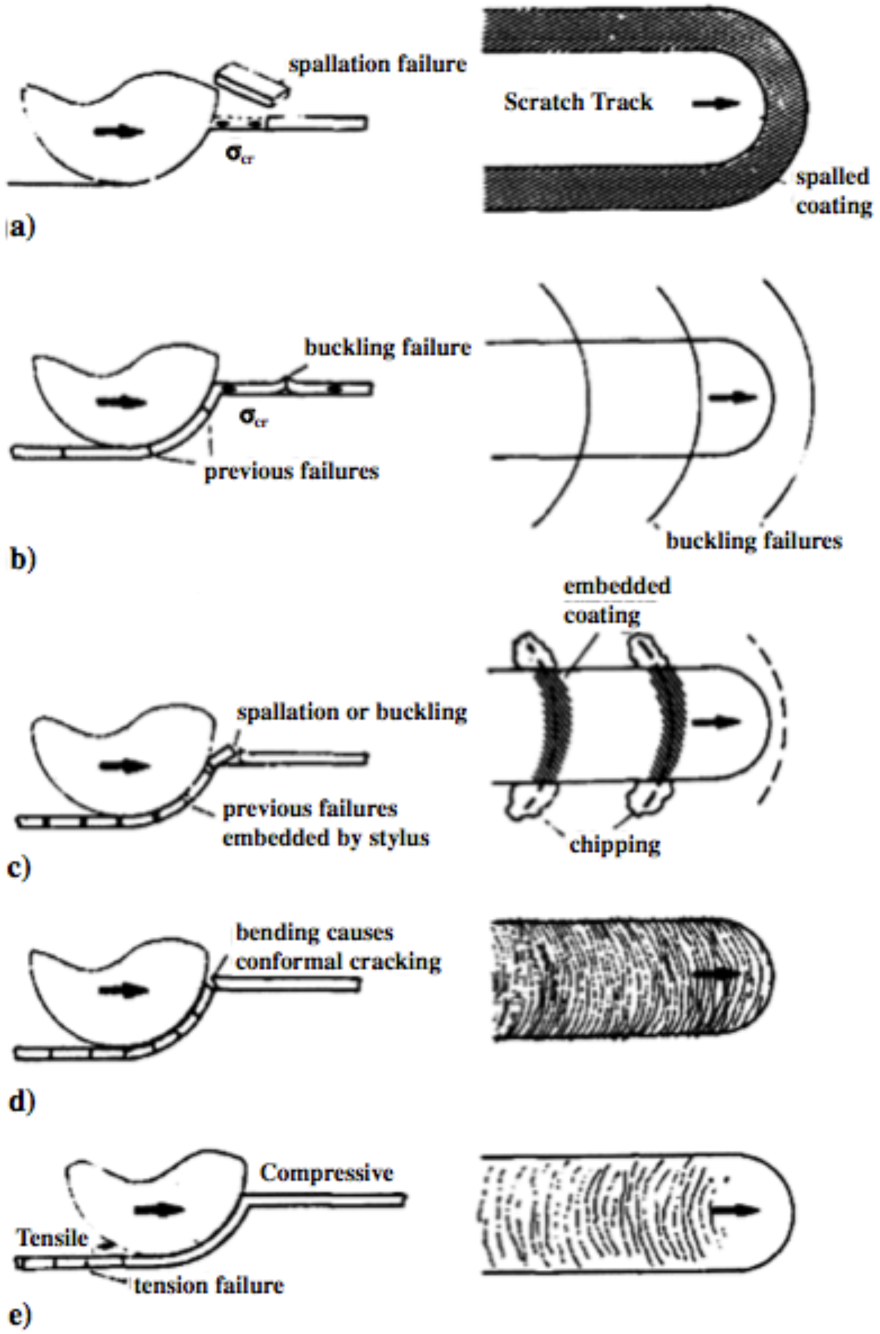

Figure 3-6. Failure modes and their ranking in terms of increasing adhesion: a) spallation failure, b) buckling failure, c) adhesion/cohesion failure, d) forward cracking, and e) rearward cracking from compressive and tensile stress (Li and Beres 2007, with permission).

The result for each scratch analysis includes a set of two values, called critical loads, which are values of force, in Newtons. A critical load was obtained from where the first obvious crack occurred. The critical value where the first signs of delamination were noticed is also important to note. This value was determined by observing the scratch in its entirety under a microscope. The first sign of consistent substrate exposure was considered to be the critical load for coating delamination, as shown in **Figure 3-7**.

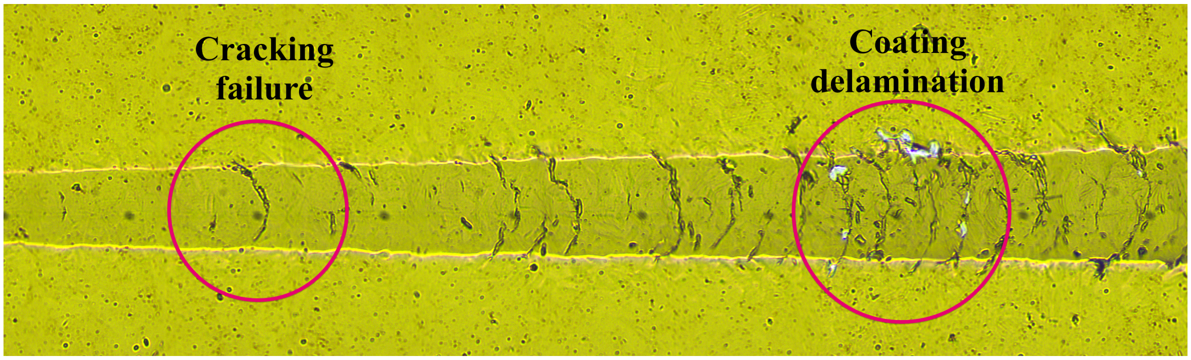

Figure 3-7. Critical loads where cracking failures and initial coating delamination occurs.

4 Results and Discussion

The initial set of samples was designed to investigate the quality of adhesion based on pretreatment methods prior to deposition. These included a comparison of the Steelforme and the McMaster cleaning methods, as well as bake time and temperature using an external furnace (Fisher Scientific, model 650-58). The sample matrix can be found in **Table 4-1**.

Table 4-1. Sample variables for cleaning method, external bake temperature and external bake time.

Sample #	Cleaning Method	Bake Temperature (°C)	Bake Time (Minutes)
7	Steelforme	N/A	0
8	McMaster	N/A	0
3	Steelforme	245	20
4	McMaster	245	20
5	Steelforme	245	40
6	McMaster	245	40
9	Steelforme	325	20
10	McMaster	325	20
11	Steelforme	325	40
12	McMaster	325	40
15	Steelforme	400	20
16	McMaster	400	20
17	Steelforme	400	40
18	McMaster	400	40

Table 4-2. CL_1 and CL_2 values with % improvement in comparison control (Sample 7).

Sample #	Average CL_1 (N)	Average CL_2 (N)	% Improvement of Control CL_1	% Improvement of Control CL_2
7	1.84	7.67	Control	Control
8	2.54	6.45	+38.04	-15.91
3	2.54	8.75	+38.04	+14.08
4	2.30	8.35	+25.00	+8.87
5	2.98	8.06	+61.96	+5.08
6	2.11	9.24	+14.67	+20.47
9	2.79	6.34	+51.63	-17.34
10	2.60	5.49	+41.30	-28.42
11	2.67	4.81	+45.11	-37.29
12	2.75	4.59	+49.46	-40.16
15	2.67	4.46	+45.11	-41.85
16	2.43	4.41	+32.07	-42.50
17	2.19	5.81	+19.02	-24.25
18	2.48	3.29	+34.78	-57.11

4.1 Scratch/Crack Resistance

The results of the crack testing experiments are summarized in Table 5 above. Samples with no external bake times experienced cracking failure at different loads: 1.84 N for the control sample, cleaned using the Steelforme cleaning method, and 2.54 N for the sample cleaned using the McMaster cleaning method in a clean room. The critical load value of 2.54 N obtained for Sample 8 was a 38.04% improvement in crack resistance over the control. As baking pretreatment was introduced, all samples experienced improvements ranging from 14.67-61.96%. The highest critical load observed for cracking failures was 2.98 N for Sample 5, which was cleaned using the Steelforme cleaning method and baked for 40 minutes at 245°C. Sample 5 showed the highest improvement of 61.96% over the average critical load obtained for the control.

Single factor analysis of variance ANOVA revealed the largest F factor of 10.14 for the group of samples that were pretreated using the Steelforme cleaning method and an external bake temperature of 245°C. The results can be found in **Table 4-3**. The F value is the mean square between distributions divided by the mean square within distributions:

$$F = \frac{MS_{Between}}{MS_{Within}}$$

where $MS_{Between} = \frac{SS_{Between}}{K-1}$, and $MS_{Within} = \frac{SS_{Within}}{N-K}$. $SS_{Between}$ and SS_{Within} are the sum of squares between groups and within groups respectively. N is the total number of samples in a survey, and K is the number of groups.

High F values indicate a significant difference between the means for each distribution. Thus, it can be concluded that the hypothesis is responsible for these differences. Alpha is a predetermined critical value commonly set to 0.05 in order for the results from variance analysis to be statistically significant. P value corresponds to the area of the distribution curve from the F value to infinity. If the P value is greater than alpha, the null hypothesis is accepted. If the P value is less than alpha, the null hypothesis is rejected. Since ANOVA revealed a large F value and small P-value such that $F > F_{crit}$ and P-value < Alpha, it can be concluded that the distributions for samples 7, 3, and 5 have little overlap between them, indicating that bake time was responsible for the difference in means between the distributions for CL_1. Similar conditions were found for the other two groups of samples that were pretreated using the Steelforme cleaning method with different bake temperatures. In all of these cases, ANOVA revealed a large F value and small P-value such that $F > F_{crit}$ and P-value < Alpha. However, for the groups of samples that were pretreated using the McMaster cleaning method, ANOVA revealed a small F value and large P-value such that $F < F_{crit}$ and P-value > Alpha, indicating the means between the distributions were relatively similar to one another.

Table 4-3. ANOVA Analysis Results for Crack Resistance (Alpha = 0.05).

Group	F	P-Value	F_{crit}	Accept/Reject Null Hypothesis
Steelforme, 245°C: 7 (0 minutes) 3 (20 minutes) 5 (40 minutes)	10.1	0.00264	3.89	Reject
McMaster, 245°C: 8 (0 minutes) 4 (20 minutes) 6 (40 minutes)	3.02	0.0864	3.89	Accept
Steelforme, 325°C: 7 (0 minutes) 9 (20 minutes) 11 (40 minutes)	6.47	0.0124	3.89	Reject
McMaster, 325°C: 8 (0 minutes) 10 (20 minutes) 12 (40 minutes)	0.351	0.711	3.89	Accept
Steelforme, 400°C: 7 (0 minutes) 15 (20 minutes) 17 (40 minutes)	3.91	0.0491	3.89	Reject
McMaster, 400°C: 8 (0 minutes) 16 (20 minutes) 18 (40 minutes)	0.0707	0.932	3.89	Accept

4.2 Adhesion

Samples with no external bake times experienced delamination at different loads: 7.67 N for the samples cleaned using the Steelforme cleaning method and 6.45 N for the sample cleaned using the McMaster cleaning method in a clean room. All samples that were externally baked at 245°C for varying times experienced a slight increase in coating adhesion, with improvements ranging from 5.08-20.47%, with the highest average critical load of 9.24 N for the sample baked for 40 minutes prior to deposition. Coating delamination was occurring at much lighter scratch loads for samples that were pretreated at temperatures of 325°C and 400°C. Sample 18 was cleaned using the McMaster cleaning method and baked externally for 40 minutes at 400°C. It showed first signs of delamination at the lowest average critical load of all samples. A reason for this may have been the possible oxidation that formed on the surface of the substrate from the high temperature environment within the furnace (Perez, et al. 2002).

Average critical load values for Sample 8, cleaned using the McMaster cleaning method and no substrate bake show a decline in adhesion of 15.91%. This may be due to sample transportation from the clean room to the cathodic arc PVD system located at Steelforme Design Inc. It is possible for residue from the plastic bags to contaminate the substrate. Also, it cannot be guaranteed that oxidation did not occur during sample transportation. Any moisture left in the plastic bags could have potentially accelerated any oxidation occurring on the substrate. For Sample 8, an external substrate bake was not performed, which may have helped evaporate any debris.

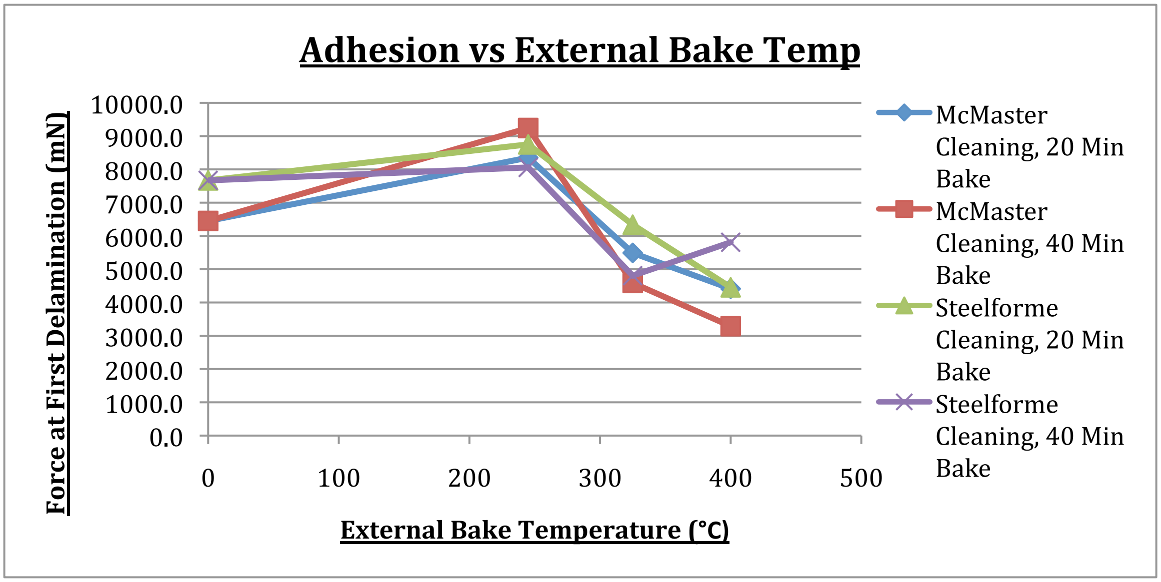

Figure 4-1. Adhesion vs External Bake Temperature for Samples 7-18.

Single factor ANOVA analysis revealed the largest F factor of 93.03 for the group of samples that were pretreated using the Steelforme cleaning method and external bake temperature of 400°C. The results can be found in **Table 4-4**. Since ANOVA revealed a large F value and small P-value such that $F > F_{crit}$ and P-value < Alpha, it can be concluded that the distributions for samples 7, 3, and 5 have little overlap between them, indicating that bake time was responsible for the difference in means between the distributions for CL_2. Similar conditions were found for all other groups of samples that were pretreated using the Steelforme or McMaster cleaning methods and different bake temperatures. In all of these cases, ANOVA revealed large F values and small P-values such that $F > F_{crit}$ and P-value < Alpha. Thus it was concluded the distributions for each group have little to no overlap between them.

Table 4-4. ANOVA Analysis Results for Adhesion (Alpha = 0.05).

Group	F	P-Value	F_{crit}	Accept/Reject Null Hypothesis
Steelforme, 245°C: 7 (0 minutes) 3 (20 minutes) 5 (40 minutes)	5.81	0.0172	3.89	Reject
McMaster, 245°C: 8 (0 minutes) 4 (20 minutes) 6 (40 minutes)	40.4	4.65E-06	3.89	Reject
Steelforme, 325°C: 7 (0 minutes) 9 (20 minutes) 11 (40 minutes)	39.9	5.00E-06	3.89	Reject
McMaster, 325°C: 8 (0 minutes) 10 (20 minutes) 12 (40 minutes)	11.3	1.74E-03	3.89	Reject
Steelforme, 400°C: 7 (0 minutes) 15 (20 minutes) 17 (40 minutes)	93.0	4.95E-08	3.89	Reject
McMaster, 400°C: 8 (0 minutes) 16 (20 minutes) 18 (40 minutes)	47.3	2.03E-06	3.89	Reject

4.3 Investigating Deposition Parameters

Table 4-5. Variables for cleaning method, ion implantation bias voltage, ion implantation duration, TiN deposition time, and nitrogen pressure.

Sample #	Cleaning Method	Ion Implant Bias Voltage (Volts)	Ion Implant Duration (Seconds)	TiN Deposition Time (Minutes)	Nitrogen Pressure (Pascal)
19a (Square)	Steelforme	300	120	10	0.4
19b (Fork)	Steelforme	300	120	10	0.4
20a	Steelforme	400	120	10	0.4
20b	Ultrasonic Only	400	120	10	0.4
20c	Alcohol Only	400	120	10	0.4
20d	Bleach (Comet) Only	400	120	10	0.4
21a (Square)	Steelforme	400	300	10	0.4
21b (Fork)	Steelforme	400	300	10	0.4
22	Steelforme	500	120	10	0.4
23	Steelforme	400	120	20	0.4
24	Steelforme	400	120	30	0.4
25	Steelforme	400	120	10	1
26	Steelforme	N/A	N/A	10	0.4

Table 4-6. CL_1 and CL_2 values with % improvement in comparison control (Sample 26).

Sample #	Average CL_1 (N)	Average CL_2 (N)	% Improvement of Control CL_1	% Improvement of Control CL_2
19a (Square)	2.32	7.62	-18.88	+2.28
19b (Fork)	3.40	8.37	+18.88	+12.35
20a	3.53	11.6	+23.42	+55.70
20b	3.81	8.84	+33.22	+18.66
20c	3.49	9.35	+22.03	+25.50
20d	3.34	9.27	+16.78	+24.43
21a (Square)	3.08	8.31	+7.69	+11.54
21b (Fork)	4.53	6.52	+58.39	-12.48
22	2.77	9.77	-3.15	+31.14
23	4.72	8.88	+65.03	+19.19
24	7.57	11.5	+164.69	+54.36
25	3.17	9.21	+10.84	+23.62
26	2.86	7.45	Control	Control

4.3.1 Comparison of Stainless Steel Square and Fork Substrates

Samples 19 and 21 contained depositions on both 25 mm by 25 mm stainless steel squares and stainless steel fork substrates. These samples were used to transition from the stainless steel squares to the tableware substrate used by Steelforme. Samples 19a and 19b were prepared using a voltage of 300 V for ion bombardment, which lasted 120 seconds. A nitrogen pressure of 0.4 Pa was set for TiN deposition lasting 10 minutes. Cracking failures occurred at 2.32 N and 3.40 N for the stainless steel square and fork respectively. Sample 19b showed delamination at a greater critical load of 8.37 N in comparison to the critical load of 7.62 N for sample 19a.

Samples 21a and 21b underwent a longer ion bombardment of 300 seconds at an increased voltage of 400 V. Cracking failures occurred at 3.08 N and 4.53 N for the stainless steel square and fork respectively. In comparison to the critical loads obtained for samples 19a and 19b, samples 21a and 21b exhibited a slight increase of 0.76 N and 1.13 N respectively. Sample 21a experienced delamination at a greater critical load of 8.31 N in comparison to sample 21b, which showed delamination at 6.52 N.

Single factor ANOVA analysis was performed in order to compare the 25 mm by 25 mm stainless steel squares and the stainless steel fork substrates. The results can be found in **Table 4-7** and **Table 4-8**. In comparing the stainless steel substrates, it is important to note the null hypothesis that change in substrate would have no effect on the TiN coatings. Both the crack and adhesion values for samples 19 and 21 show small P-values such that P-Value < Alpha and large F values such that $F > F_{crit}$. Thus, in all cases, the null hypothesis is rejected. It was concluded that distributions for crack resistance and adhesion of the two different stainless steel substrates experience little to no overlap with one another, which allows the interpretation that changing the substrate influenced scratch resistance and adhesion of TiN coatings.

Table 4-7. Single factor ANOVA analysis on crack values for Samples 21a, 21b, 19a and 19b (Alpha = 0.05).

Group	F	P-Value	F_{crit}	Accept/Reject Null Hypothesis
19a (Square) 19b (Fork)	14.5	0.00522	5.32	Reject
21a (Square) 21b (Fork)	30.8	0.000541	5.32	Reject

Table 4-8. Single factor ANOVA analysis on adhesion values for Samples 21a, 21b, 19a and 19b (Alpha = 0.05).

Group	F	P-Value	F_{crit}	Accept/Reject Null Hypothesis
21a (Square) 21b (Fork)	6.79	0.0314	5.32	Reject
19a (Square) 19b (Fork)	13.4	0.00641	5.32	Reject

4.3.2 Ion Bombardment Duration

The duration of ion bombardment was varied to monitor its effects on substrate pretreatment and whether scratch resistance was dependent on it. Samples were placed under ion bombardment for durations of 120 and 300 seconds. Post deposition observations of sample 21b that had undergone ion bombardment for an increased duration of 300 seconds, showed a noticeably rough texture believed to have been caused by the longer duration and increased bias voltage for ion bombardment.

Similar findings for TiN hard coatings deposited using cathodic arc PVD were discussed by H. Randhawa et al. A major difference in topography was observed for TiN deposited through arc PVD processes. The surfaces of TiN obtained through cathodic arc PVD deposition were rough in texture in comparison to TiN deposited using ion plating and sputtering processes. TiN obtained though ion plating demonstrated a roughness root mean square value of 0.085 μm while roughness through sputtering process was 0.092 μm. These values for roughness were significantly less than the 0.345 μm roughness value obtained for arc PVD. TiN films deposited through cathodic arc PVD contained microdroplets that are rich in titanium, ranging in size from 0.2 to 1.0 μm. H. Randhawa et al. discovered through fractured surface analysis, that these microdroplets were present throughout the thickness of the coating. It was suggested these microdroplets were loosely held within the TiN coating and may chip off easily. Microdroplets arise from cathode spots, formed when a high current pulse is placed near the cathode of the arc. Cathode spots are subjected to extreme forces and elevated, localized temperatures, listed in **Table 4-9**, that are responsible for high velocity vaporized cathode material (Randhawa and Johnson, Technical Note: A Review of Cathodic Arc Plasma Deposition Processes and their Applications 1987).

Table 4-9. Cathode arc spot physical conditions (Randhawa and Johnson, Technical Note: A Review of Cathodic Arc Plasma Deposition Processes and their Applications 1987**).**

Temperature (K)	4×10^3-10^4
Pressure (MPa)	0.1-10
Power Density (W/cm^2)	10^7-10^9
Electric field (V/cm)	10^4-10^5
Current Density (A/cm^2)	10^6-10^8

Microdroplets, electrons, neutral vapour particles, and ions are emitted at high velocities from the cathode spot, leaving behind a crater in the target material. **Figure 4-2** shows resulting emission craters present on a titanium cathode surface (Randhawa and Johnson, Technical Note: A Review of Cathodic Arc Plasma Deposition Processes and their Applications 1987).

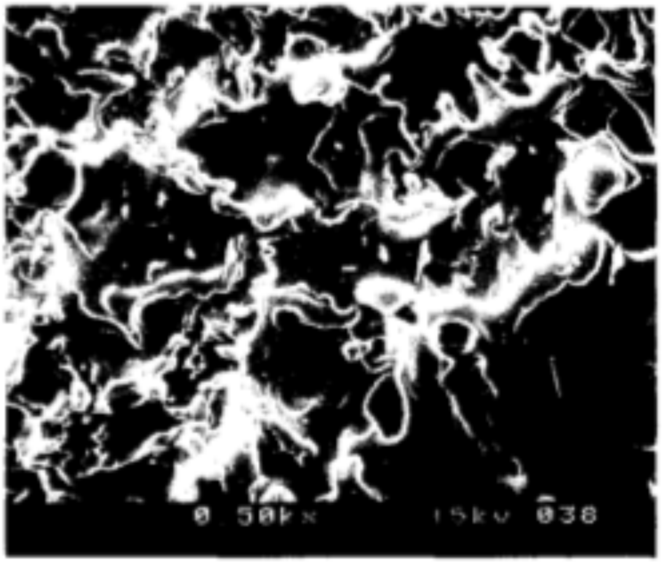

Figure 4-2. Scanning electron micrograph of emission craters present on the cathodic surface of titanium (Randhawa and Johnson, Technical Note: A Review of Cathodic Arc Plasma Deposition Processes and their Applications 1987, with permission)**.**

Figure 4-3 shows Daalder's model of cathode spot emission. The positive ions discharge from the target material in the direction that is nearly perpendicular to the surface of the cathode spot. It is suggested that the microdroplets are ejected at very small angles of up to 30° from the cathode surface (Daalder, Cathode Erosion of Metal Vapor Arcs in Vacuum 1978).

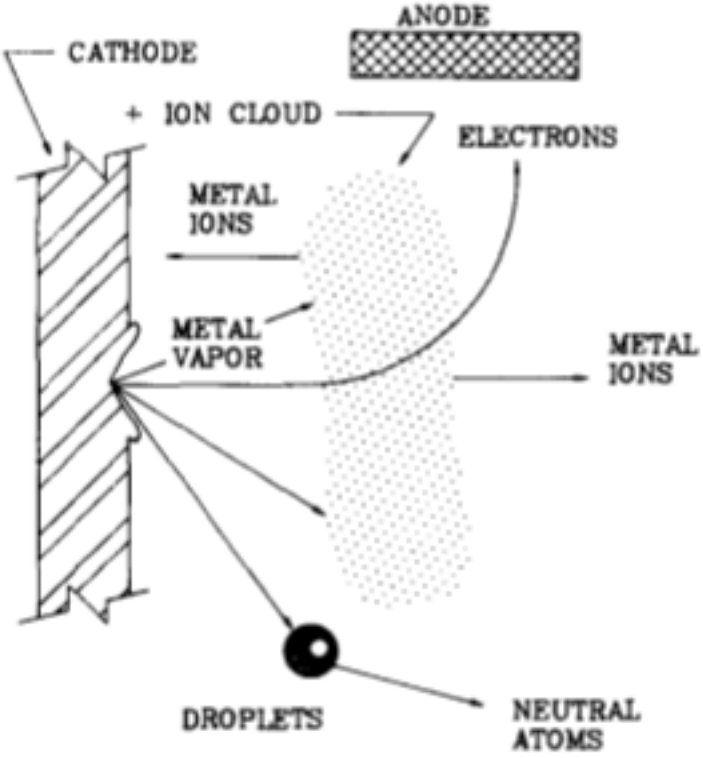

Figure 4-3. Daalder's model of cathode spot emission (Daalder, Cathode Erosion of Metal Vapor Arcs in Vacuum 1978)(Randhawa and Johnson, Technical Note: A Review of Cathodic Arc Plasma Deposition Processes and their Applications 1987, with permission).

H. Randhawa et al. suggested that it was possible to decrease the amount of microdroplet emission through modified cathodic arc PVD processes. Adjusting deposition parameters as well as cathodic spot movement provides the required modifications to significantly decrease the emission of microdroplets during thin film deposition (Randhawa and Johnson, Technical Note: A Review of Cathodic Arc Plasma Deposition Processes and their Applications 1987).

Upon microscopic observation of samples 21a and 21b, impurities were clearly visible on the surface of the sample. Sample 21a experienced delamination at 8.31 N while sample 21b experienced premature delamination at 6.52 N believed to have been influenced by microdroplets present within the TiN coating, shown in **Figure 4-4.**

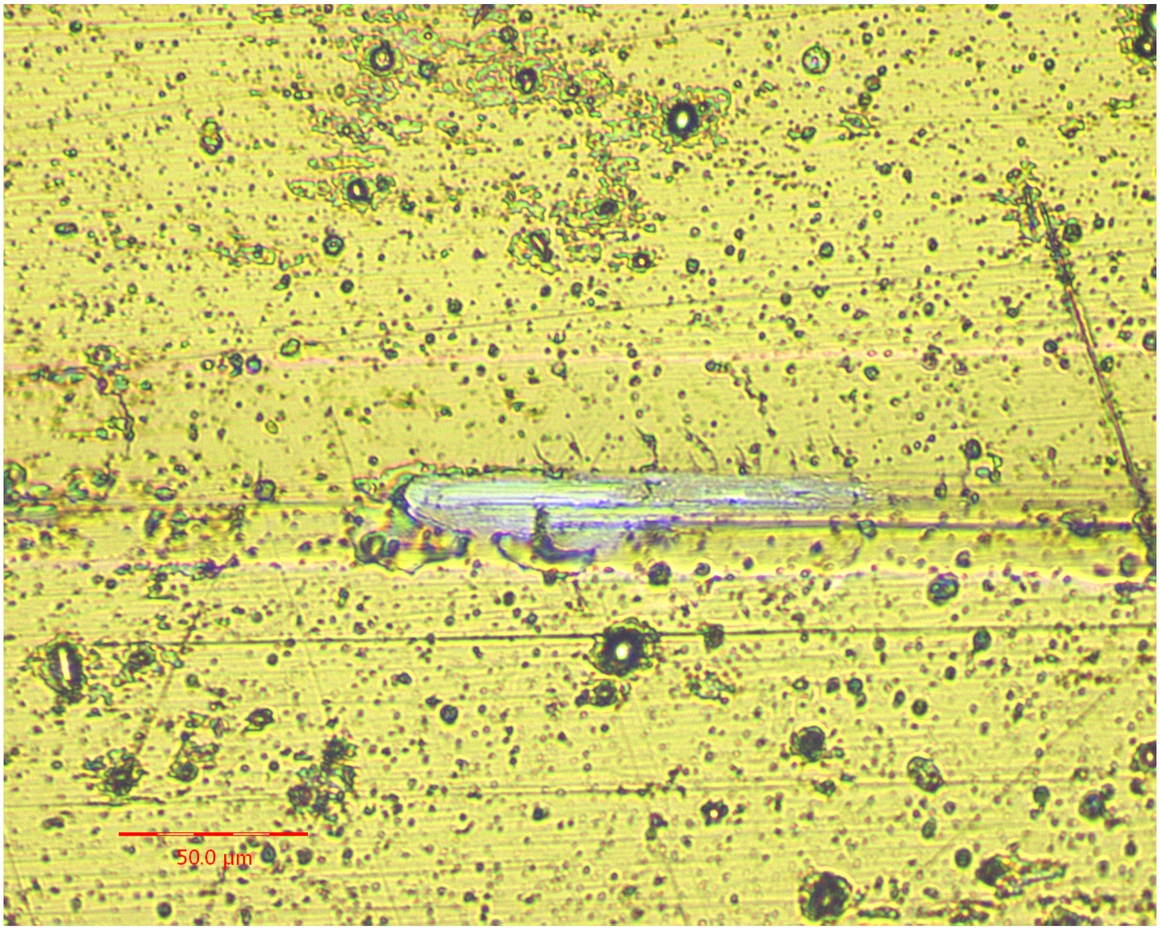

Figure 4-4. Influenced delamination on Sample 21b.

Similarly, H. Randhawa et al. investigated the performance of TiN coated drills and the effects caused by microdroplet emission. Test conditions included the use of 6mm drills that were coated with TiN. It was determined that drills with the largest density of microdroplets demonstrated poor performance in comparison to drills that were coated using ion plating and sputtering processes. H. Randhawa et al. suggested the concentration of microdroplet emission is greater for target material with lower boiling points (Randhawa and Johnson, Technical Note: A Review of Cathodic Arc Plasma Deposition Processes and their Applications 1987). A proposed solution was to coat the tools with zirconium nitride (ZrN) since Zirconium (Zr) has a much higher boiling point of 4409°C and lower vapour pressure in comparison to Ti, which has a lower boiling point of 3287°C and high vapour pressure. It was confirmed through experimentation that ZrN coated drills demonstrated significantly better performance than the TiN coated tools (Johnson and Randhawa 1987).

Another proposed solution to reduce the amount of microdroplets found within functional coatings is the use of macroparticle magnetic filtering (Bilek and Anders 1999). A. Morozov first discussed plasma optics calculations for curved magnetic fields in 1966 (Morozov 1966), which became the fundamental concept behind the development of a 90 degree curved solenoid macroparticle filter in 1978 by Aksenov et al. (Aksenov, Belous, et al., Apparatus to Rid the Plasma of a Vacuum Arc of Macroparticles 1978)(Aksenov, Belous, et al., Transport of Plasma Streams in a Curvilinear Plasma Optics System 1978). A curved magnetic field guides ions through a coil design to the target substrate, shown in **Figure 4-5** (Bilek and Anders 1999).

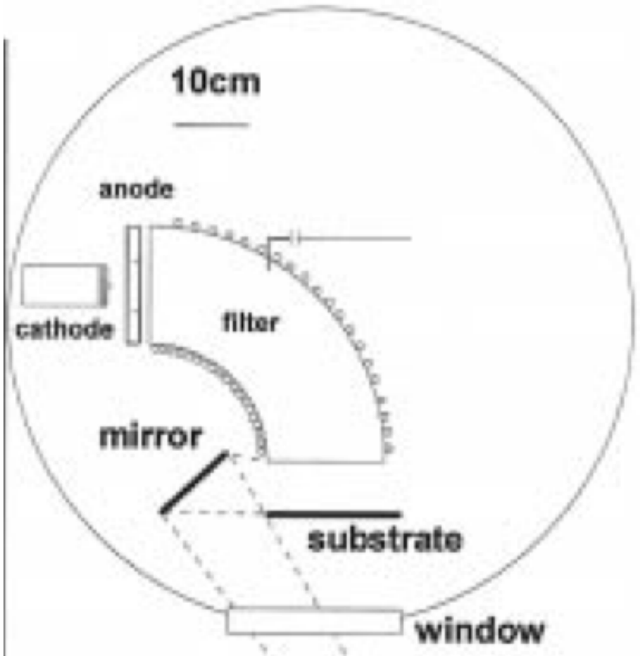

Figure 4-5. Schematic of macroparticle filtering using a 90 degree curved solenoid design (Schulke, Anders and Siemroth 1997, with permission).

Single factor ANOVA analysis was performed in order to compare crack and delamination values for various ion bombardment durations including 120, 300, and 0 seconds as set by the control. The results can be found in **Tables 4-10** and **4-11**. In comparing the ion bombardment durations, it is important to note the null hypothesis that change in ion bombardment duration would have no effect on the TiN coatings. Both crack and adhesion values for samples 20a, 21b, and 26 all show small P-values such that P-Value < Alpha and large F values such that $F > F_{crit}$. Thus, in all cases, the null hypothesis is rejected. It was concluded that distributions for crack resistance and adhesion of varying ion bombardment durations experience little to no overlap with one another, which allows the interpretation that change in ion bombardment duration influenced scratch resistance and adhesion of TiN coatings.

Table 4-10. Single factor ANOVA analysis on crack values for Samples 20a, 21b, and 26 (Alpha = 0.05).

Group	F	P-Value	F_{crit}	Accept/Reject Null Hypothesis
20a (120 s) 21b (300 s) 26 (0 s)	20.6	0.000133	3.89	Reject

Table 4-11. Single factor ANOVA analysis on adhesion values for Samples 20a, 21b, and 26 (Alpha = 0.05).

Group	F	P-Value	F_{crit}	Accept/Reject Null Hypothesis
20a (120 s) 21b (300 s) 26 (0 s)	32.1	1.53E-05	3.89	Reject

4.3.3 Cleaning methods

Samples 20a, 20b, 20c, and 20d were pretreated using the standard Steelforme method, ultrasonic cleaning only, alcohol only, and Comet bleach dissolved in water respectively. These samples underwent a 400 V ion bombardment for 120 seconds and TiN deposition lasting 10 minutes with a nitrogen pressure of 0.4 Pa. Visual observations determined possible scratching of the substrate using Comet bleach, as the powder is known to be very abrasive. Cracking failures for these samples were relatively consistent since the first critical loads all occurred within a range of 0.47 N: Sample 20a experienced cracking failure at 3.53 N, 3.81 N for sample 20b, 3.49 N for sample 20c, and 3.34 N for sample 20d.

Investigating pretreatment solutions separately and in combination was beneficial in determining the most effective substrate pretreatment that improved coating adhesion. Alcohol only and bleach only pretreatments showed improved resistance to surface delamination with critical loads occurring at 9.35 N and 9.27 N for samples 20c and 20d respectively. Ultimately, the optimal substrate pretreatment was the Steelforme cleaning method, which utilized both ultrasonic cleaning and rinsing in alcohol. Sample 20a showed coating delamination at 11.6 N.

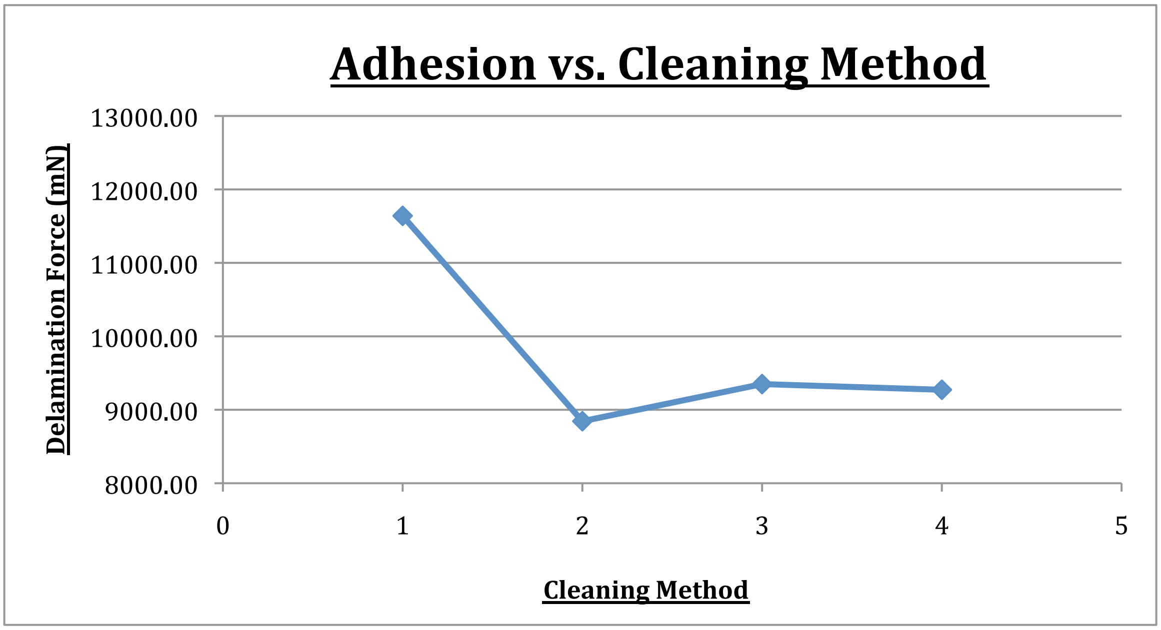

Figure 4-6. Adhesion vs cleaning method for samples 20a, 20b, 20c, 20d.

Single factor ANOVA analysis was performed in order to compare crack and delamination values for different cleaning method steps including the complete Steelforme cleaning method, ultrasonic cleaning only, alcohol cleaning only and cleaning using bleach only. The results can be found in **Tables 4-12** and **4-13**. In comparing the cleaning methods, it is important to note the null hypothesis that differences in cleaning steps would have no effect on the TiN coatings. In the case of critical values where cracking occurs, Samples 20a, 20b, 20c, 20d show large P-values such that P-Value > Alpha and small F values such that $F < F_{crit}$. Therefore, the null hypothesis is accepted. It was concluded that distributions for crack resistance of different cleaning steps are relatively similar, which allows the interpretation that substrate cleaning would have little to no influence on scratch resistance of the TiN film. Samples 20a, 20b, 20c, 20d show small P-values for adhesion such that P-Value < Alpha and large F values such that $F > F_{crit}$. Thus, the null hypothesis is rejected. It was concluded that distributions for adhesion after employing various cleaning methods experience little to no overlap with one another, which allows the interpretation that substrate cleaning influenced adhesion of TiN coatings.

Table 4-12. Single factor ANOVA analysis on crack values for Samples 20a, 20b, 20c, and 20d (Alpha = 0.05).

Group	F	P-Value	F_{crit}	Accept/Reject Null Hypothesis
20a (Steelforme) 20b (Ultrasonic) 20c (Alcohol) 20d (Bleach)	0.755	0.536	3.24	Accept

Table 4-13. Single factor ANOVA analysis on adhesion values for Samples 20a, 20b, 20c, and 20d (Alpha = 0.05).

Group	F	P-Value	F_{crit}	Accept/Reject Null Hypothesis
20a (Steelforme) 20b (Ultrasonic) 20c (Alcohol) 20d (Bleach)	9.42	0.000802	3.24	Reject

4.3.4 Ion Bombardment Voltage

Ion bombardment voltage was increased to 500 V and ran for 120 seconds for trial 22, where cracking failure occurred at 2.77 N. Sample 19b had undergone ion bombardment at 300V for 120 seconds. Cracking failure occurred at 3.40 N. Sample 20a had undergone ion bombardment at 400V for 120 seconds and demonstrated cracking failure at 3.53 N.

An ion bombardment step was not performed on Sample 26, the control sample. Sample 26 experienced film delamination at 7.45 N. Samples 19b, 20a, and 22 all showed improvements in comparison to the control. Critical loads for delamination occurred at 8.37 N for bias voltage of 300 V, 11.6 N for bias voltage of 400 V, and 9.77 N for bias voltage of 500V.

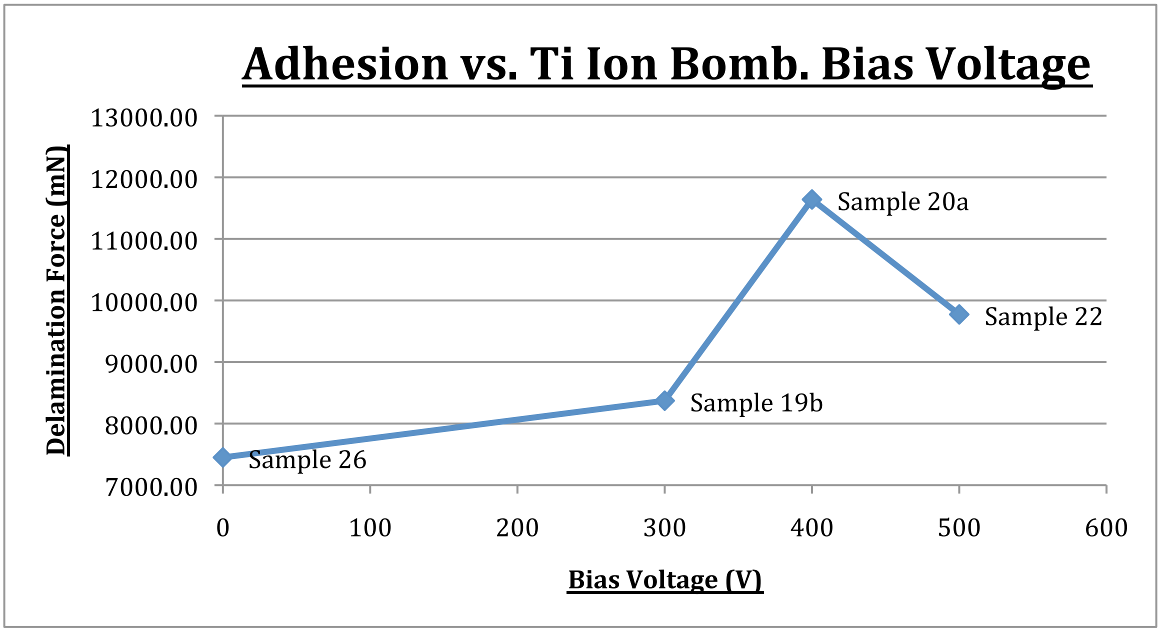

Figure 4-7. Adhesion vs Ti ion bombardment bias voltage for samples 19b, 20a, 22, and 26.

Single factor ANOVA analysis was performed in order to compare crack and delamination values for various ion bombardment bias voltages including 300 V, 400 V, 500 V, and no ion bombardment as set by the control. The results can be found in **Tables 4-14** and **4-15**. In comparing the ion bombardment bias voltages, it is important to note the null hypothesis that change in ion bombardment bias voltage would have no effect on the TiN coatings. Both the crack and adhesion values for samples 19b, 20a, 22, and 26, all show small P-values such that P-Value < Alpha and large F values such that $F > F_{crit}$. Thus, in both cases, the null hypothesis is rejected. It was concluded that distributions for crack resistance and adhesion of different ion bombardment bias voltages experience little to no overlap with one another, which allows the interpretation that changes in bias voltage influenced crack resistance and adhesion of TiN coatings.

Table 4-14. Single factor ANOVA analysis on crack values for Samples 19b, 20a, 22, and 26 (Alpha = 0.05).

Group	F	P-Value	F_{crit}	Accept/Reject Null Hypothesis
19b (300 V) 20a (400 V) 22 (500 V) 26 (N/A)	4.48	0.0183	3.24	Reject

Table 4-15. Single factor ANOVA analysis on adhesion values for Samples 19b, 20a, 22, and 26 (Alpha = 0.05).

Group	F	P-Value	F_{crit}	Accept/Reject Null Hypothesis
19b (300 V) 20a (400 V) 22 (500 V) 26 (N/A)	24.7	3.04E-06	3.24	Reject

4.3.5 Coating Thickness

Varying TiN deposition times affected the thickness of coatings. Trials 23 and 24 were performed with ion bombardment at 400V for 120 seconds and nitrogen pressure of 0.4 Pa for TiN deposition times of 20 and 30 minutes respectively. In comparison to Sample 20a, Sample 23, with a TiN deposition time of 20 minutes, showed cracking failure at 4.72 N. Ultimately, the sample on which TiN was deposited for 30 minutes proved to be the most scratch resistant with first signs of cracking failure occurring at 7.57 N. Longer TiN deposition times lead to thicker TiN layers. In this case, thicker TiN coatings produced coatings that were more resistant to visible scratches and cracking failures.

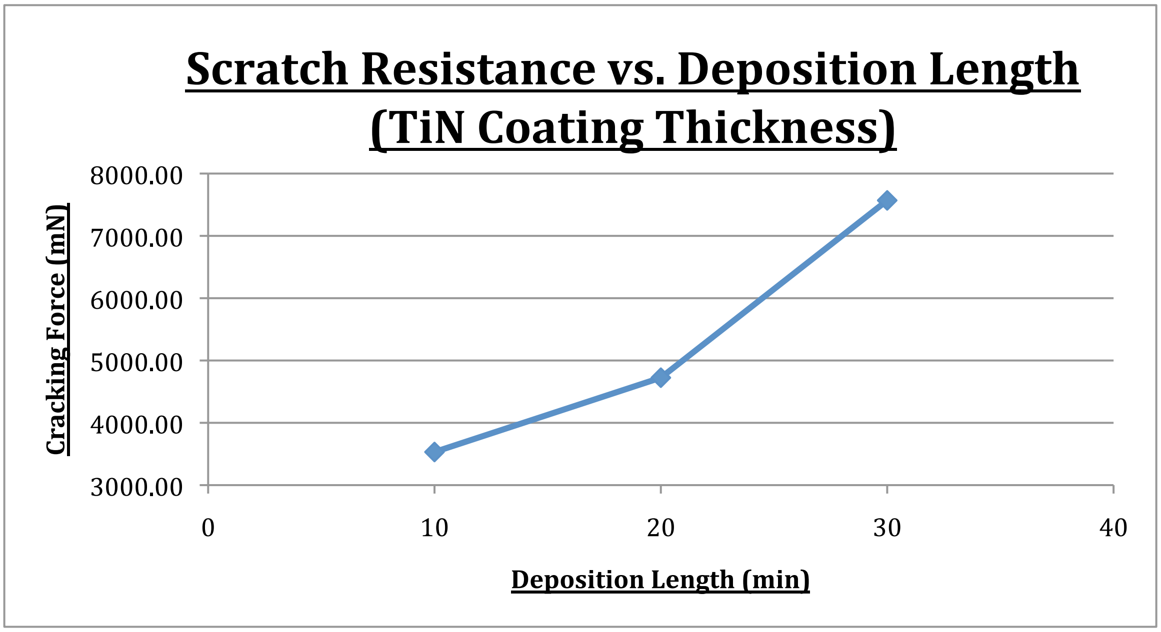

Figure 4-8. Scratch resistance vs deposition length for deposition times of 10 minutes (Sample 20a), 20 minutes (Sample 23), and 30 minutes (Sample 24).

Longer deposition times become more costly due to the amount of power being used during the process, but arc PVD processes still prove to be cost effective due to its high deposition rates as opposed to other deposition processes (Randhawa and Johnson, Technical Note: A Review of Cathodic Arc Plasma Deposition Processes and their Applications 1987).

Single factor ANOVA analysis was performed in order to compare crack and delamination values for various TiN deposition times including 10, 20, and 30 minutes. The results can be found in **Tables 4-16** and **4-17**. In comparing TiN deposition times, it is important to note the null hypothesis that change in TiN deposition time would have no effect on crack resistance or adhesion of the TiN coatings. Both the crack and adhesion values for samples 20a, 23, and 24, all show small P-values such that P-Value < Alpha and large F values such that $F > F_{crit}$. Thus, in both cases, the null hypothesis is rejected. It was concluded that distributions for crack resistance and adhesion of samples prepared using different TiN deposition times experience little to no overlap with one another, which allows the interpretation that TiN deposition duration influenced scratch resistance and adhesion of TiN coatings.

Table 4-16. Single factor ANOVA analysis on crack values for Samples 20a, 23, and 24 (Alpha = 0.05).

Group	F	P-Value	F_{crit}	Accept/Reject Null Hypothesis
20a (10 minutes) 23 (20 minutes) 24 (30 minutes)	159	2.28E-09	3.89	Reject

Table 4-17. Single factor ANOVA analysis on adhesion values for Samples 20a, 23, and 24 (Alpha = 0.05).

Group	F	P-Value	F_{crit}	Accept/Reject Null Hypothesis
20a (10 minutes) 23 (20 minutes) 24 (30 minutes)	18.3	0.000225	3.89	Reject

4.3.6 Nitrogen Pressure

Including nitrogen pressure in the controllable parameters of this experiment may provide insight into deposition optimization, as running longer TiN depositions may be too costly in the long term. J. Bujak et al. conducted experiments where TiAlN films were deposited on tempered HSS disks, 27 mm in diameter and a thickness of 10 mm, with mirrored finishes. The substrates were ultrasonically cleaned and preheated to 200°C. During deposition, argon cleaning and Ti ion bombardment were performed. Nitrogen pressures were set to $3.0\text{x}10^{-3}$, $8.0\text{x}10^{-3}$, $1.3\text{x}10^{-2}$ and $3.0\text{x}10^{-2}$ mbar with an arc current and bias voltage of 50 A and 100V respectively.

Experimental results by J. Bujak et al. suggested that deposition rates increase with increasing nitrogen pressures for TiAlN films, as shown in **Figure 4-9** (Bujak, Walkowicza and Kusinski 2004). It was important to investigate this observation as it may allow for a decrease in TiN deposition times, while maintaining the film properties, thus, increasing productivity and saving on expenses due to power required by the system.

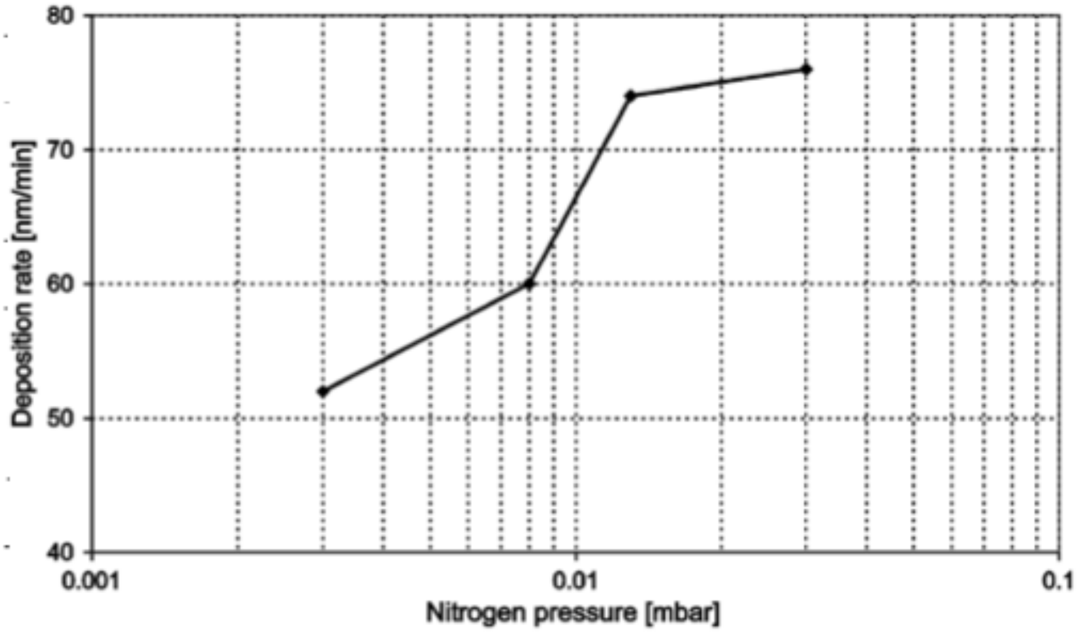

Figure 4-9. Experimental results by J. Bujak et al. for Deposition rate vs Nitrogen pressure (Bujak, Walkowicza and Kusinski 2004, with permission).

Since J. Bujak et al. suggested that deposition rate increased with increased nitrogen pressures (Bujak, Walkowicza and Kusinski 2004), it was expected that Sample 25 would exhibit similar critical loads for cracking and delamination as samples that had undergone longer TiN deposition times. Trial 25 was performed with a 400 V ion bombardment for 120 seconds, followed by TiN deposition for 10 minutes using 1.0 Pa nitrogen pressure. Cracking failure occurred at 3.17 N, which was slightly less than the 3.53 N obtained with 0.4 Pa nitrogen pressure.

C. Chokwatvikul et al. observed opposing experimental results. TiAlN films were deposited onto mirror finished SKD11 modified cold-worked tool steel substrates with a diameter of 32mm and thickness of 5mm. All substrates were ultrasonically cleaned and dried in hot air. During deposition, argon cleaning and Ti ion bombardment were performed. A bias voltage of 100 V and arc current of 70 A was set during deposition. Each film deposition ran for 90 minutes with varying nitrogen pressures of 1, 1.5, and 2 Pa. It was discovered that the thickness of these coatings decreased with increasing nitrogen pressure during deposition, shown in **Figure 4-10** (Chokwatvikul, et al. 2011).

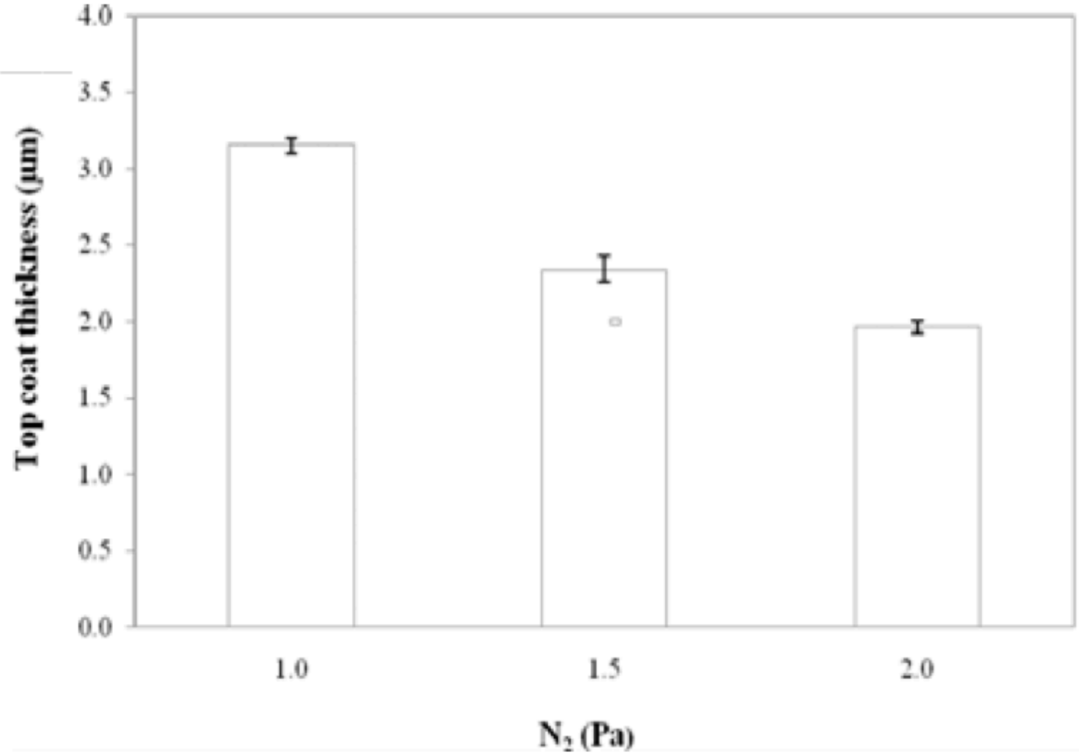

Figure 4-10. Experimental results by C. Chokwatvikul et al. for Deposition rate vs Nitrogen pressure (Chokwatvikul, et al. 2011, with permission).

With an increase in nitrogen gas pressure, more gas particles are present within the system. This results in a significant increase in the number of collisions between the gas particles, but decreases the mean free paths and kinetic energy of the ions. Thus, the deposition rate is lowered and film thickness is decreased (Chokwatvikul, et al. 2011). While J. Bujak et al. discussed the same phenomenon; it appears their experimental results show an increase in deposition rates and thus, are different from the results obtained by C. Chokwatvikul et al.

4.3.6.1 Young's Modulus and Hardness

Young's modulus is helpful in determining adhesion of thin films. It is a measure of elasticity defined by the ratio between stress acting on the material and the strain that is produced. J. Bujak et al. studied the effects of nitrogen pressure on coating hardness and Young's modulus of TiAlN films, shown in **Figure 4-11**. It was found that increasing nitrogen pressures up to $1.3\text{x}10^{-2}$ mbar produced increasing values for hardness and Young's modulus. Films fabricated at nitrogen pressure of $3.0\text{x}10^{-2}$, however, demonstrated a significant decrease in both coating hardness and Young's modulus (Bujak, Walkowicza and Kusinski 2004). Results for samples 20a and 25 show a decrease in hardness as cracking failures occurred at 3.53 N for 0.4 Pa and 3.17 N for 1.0 Pa nitrogen pressures.

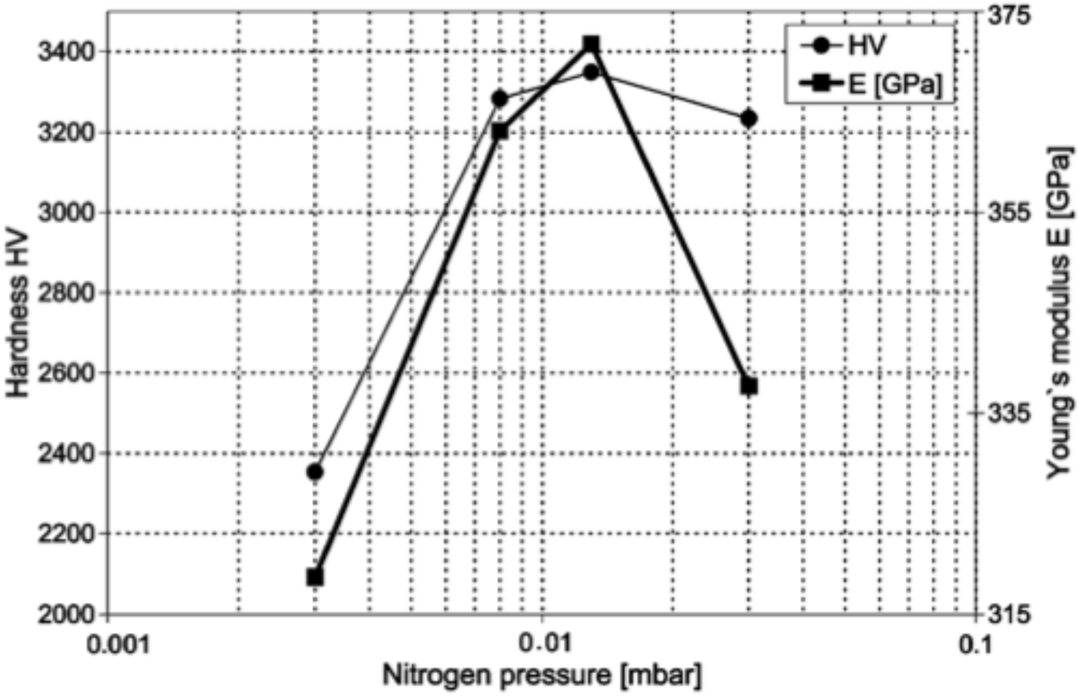

Figure 4-11. Hardness and Young's modulus vs Nitrogen pressure for TiAlN thin films (Bujak, Walkowicza and Kusinski 2004, with permission).

C. Chokwatvikul et al. obtained similar results for hardness and Young's modulus of TiAlN films, shown in **Figures 4-12** and **4-13**. The hardness and Young's modulus values were obtained through Rockwell C nanoindentation testing, and were found to be lower for the sample deposited using 2.0 Pa nitrogen pressure.

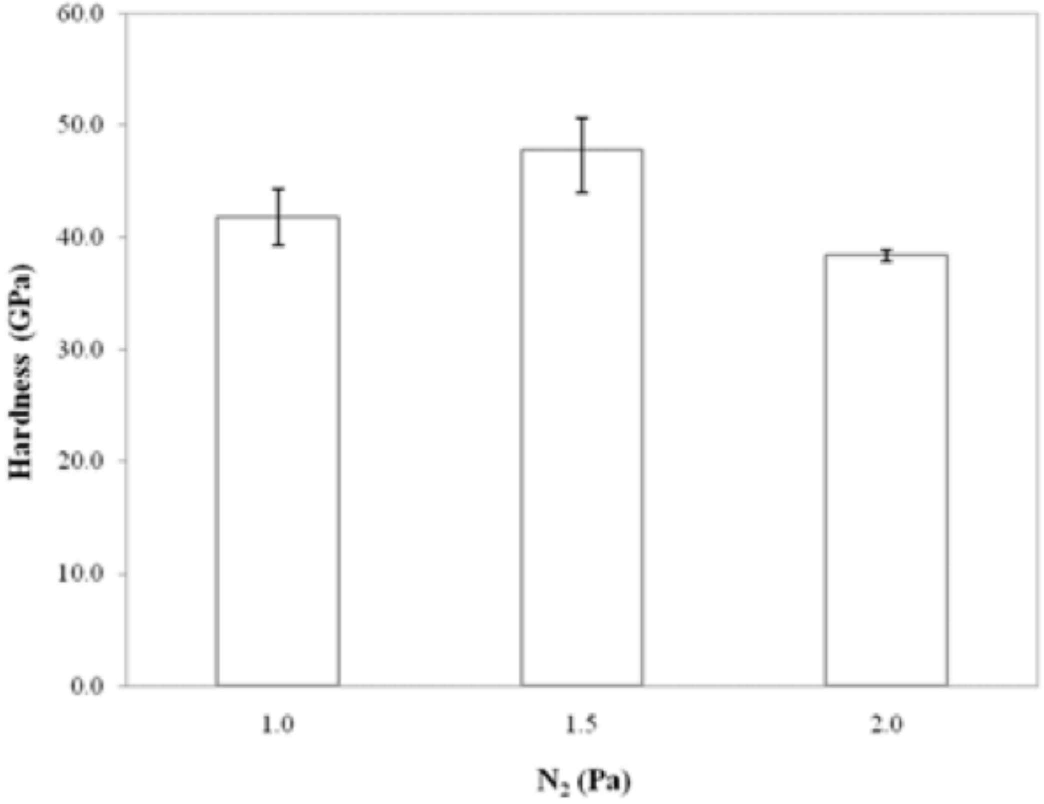

Figure 4-12. Hardness vs Nitrogen pressure for TiAlN thin films (Chokwatvikul, et al. 2011, with permission).

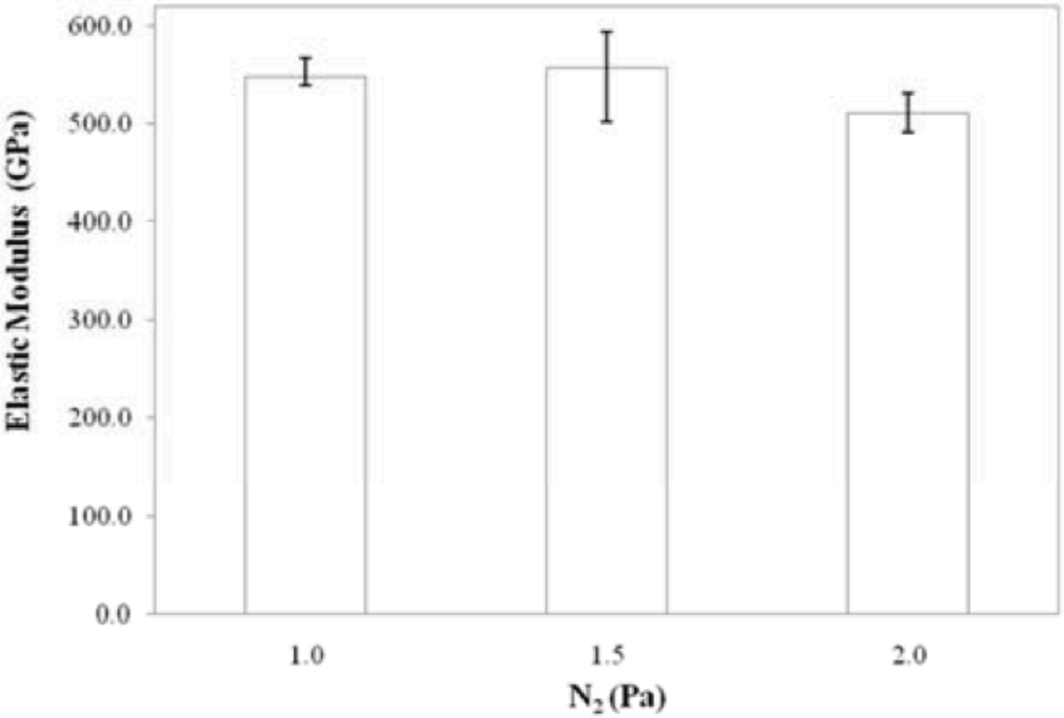

Figure 4-13. Elastic modulus vs Nitrogen pressure for TiAlN thin films (Chokwatvikul, et al. 2011, with permission).

4.3.6.2 Adhesion

J. Bujak et al. investigated adhesion properties of TiAlN coatings on tempered HSS disks by observing the first signs of breaking up within the coating along the edges of the scratch path. The results are shown in **Figure 4-14**. The maximum value of critical load was 90 N for the lowest nitrogen pressure of $3x10^{-3}$ mbar. Increasing nitrogen pressure above $8.0x10^{-3}$ mbar showed a dramatic decrease in the values obtained for critical loads, ranging from 48-54 N. These results suggested an inverse relationship between the increasing nitrogen pressure and decreasing adhesion of the TiAlN coatings caused by higher levels of stress and hardness of these films (Bujak, Walkowicza and Kusinski 2004).

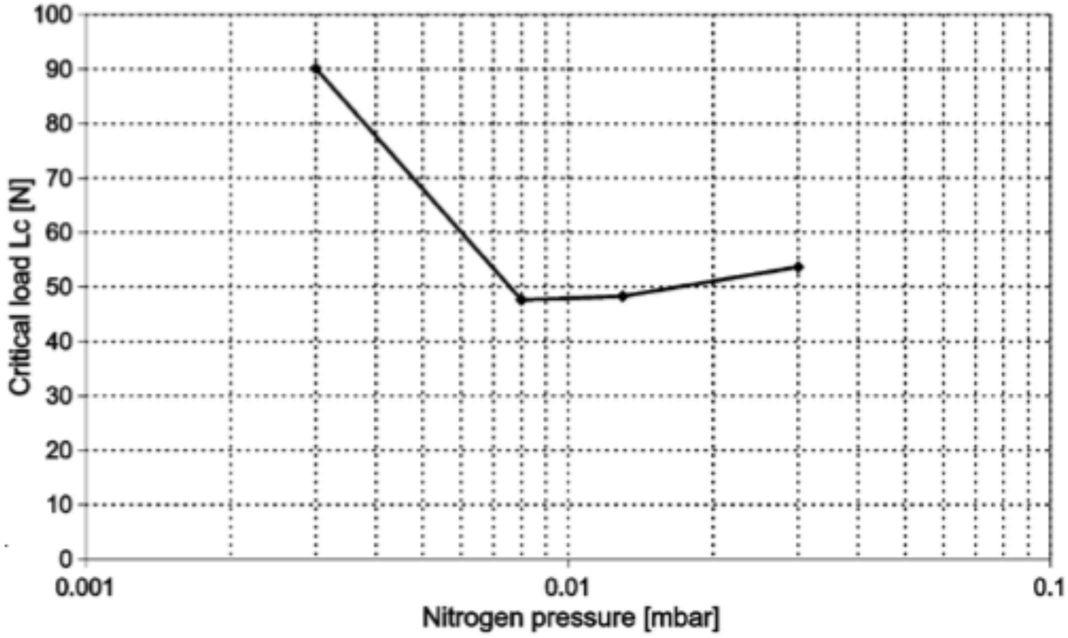

Figure 4-14. Adhesion vs Nitrogen pressure (Bujak, Walkowicza and Kusinski 2004, with permission).

C. Chokwatvikul et al. confirmed the inverse correlation between nitrogen pressure and coating adhesion with their experimental results. Scratch tests were performed on TiAlN coatings deposited with 1.0, 1.5, and 2.0 Pa nitrogen pressures, with loads exceeding 150 N. Their results are tabulated in **Table 4-18**. Samples deposited with 1.0 Pa and 1.5 Pa nitrogen pressures demonstrated the strongest adhesion with critical loads occurring at values greater than 150N. The TiAlN coating deposited using the largest nitrogen pressure of 2.0 Pa showed the weakest adhesion with minimum failure modes occurring at 128 N. A probable cause for poor adhesion is the greater probability that nitrogen gas may diffuse into the coating, creating voids within the film and at the interface between the substrate and the coating (Chokwatvikul, et al. 2011). From the results of this experiment, substrate exposure began to occur at 9.21 N for sample 25, which was a decrease for coating adhesion in comparison to sample 20a, which was run at 0.4 Pa nitrogen pressure, showing a value of 11.6 N.

Table 4-18. Critical loads where full delamination was evident for varying nitrogen pressures. Experimental results by C. Chokwatvikul et al. (Chokwatvikul, et al. 2011).

Nitrogen pressure (Pa)	Load at full delamination from Scratch test (N)
1.0	>150
1.5	>150
2.0	128.43 ± 3.95

Single factor ANOVA analysis was performed on Samples 20a and 25 in order to compare crack and delamination values for different nitrogen pressures 0.4 Pa and 1.0 Pa. The results can be found in **Tables 4-19** and **4-20**. In comparing the two different nitrogen pressures, it is important to note the null hypothesis that differences in nitrogen pressure during TiN deposition would have no effect on crack resistance and adhesion of the TiN coatings. In the case of critical values where cracking occurs, Samples 20a and 25 show large P-values such that P-Value > Alpha and small F values such that $F < F_{crit}$. Thus, the null hypothesis is accepted. It was concluded that distributions for crack resistance of samples prepared under varying nitrogen pressures experience little to no overlap with one another, which allows the interpretation that change in nitrogen pressure influenced the scratch resistance of TiN coatings. Samples 20a and 25 show small P-values for adhesion such that P-Value < Alpha and large F values such that $F > F_{crit}$. Thus, the null hypothesis is rejected. It was concluded that distributions for adhesion of samples prepared under varying nitrogen pressures experience little to no overlap with one another, which allows the interpretation that changes in nitrogen pressure influenced adhesion of TiN coatings.

Table 4-19. Single factor ANOVA analysis on crack values for Samples 20a and 25 (Alpha = 0.05).

Group	F	P-Value	F_{crit}	Accept/Reject Null Hypothesis
20a (0.4 Pa) 25 (1 Pa)	2.22	0.175	5.32	Accept

Table 4-20. Single factor ANOVA analysis on adhesion values for Samples 20a and 25 (Alpha = 0.05).

Group	F	P-Value	F_{crit}	Accept/Reject Null Hypothesis
20a (0.4 Pa) 25 (1 Pa)	15.6	0.00423	5.32	Reject

4.3.7 Control Sample

For the control sample we used all the initial parameters for the original TiN coating recipe developed by Steelforme Design Inc., demonstrated by sample 26. The substrate was cleaned using the standard Steelforme cleaning method and the TiN layer deposition lasted 10 minutes at a nitrogen pressure of 0.4 Pa. Cracking failures occurred at 2.86 N and delamination became evident at a critical load of 7.45 N. The original TiN coating recipe excluded the ion bombardment pretreatment step, which proved crucial for superior quality coatings with good adhesion. This result was proven by the experimental results obtained for Sample 20a. The substrate was pretreated using the same Steelforme cleaning method as the control. TiN deposition lasted 10 minutes at a nitrogen pressure of 0.4 Pa. Ion bombardment was performed on the sample at 400V for 120 seconds, demonstrating a 23% improvement in crack resistance and 56% for adhesion.

4.4 TiN Coating Optimization

Although experimental results for sample 20a demonstrated a significant improvement in coating adhesion by showing the highest critical load value for delamination, it is important to optimize bias voltage and ion bombardment duration parameters for superior quality coatings. Running ion bombardment for a longer duration, as in Sample 21b, contributed to a significant increase of microdroplets present within the coating. Premature coating delamination became evident during scratch testing. This may have been influenced by the increased amount of microdroplets present within the film. While crack resistance for this trial was improved by 58%, the adhesion of the coating showed a decrease of 12.5%

Coating thickness also plays an important role in the quality of TiN coatings. Single factor ANOVA analysis confirmed the significance of TiN deposition times for scratch resistance of the TiN coatings. An F value of 159 was obtained, which far exceeded the F_{crit} value of 3.89. The P-value for this factor was noted to be $2.28x10^{-9}$, much smaller than the set alpha constant of 0.05. These extreme values prove that there is little to no overlap between the critical load distributions for each sample obtained through scratch testing. Samples 23 and 24 were fabricated using longer TiN deposition times (20 and 30 minutes), resulting in an increase in the TiN coating thickness. In comparison to the control, the TiN deposition time of 20 minutes presented a 65% improvement in crack resistance and an improvement of 34% in comparison to sample 20a, which was run for 10 minutes. TiN deposition lasting 30 minutes demonstrated an improvement of 165% in crack resistance in comparison to the control and an overall improvement of 114 % in crack resistance in comparison to TiN deposition lasting 10 minutes.

The two samples with the highest experimentally obtained CL_2 averages as well as the control sample were scratched with a larger final load of 30 N. The samples were then compared under a microscope to find critical values where full delamination occurred. The control sample experienced obvious delamination at 25.5 N and full delamination at the end of the scratch track, as shown in **Figures 4-15** and **4-16**.

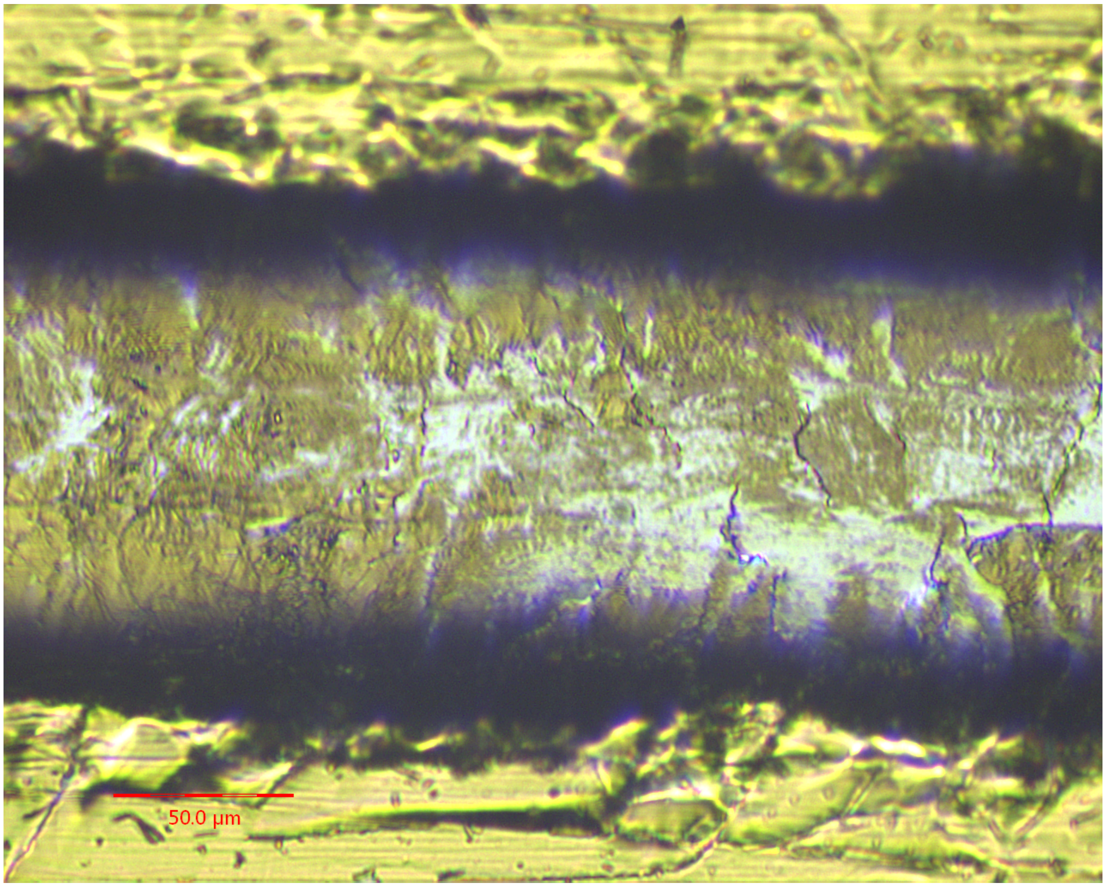

Figure 4-15. Partial delamination occurring at 25.5 N on the control sample.

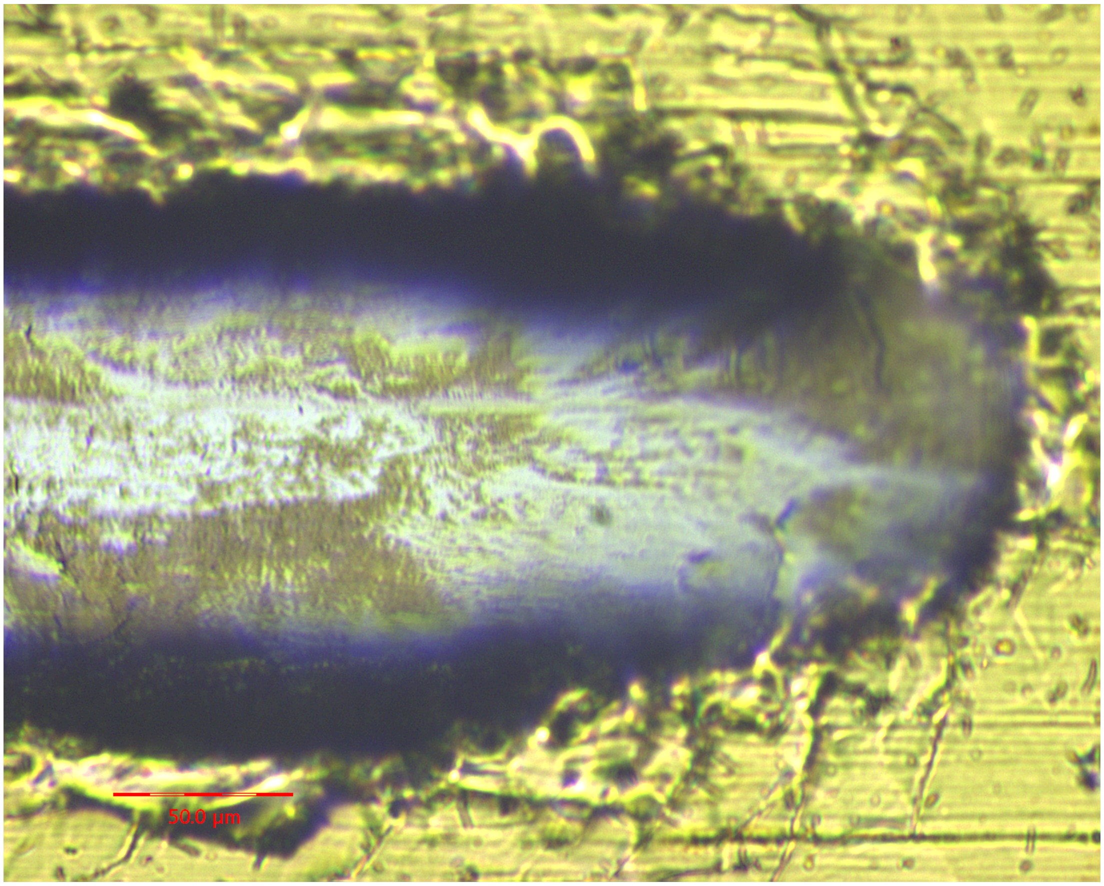

Figure 4-16. Full delamination occurring at the end of the scratch with load value of 30 N on the control sample.

Sample 20a exhibited the best coating adhesion as experimental results have shown the highest LC_2 average of 11.64 N. The second highest LC_2 average was obtained for Sample 24, which had undergone the longest TiN deposition time of 30 minutes. It was discovered that both Samples 20a and 24 exhibited partial delamination at 30 N, shown in **Figures 4-17** and **4-18**. This result suggested that full delamination for these coatings would occur at loads greater than 30 N, thus demonstrating improved adhesion in comparison to the control.

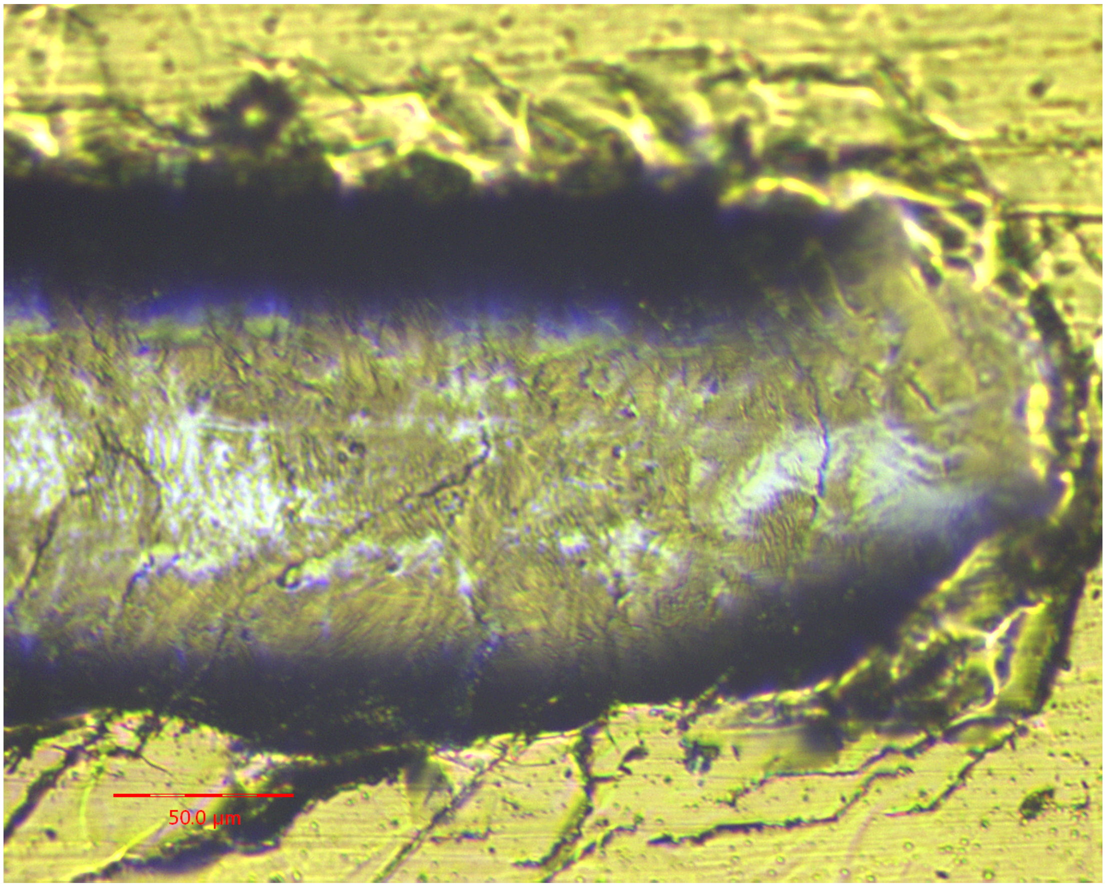

Figure 4-17. Partial delamination occurring at 30 N for Sample 20a.

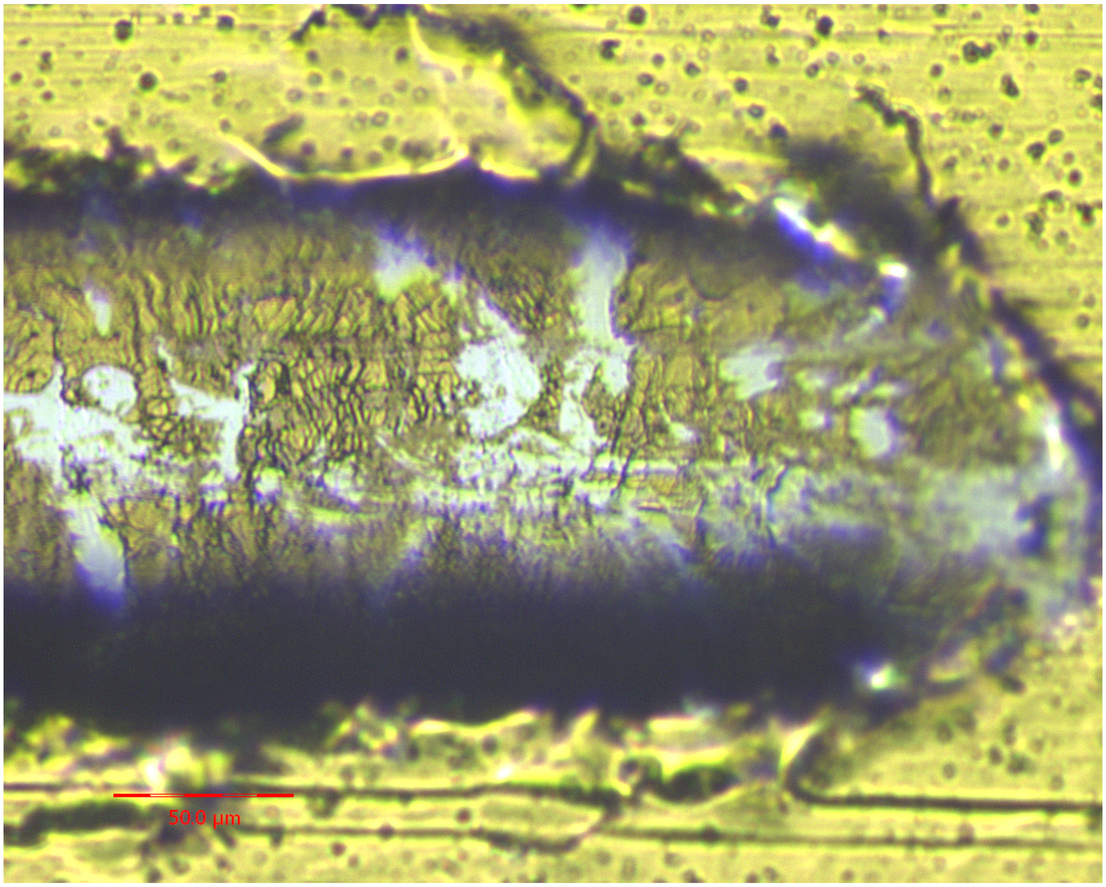

Figure 4-18. Partial delamination occurring at 30 N for Sample 24.

4.5 Limitations

Investigating various deposition parameters proved insightful in TiN coating optimization on stainless steel substrates. During the duration of this project, the cathodic arc PVD system experienced occasional performance failure and required immediate maintenance. Due to time limitations from system down time, it was important to maintain equal importance across all parameters being investigated as to efficiently use experimental time. Further investigation into the parameters that showed the most coating enhancement would provide detailed information on further optimizing coating adhesion and scratch resistance.

Scratch tests using the MCT showed consistent results for coating adhesion and scratch resistance. The MCT system was able to provide scratch loads of up to 30 N. As coating adhesion improved, it became impossible to determine critical loads where full delamination would occur since only partial delamination was evident at 30 N, indicating a critical load value of greater than what the MCT was able to deliver.

4.6 Sources of Uncertainty

The experimental results provided insight into crucial parameters for coating optimization specific to the cathodic arc PVD system at Steelforme Design Inc. A source of uncertainty lies in determining the precise load where cracking or delamination failures occur. The scratches were observed under a microscope and a judgment had to be made where these failure modes began to occur. Once the critical load was marked, the system noted the load value associated with that position. In order to minimize any uncertainty, judgments for each critical load was made by two students observing the same scratch path.

It is important for all arcs to be triggered during coating deposition in order to ensure thorough substrate coverage. For a number of coating depositions, a couple of arcs would not trigger and had to be shut off for the remainder of the trial. The rotating carousel increased substrate coverage for all samples as well as helped reduce any uncertainties in coating deposition when certain arcs failed to trigger.

Coating contamination is always possible. The arc PVD system at Steelforme Design Inc. is frequently used for production of various coatings. Some of the coating materials are deposited on the chamber walls. Coating purity cannot be guaranteed. Since the chamber is heated to high temperatures during deposition, it is possible that particles from the walls break off and redeposit onto the substrate as impurities.

4.7 Next Research Steps

4.7.1 Investigating Ti/TiN Ratio

Investigating varying thicknesses of TiN coatings provided significant results in coating hardness and resistance to crack failures. While thicker coatings allow for TiN properties to become more evident, it creates a high degree of internal stress within the film, making it difficult to deposit TiN coatings thicker than 6-7 μm without exhibiting poor adhesion (Jonsson and Hogmark 1984) (Burnett and Rickerby 1987) (Chicot and Lesage 1995). Instead of investigating varying TiN layer thickness, the importance of the Ti interlayer may prove to have extreme significance in lowering compressive stresses within the film. It may be important to consider the ratio between the Ti interlayer and TiN coating and examine through tribological testing whether there are improvements in film adhesion. The goal of this investigation would be to obtain an optimal ratio between the Ti interlayer and TiN coating with the strongest adhesion. E. Bemporad et al.

modeled, deposited and tested three sets of multilayered Ti/TiN coatings with constant and variable Ti interlayer thickness. The coatings were deposited using a cathodic arc PVD system and included multilayer films with constant Ti thickness, increasing Ti thickness in the direction toward the substrate, and increasing Ti thickness in the direction away from the substrate, as shown in **Figure 4-19**. Experimental results by E. Bemporad et al. showed hardness and wear rates were directly influenced by the total amount of Ti present within the coating. Multilayer films with lower average Ti/TiN ratio demonstrated increased wear resistance, while films with higher average Ti/TiN ratio showed a significant decrease in coating hardness. E. Bemporad et al. also noted stronger adhesion for the multilayer film with increasing Ti thickness toward the substrate, which was confirmed by finite element modeling as it showed a decrease in residual stress and strain (Bemporad, et al. 2006)**.**

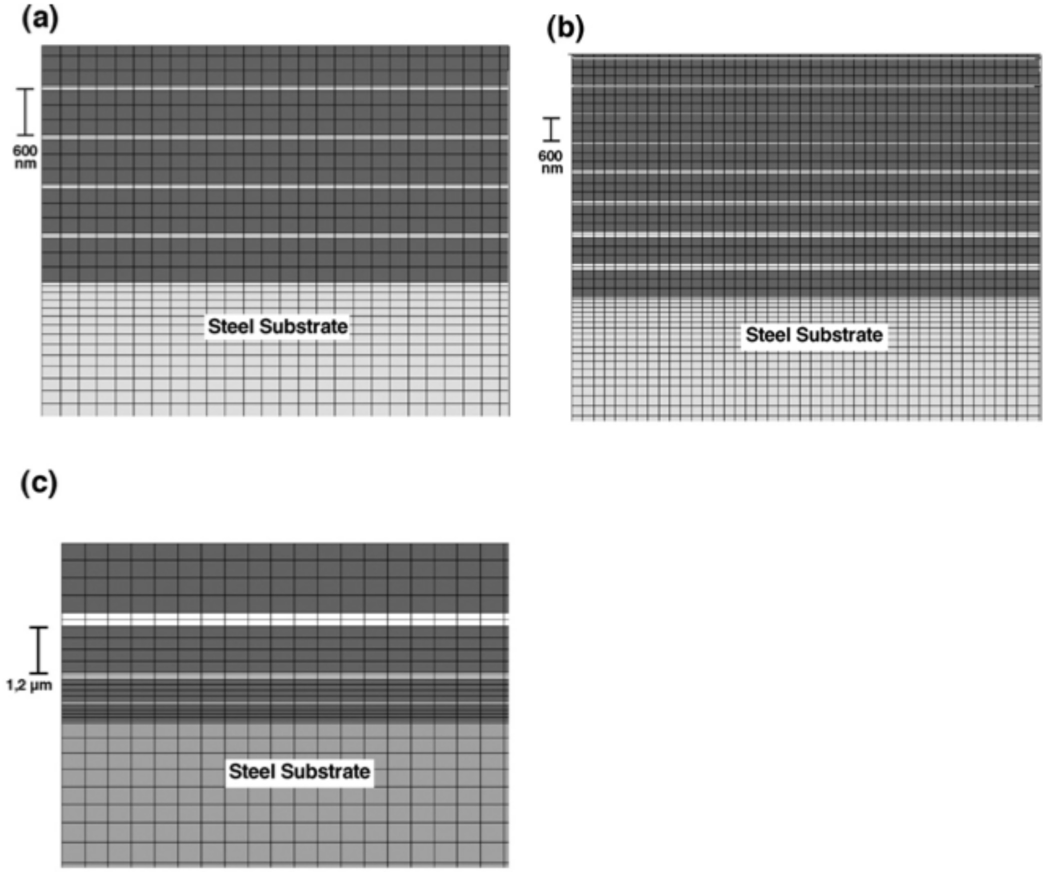

Figure 4-19. Multilayer systems analyzed by E. Bemporad et al. Multilayer system with (a) constant Ti thickness, (b) increasing thickness toward the substrate, (c) increasing thickness away from the substrate (Bemporad, et al. 2006, with permission).

4.7.2 Macroparticle Filter Design

Experimental results revealed that microdroplets might be the cause of premature coating delamination. A proposed solution of minimizing microdroplets within coatings was the concept of macroparticle filtering. While the most common design for macroparticle filters is a 90° coiling arrangement, there have been suggested design advancements such as the S-shaped macroparticle filter, formed by two 90° filters, shown in **Figure 4-20**. S. Anders et al. studied macroparticle behaviour in cathodic arc deposition systems by depositing films of amorphous hard carbon using 90° and S-shaped magnetic filters. The films were deposited onto silicon substrates and were approximately 200 nm thick. Their filter design consisted of metal bellows that curved into an “S” shape, with inner radii of 4cm and outer radii of 15 cm. Deposition rates varied between the 90° and S-shaped filters. The 90° filter had a deposition rate of 8 nm/minute, while the S-shaped filter led to a slower deposition rate of approximately 2 nm/minute. The samples were visually inspected using scanning electron microscopy. While it is difficult to measure particle density using a magnification of 5000 or higher, S. Anders et al. determined a rough estimate of 100 particles/cm^2 for the film deposited using the 90° magnetic filter and found that particle density was reduced by at least three orders of magnitude using the S-shaped magnetic filter (Anders, et al. 1997).

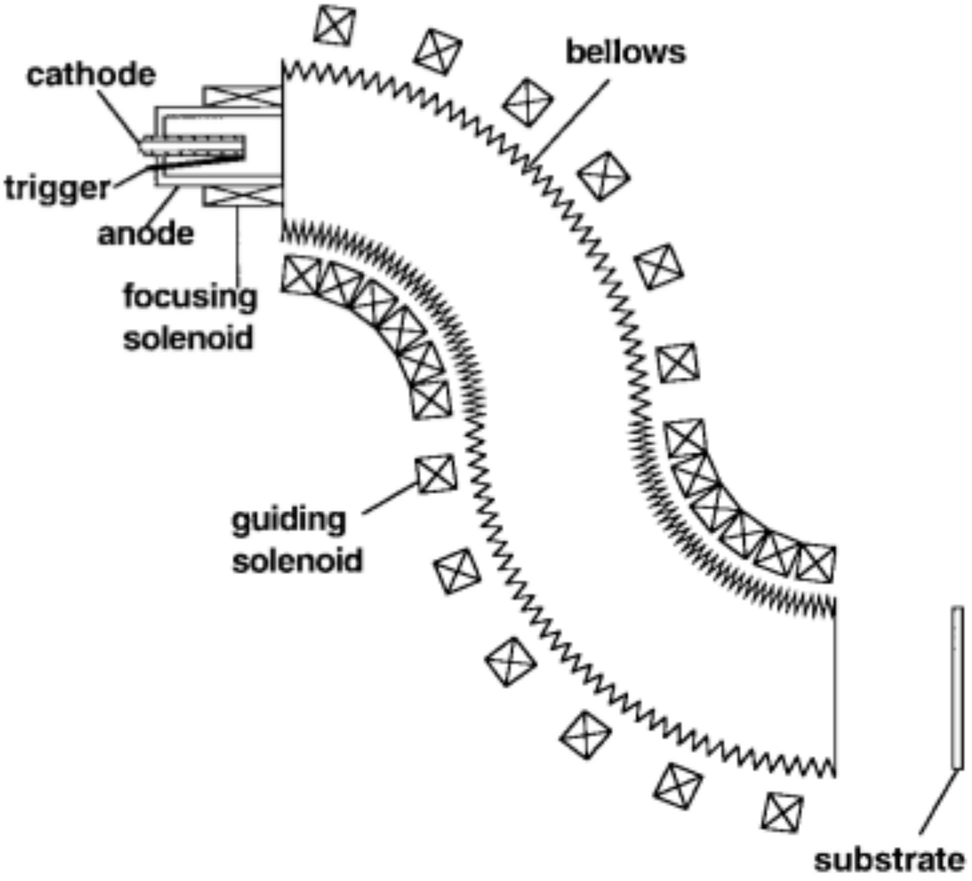

Figure 4-20. Schematic of the S-Shaped macroparticle filter design by S. Anders et al. (Anders, et al. 1997, with permission).

4.7.3 Other Types of Nitride Films

While TiN exhibits desirable properties such as hardness and durability, limitations exist since single metal nitride films are believed to deteriorate at higher temperatures. Literature suggests that TiN films experience rapid oxidation at temperatures above 550°C (Ikeda and Satoh 1991) (Cselle and Barimani 1995). Investigating compound nitride films may demonstrate increased durability for coatings that are required to function under extreme thermal conditions. TiAlN (Zhao, et al. 2010)

(Hsu, Lee and Ho 2008) (Kimura, Hasegawa, et al. 1999) (Ohnuma, et al. 2004) (Larpkiattaworn, Ikeuchi and Eamchotchawalit 2009) (Chokwatvikul, et al. 2011), TiZrN (Randhawa, Johnson and Cunningham, Deposition and Characterization of Ternary Nitrides 1988), and TiSiN (Wo, et al. 2010) (Kimura, Murakami, et al. 2001) are just a few examples of possible nitride coating variations that may be useful to investigate.

4.7.4 TiAlN Coatings

H. Zhao et al. deposited TiN and TiAlN coatings onto AZ91 magnesium alloy substrates using a reactive multi-arc ion plating system and tested the microhardness and wear volume loss of the uncoated substrate, and the substrate coated with TiN and TiAlN films. The sample containing TiN exhibited enhancement in microhardness with a hardness value that was two times greater than that of the uncoated AZ91 alloy, while the sample containing TiAlN showed to have the highest hardness value overall, shown in **Figure 4-21**. Both alloys coated with TiN and TiAlN demonstrated a significant decrease in wear volumes in comparison to the uncoated AZ91 alloy, shown in **Figure 4-22**. H. Zhao et al. suggested the decrease in wear volumes was related to the high hardness of both TiN and TiAlN films (Zhao, et al. 2010).

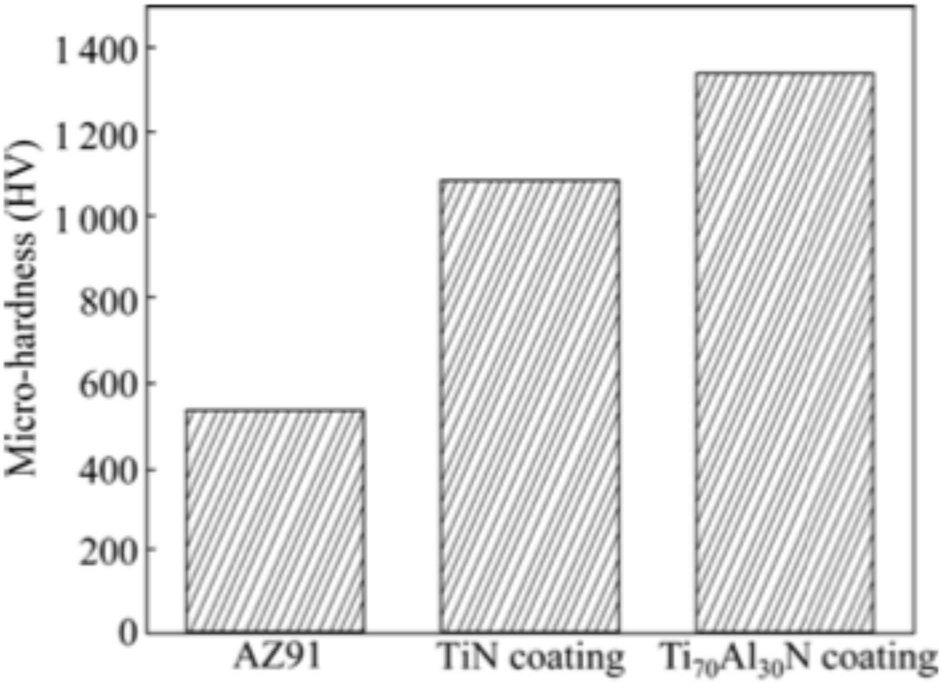

Figure 4-21. Microhardness values obtained by H. Zhao et al. for AZ91 alloy substrate, AZ91 alloy coated with TiN, and AZ91 alloy coated with TiAlN (Zhao, et al. 2010, with permission).

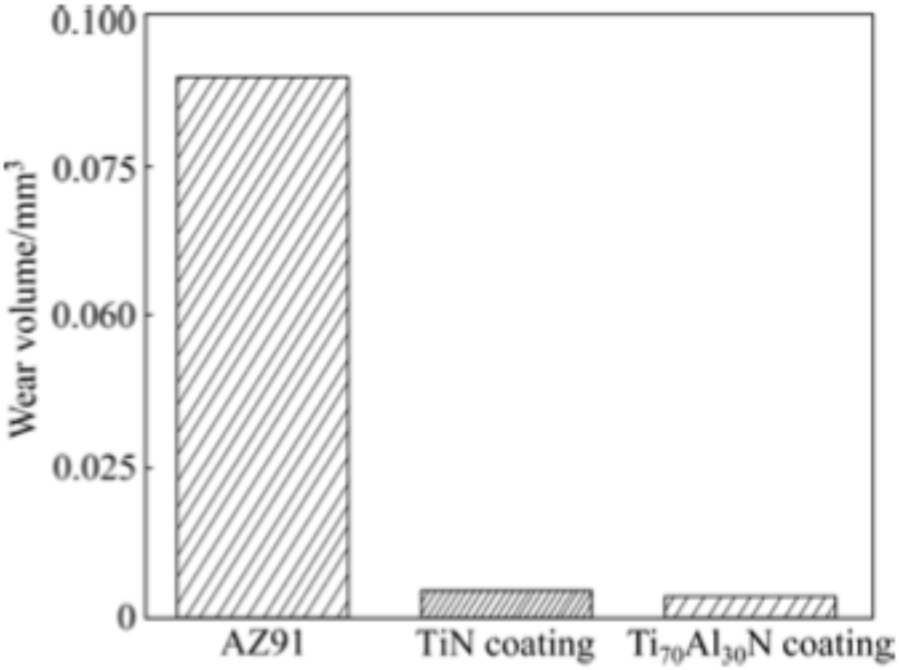

Figure 4-22. Wear volumes obtained by H. Zhao et al. for AZ91 alloy substrate, AZ91 alloy coated with TiN, and AZ91 alloy coated with TiAlN (Zhao, et al. 2010, with permission).

4.7.5 TiZrN Coatings

V. Rogov et al. deposited TiN and TiZrN on steel cutting plates and measured wear after intervals of 5 minutes for a total of 20 minutes for the cutting plates that were uncoated, coated with TiN or coated with TiZrN. The plate coated with TiZrN showed the least amount of wear as a function of operating time, followed by the plate coated with TiN. Lastly, the uncoated substrate showed the most amount of wear, proving that TiN and TiZrN improve wear resistant properties with TiZrN being the superior coating for this purpose, shown in **Figure 4-23** (Rogov, Fomin and Fomin 2010).

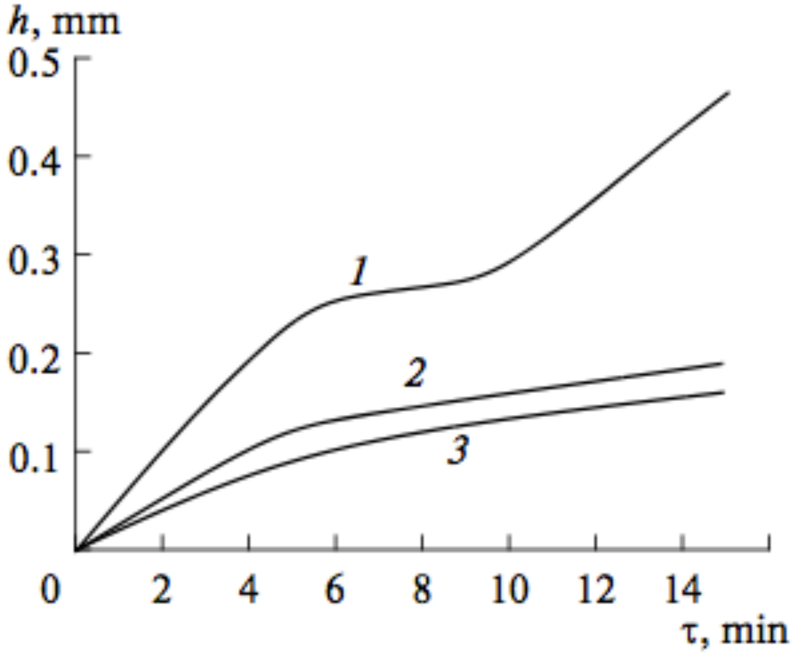

Figure 4-23. Wear *h* vs operating time *τ* obtained by V. A. Rogov et al. for (1) uncoated substrate, (2) substrate coated with TiN, and (3) substrate coated with TiZrN (Rogov, Fomin and Fomin 2010, with permission).

4.7.6 TiSiN Coatings

C. Guo et al. deposited TiSiN coatings on tungsten cemented carbide tools using a cathodic arc ion plating system and tested cutting and drilling performance of end mills and drillers under high-speed cutting conditions. Results by C. Guo et al. showed tools coated with TiSiN demonstrated superior cutting and drilling performance to those that were uncoated or coated with TiN. **Figure 4-24** shows the relationship between cutting lengths and wear for tools that were uncoated, coated with TiN, or coated with TiSiN. C. Guo et al. suggested Si components within the TiSiN films contributed to an increase in overall hardness, which reduced the amount of chipping and wear of the tools. **Figure 4-25** shows the relationship between the numbers of drilled holes and wear for tools that were uncoated, coated with TiN, or coated with TiSiN. Tools coated with TiSiN demonstrated enhanced performance, lasting for more than 50 holes. In comparison to uncoated drills, TiSiN coated drills performed seven times as many holes with minimal damage, and 3 times as many holes as drills coated with TiN (Guo, Lee and Chen 2008).

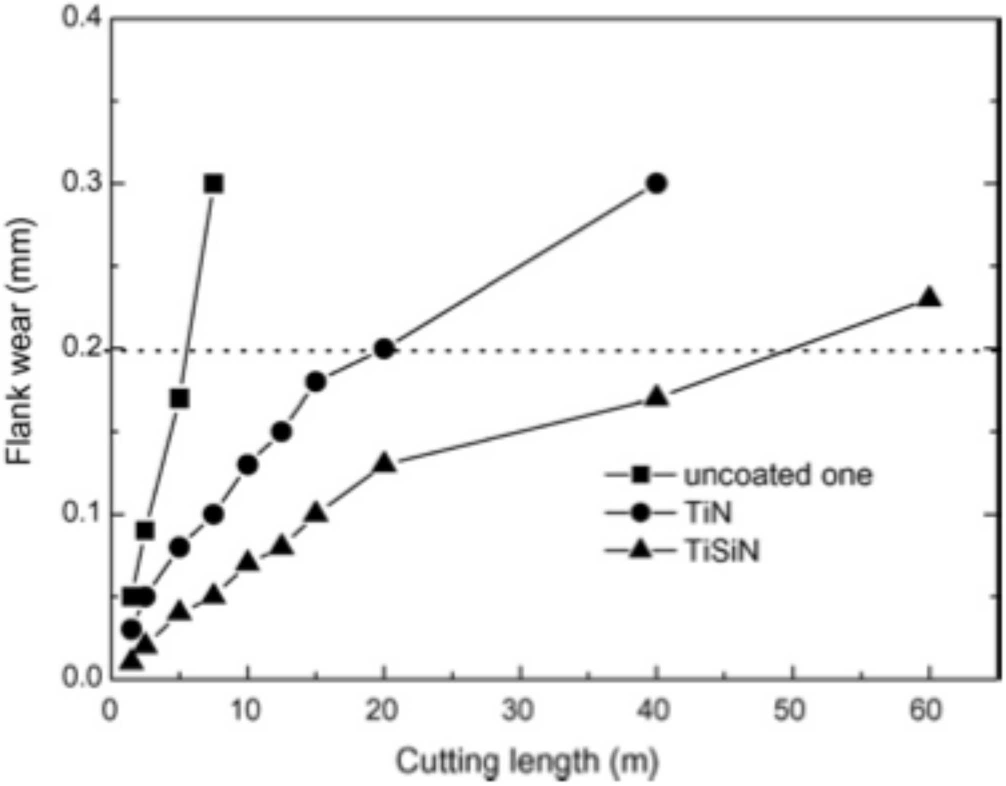

Figure 4-24. Cutting length vs wear for tools that were uncoated, coated with TiN, and coated with TiSiN (Guo, Lee and Chen 2008, with permission).

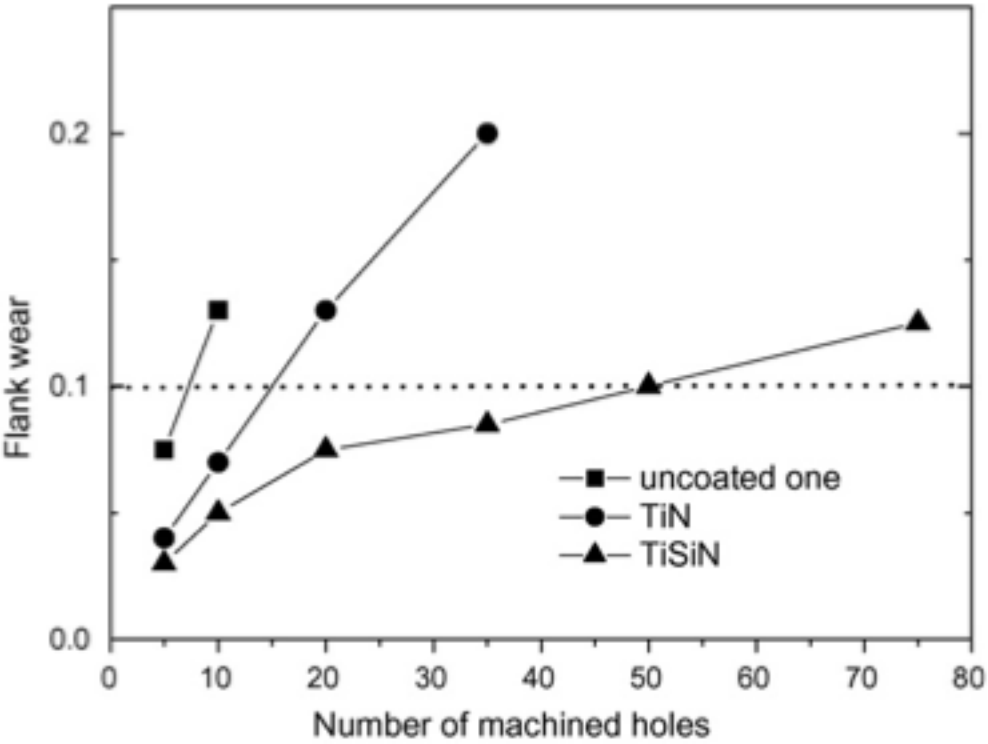

Figure 4-25. Number of machined holes vs wear for tools that were uncoated, coated with TiN, and coated with TiSiN (Guo, Lee and Chen 2008, with permission).

5 Conclusions

The original coating recipe used at Steelforme Design Inc. was the control in this experiment. The control experienced cracking failure at an average critical load of 2.86 N and delamination failure at an average critical load of 7.45 N. Samples with longer ion bombardment durations exhibited imperfections along the surface believed to have been the result of an increased presence of microdroplets within the coating. Samples with an ion bombardment voltage of 400 V proved to have best adhesion in comparison to 300 V and 500 V. Coating thickness showed a dramatic increase in scratch resistance with increasing TiN deposition time. The sample with the highest TiN deposition time of 30 minutes showed cracking failures at an average critical load of 7.57 N and delamination at an average critical load of 11.53 N. ANOVA analysis of scratch resistance revealed the highest F value of 159.36 and lowest P value of 2.28×10^{-9}. Ion bombardment and longer TiN deposition time exhibited the highest improvement in comparison to the control. Further experimental analysis showed the control experienced full delamination at the maximum 30 N performed by the MCT. Samples 20a and 24 experienced partial delamination at 30 mN, indicating excellent progress in coating optimization.

Works Cited

Adler, T. A., and R. P. Walters. “Corrosion and Wear of 304 Stainless Steel Using a Scratch Test.” *Corrosion Science* 33, no. 12 (1992): 1855-1876.

Aksenov, I. I., V. A. Belous, V. G. Padalka, and Khoroshikh V. M. “Transport of Plasma Streams in a Curvilinear Plasma Optics System.” *Soviet Journal of Plasma Physics* 4, no. 4 (1978): 425-428.

Aksenov, I. I., V. A. Belous, V. G. Padalka, and V. M. Khoroshikh. “Apparatus to Rid the Plasma of a Vacuum Arc of Macroparticles.” *Instruments and Experimental Techniques* 21, no. 5 (1978): 1416-1418.

Anders, S., A. Anders, M. R. Dickinson, R. A. MacGill, and I. G. Brown. “S-Shaped Magnetic Macroparticle Filter for Cathodic Arc Deposition.” *IEEE Transactions on Plasma Science* 24, no. 4 (1997): 670-674.

Andreev, A. A., L. V. Bulatova, G. N. Kartmazov, T. V. Kostritsa, and A. A. Romanov. “Effect of Annealing on the Structure and Properties of Molybdenum Coatings on Steel KhI2M.” *Metal Science and Heat Treatment* 24, no. 7-8 (1982): 481-484.

Bemporad, E., M. Sebastiani, C. Pecchio, and S. De Rossi. “High Thickness Ti/TiN Multilayer Thin Coatings for Wear Resistant Applications.” *Surface & Coatings Technology* 201, no. 6 (2006): 2155-2165.

Bendavid, A., P. J. Martin, R. P. Netterfield, and T.J. Kinder. “The Properties of TiN Films by Filtered Arc Evaporation.” *Surface and Coatings Technology* 70, no. 1 (1994): 97-106.

Bilek, M., and A. Anders. “Designing Advanced Filters for Macroparticle Removal from Cathodic Arc Plasmas.” *Plasma Sources* 8, no. 3 (1999): 488-493.

Borrero-López, O., M. Hoffman, A. Bendavid, and P. J. Martin. “The Use of the Scratch Test to Measure the Fracture Strength of Brittle Thin Films.” *Thin Solid Films* 518, no. 17 (2010): 4911-4917.

Bujak, J., J. Walkowicza, and J. Kusinski. “Influence of the Nitrogen Pressure on the Structure and Properties of (Ti,Al)N Coatings Deposited by Cathodic Vacuum Arc PVD Process.” *Surface & Coatings Technology* 180-181 (2004): 150-157.

Bull, S. J., and D. S. Rickerby. “The Sliding Wear of Titanium Nitride Coatings.” *Surface and Coatings Technology* 41, no. 3 (1990): 269-283.

Burnett, P. J., and D. S. Rickerby. “The Mechanical Properties of Wear-Resistant Coatings: I: Modelling of Hardness Behaviour.” *Thin Solid Films* 148, no. 1 (1987): 41-50.

Celis, J. P., P. Ponthiaux, and F. Wenger. “Tribo-Corrosion of Materials: Interplay Between Chemical, Electrochemical, and Mechanical Reactivity of Surfaces.” *Wear* 261, no. 9 (2006): 939-946.

Cheng, C. C., A. Erdemir, and G. R. Fenske. “Correlation of Interface Structure with Adhesive Strength of Ion-Plated TiN Hard Coatings.” *Surface and Coatings Technology* 39-40, no. 1-3 (1989): 365-376.

Chicot, D., and J. Lesage. “Absolute Hardness of Films and Coatings.” *Thin Solid Films* 254, no. 1-2 (1995): 123-130.

Chokwatvikul, C., S. Larpkiattaworn, S. Surinphong, C. Busabok, and P. Termsuksawad. “Effect of Nitrogen Partial Pressure on Characteristic and Mechanical Properties of Hard Coating TiAlN Film.” *Journal of Metals, Materials and Minerals* 21, no. 1 (2011): 115-119.

Cselle, T., and A. Barimani. “Today’s Applications and Future Developments of Coatings for Drills and Rotating Cutting Tools.” *Surface and Coatings Technology* 77, no. 1-3 (1995): 712-718.

Daalder, J. E. *Cathode Erosion of Metal Vapor Arcs in Vacuum.* Ph.D. Thesis, Eindhoven, Holland: Technische Hugelschol, 1978.

Daalder, J. E. “Cathode Spots and Vacuum Arcs.” *Physica B & C* 104, no. 1-2 (1981): 91-106.

Daalder, J. E. “Random Walk of Cathode Arc Spots in Vacuum.” *Journal of Applied Physics D: Applied Physics* 16, no. 1 (1983): 17-27.

Davis, W. D., and H. C. Miller. “Analysis of the Electrode Products Emitted by DC Arcs in a Vacuum Ambient.” *Journal of Applied Physics* 40, no. 5 (1969): 2212.

Ding, X. Z., M. K. Samani, and G. Chen. “Thermal Conductivity of PVD TiAlN Films Using Pulsed Photothermal Reflectance Technique.” *Applied Physics A: Materials Science & Processing* 101, no. 3 (2010): 573-577.

Guo, C. T., D. Lee, and C. Chen. “Deposition of TiSiN Coatings by Arc Ion Plating Process.” *Applied Surface Science* 254, no. 10 (2008): 3130-3136.

Hansen, D. C., S. C. Dexter, and J. H. Waite. “The Inhibition of Corrosion of S30403 Stainless Steel by a Naturally Occuring Catecholic Polymer.” *Corrosion Science* 37, no. 9 (1995): 1423-1441.

Hariharan, K., G. Balachandran, and M. Sathya Prasad. “Application of Cost-Effective Stainless Steel for Automotive Components.” *Materials and Manufacturing Processes* 24, no. 10-12 (2009): 1442-1452.

Harris, N. S. “Diffusion Pump Back-Streaming.” *Vacuum* 27, no. 9 (1977): 519-530.

Higgins, M., D. Smith, J. Mattzela, and G. Barone. “Protective Chemical Vapor Deposition Coatings for Stainless Steel Surfaces Used in Produced Water Environments.” *20th Annual Produced Water Seminar 2010.* Houston, Texas: Produced Water Society, 2010. 87-100.

Hsu, C., C. Lee, and W. Ho. “Filter Effects on the Wear and Corrosion Behaviors of Arc Deposited (Ti,Al)N Coatings for Application on Cold-Work Tool Steel.” *Thin Solid Films* 516, no. 15 (2008): 4826-4832.

Ikeda, T., and H. Satoh. “Phase Formation and Characterization of Hard Coatings in the Ti-Al-N System Prepared by the Cathodic Arc Ion Plating Method.” *Thin Solid Films* 195, no. 1-2 (1991): 99-110.

Jehn, H. A. “PVD and ECD-Competition, Alternative or Combination?” *Surface and Coatings Technology* 112, no. 1 (1999): 210-216.

Johnson, P. C., and H. Randhawa. “Zirconium Nitride Films Prepared by Cathodic Arc Plasma Deposition Process.” *Surface and Coatings Technology* 33 (1987): 53-62.

Jonsson, B., and S. Hogmark. “Hardness Measurements of Thin Films.” *Thin Solid Films* 114, no. 4 (1984): 257-269.

Kimblin, C. W. “Cathode Spot Erosion and Ionization Phenomena in the Transition from Vacuum to Atmospheric Pressure Arcs.” *Journal of Applied Physics* 45, no. 12 (1974): 5235-5244.

Kimura, A., H. Hasegawa, K. Yamada, and T. Suzuki. “Effects of Al Content on Hardness, Lattice Parameter and Microstructure of TiAlN Films.” *Surface and Coatings Technology* 120-121 (1999): 438-441.

Kimura, A., T. Murakami, K. Yamada, and T. Suzuki. “Hot-Pressed Ti-Al Targets for Synthesizing TiAlN Films by the Arc Ion Plating Method.” *Thin Solid Films* 382, no. 1-2 (2001): 101-105.

Knotek, O., F. Liiffler, and G. Kriimer. “Process and Advantage of Multicomponent and Multilayer PVD Coatings.” *Surface and Coatings Technology* 59, no. 1-3 (1993): 14-20.

Kobayashi, M., and Y. Doi. “TiN and TiC of Cemented Carbides by Ion Plating.” *Thin Solid Films* 54, no. 1 (1978): 67-74.

Laing, K., J. Hampshire, D. Teer, and G. Chester. “The Effect of Ion Current Density on the Adhesion and Structure of Coatings Deposited by Magnetron Sputter Ion Plating.” *Surface and Coatings Technology* 112, no. 1-3 (1999): 177-180.

Larpkiattaworn, S., J. Ikeuchi, and C. Eamchotchawalit. “Comparison of Properties of Titanium Aluminium Nitride Film Produced by Using Two Different Types of Ti–Al Target.” *Surface and Interface Analysis* 41, no. 10 (2009): 794-798.

Lee, Y. K., and J. W. Lee. “Direct Simulation of Pumping Characteristics for a Model Diffusion Pump.” *Vacuum* 47, no. 3 (1996): 297-306.

Li, J., and W. Beres. “Scratch Test for Coating/Substrate Systems – A Literature Review.” *Canadian Metallurgical Quarterly* 46, no. 2 (2007): 155-173.

Lima, P., P. Pedrosa, A. V. Machado, C. Fonseca, and F. Vaz. “Plasma Surface Activation and TiN Coating of a TPV Substrate for Biomedical Applications.” *Plasma Processes and Polymers* 8, no. 12 (2011): 1174-1183.

Lugscheider, E., O. Knotek, H. Zimmermann, and S. Hellmann. “Investigation of the Mechanical and Structural Properties of Ti–Hf–C–N Arc PVD Coatings.” *Surface and Coatings Technology* 116-119 (1999): 239-243.

Lunev, V. M., V. G. Padalkaand, and V. M. Khoroshikh. “Plasma Properties of a Metal Vacuum Arc.” *Soviet Physics - Technical Physics* 22, no. 7 (1977): 855-861.

Marder, M. “How Things Break.” *Physics Today* 49, no. 9 (1996): 24-29.

Mattox, D. M. “Fundamentals of Ion Plating.” *Journal of Vacuum Science and Technology* 10, no. 1 (1973): 47-52.

—. *Handbook of Physical Vapor Deposition (PVD) Processing.* 2nd Edition. William Andrew, 2010.

Mattox, D. M. “Thin Film Adhesion and Adhesive Failure – a Perspective.” *Adhesion Measurement of Thin Films, Thick Films and Bulk Coatings*, 1978: 54-62.

Merl, D. K., P. Panjan, M. Cekada, P. Gselman, and S. Paskvale. “Tribocorrosion Degradation of Protective Coatings on Stainless Steel.” *Materiali in Tehnologije* 47, no. 4 (2013): 435-439.

Miller, H. C. “On Sputtering in Vacuum Arcs.” *Journal of Physics D: Applied Physics* 12, no. 8 (1979): 1293-1298.

Mohrbacher, H., B. Blanpain, J. P. Celis, J. R. Roos, L. Stals, and M. Van Stappen. “Oxidational Wear of TiN Coatings on Tool Steel and Nitrided Tool Steel in Unlubricated Fretting.” *Wear* 188, no. 1-2 (1995): 130-137.

Mohseni, E., E. Zalnezhad, A. R. Bushroa, A. M. Hamouda, B. T. Goh, and G.H Yoon. “Ti/TiN/HA Coating on Ti–6Al–4V for Biomedical Applications.” *Ceramics International* 41 (2015): 14447-14457.

Morozov, A. I. "Focussing of Cold Quasineutral Beams in Electromagnetic Fields." *Soviet Physics - Doklady* 10 (1966): 775-777.

Nicolet, M. A. "Diffusion Barriers in Thin Films." *Thin Solid Films* 52, no. 3 (1978): 415-443.

Nordin, M., M. Larsson, and S. Hogmark. "Mechanical and Tribological Properties of Multilayered PVD TiNrCrN." *Wear* 232 (1999): 221-225.

Nuraje, N., W. S. Khan, Y. Lei, M. Ceylan, and R. Asmatulu. "Superhydrophobic Electrospun Nanofibers." *Journal of Materials Chemistry A* 1, no. 6 (2013): 1929-1946.

Ohnuma, H., N. Nihira, A. Mitsuo, K. Toyoda, K. Kubota, and T. Aizawa. "Effect of Aluminum Concentration on Friction and Wear Properties of Titanium Aluminum Nitride Films." *Surface & Coatings Technology* 177-178 (2004): 623-626.

Perez, F. J., F. Pedraza, M. P. Hierro, J. Balmain, and G. Bonnet. "Comparison of the High-Temperature Oxidation of Uncoated and CVD–FBR Aluminized AISI-304 Stainless Steel." *Oxidation of Metals* 58, no. 5-6 (2002): 563-588.

Ponthiaux, P., F. Wenger, D. Drees, and J. P. Celis. "Electrochemical Techniques for Studying Tribocorrosion Processes." *Wear* 256, no. 5 (2004): 459-468.

Quaeyhaegens, C., L. M. Stals, M. Van Stappen, and L. De Schepper. "Interface Study of TiN- and Steel AISI 304 with Asymmetric Diffraction and Classical Bragg-Brentano Diffraction." *Thin Solid Films* 197, no. 1-2 (1991): 37-46.

Randhawa, H., and P. C. Johnson. "Technical Note: A Review of Cathodic Arc Plasma Deposition Processes and their Applications." *Surface and Coatings Technology* 31, no. 4 (1987): 303-318.

Randhawa, H., P. C. Johnson, and R. Cunningham. "Deposition and Characterization of Ternary Nitrides." *Journal of Vacuum Science & Technology A (Vacuum, Surfaces, and Films)* 6, no. 5 (1988): 2136-2139.

Rogov, V. A., E. V. Fomin, and A. V. Fomin. "Effectiveness of Wear-Resistant TiN and (TiZr)N Coatings in Face Milling of Low-Temperature Steel." *Russian Engineering Research* 30, no. 11 (2010): 1180-1181.

Sakharova, N. A., J. V. Fernandes, J. M. Antunes, and M. C. Oliveira. "Comparison Between Berkovich, Vickers and Conical Indentation Tests: A Three-Dimensional Numerical Simulation Study." *International Journal of Solids and Structures* 46, no. 5 (2009): 1095-1104.

Schade, K., et al. "High Temperature Line Electrode Assembly for Continuous Substrate Flow VHF PECVD." *Thin Solid Films* 502, no. 1-2 (2006): 59-62.

Schulke, T., A. Anders, and P. Siemroth. "Macroparticle Filtering of High-Current Vacuum Arc Plasmas." *IEEE Transactions on Plasma Science* 25, no. 4 (1997): 660-664.

Taiwade, R. V., A. P. Patil, S. J. Patre, and R. K. Dayal. "A Comparative Study of Intergranular Corrosion of AISI 304 Stainless Steel and Chrome-Manganese Austenitic Stainless Steel." *ISIJ International* 52, no. 10 (2012): 1879-1887.

Tarefder, R. A., A. M. Zaman, and W. Uddin. "Determining Hardness and Elastic Modulus of Asphalt by Nanoindentation." *International Journal of Geomechanics* 10, no. 3 (2010): 106-116.

Tuffy, K., G. Byrne, and D. Dowling. "Determination of the Optimum TiN Coating Thickness on WC Inserts for Machining Carbon Steels." *Journal of Materials Processing Technology* 155-156, no. 1-3 (2004): 1861-1866.

Tuma, D. T., C. L. Chen, and D. K. Davies. "Erosion Products from the Cathode Spot Region of a Copper Vacuum Arc." *Journal of Applied Science* 49, no. 7 (1978): 3821-31.

Vuorinen, S., E. Niemi, and A. S. Korhonen. "Microstructural Study of TiN-Coated Threading Taps." *Journal of Vacuum Science and Technology A* 3, no. 6 (1985): 2445-2449.

Whittaker, J. T., and D. P. Hess. "Ductility of Titanium Alloy and Stainless Steel Aerospace Fasteners." *Journal of Failure Analysis and Prevention* 15, no. 5 (2015): 571-575.

Wittmer, M., B. Struder, and H. Melchior. "Electrical Characteristics of TiN Contacts to N Silicon." *Journal of Applied Physics* 52, no. 9 (1981): 5722-5726.

Wo, P. C., P. R. Munroe, Z. F. Zhou, K. Y. Li, and Z. H. Xie. "Effects of TiN Sublayers on the Response of TiSiN Nanocomposite Coatings to Nanoidentation and Scratching Contacts." *Materials Science & Engineering: A (Structural Materials: Properties, Microstructure and Processing)* 527, no. 16-17 (2010): 4447-4457.

Wu, P. Q., H. Mohrbacher, and J. P. Celis. "The Fretting Behaviour of PVD TiN Coatings in Aqueous Solutions." *Wear* 201, no. 1-2 (1996): 171-177.

Xu, K. W., et al. "Prediction of Nanoindentation Hardness Profile from a Load-Displacement Curve." *Journal of Materials Research* 13, no. 12 (1998): 3519-3526.

Yan, J., H. Jianjun, and X. Hongbin. "Design of Applied Diffusion Pump System for Electron Beam Process." *Applied Mechanics and Materials* 80-81, no. 2 (2011): 1295-1299.

Yuan, J. P., W. Li, and C. Wang. "Effect of the La Alloying Addition on the Antibacterial Capability of 316L Stainless Steel." *Materials Science and Engineering: C (Materials for Biological Applications)* 33, no. 1 (2013): 446-452.

Zalnezhad, E., A. A. D. Sarhan, and M. Hamdi. "A Fuzzy Logic Based Model to Predict Surface Hardness of Thin Film TiN Coating on Aerospace AL7075-T6 Alloy." *International Journal of Advanced Manufacturing Technology* 68, no. 1-4 (2013): 415-423.

Zhao, H., X. Wang, Q. Liu, L. Chen, and Z. Liu. "Structure and Wear Resistance of TiN and TiAlN Coatings on AZ91 Alloy Deposited by Multi-Arc Ion Plating." *Transactions of Nnferrous Metals Society of China* 20, no. 2 (2010): 679-682.